





UNIVERSITÀ DEGLI STUDI DI TRIESTE
SCUOLA DI DOTTORATO IN BIOMEDICINA MOLECOLARE
XXIX CICLO

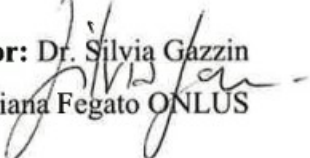
***In vivo* evaluation of biomolecular
mechanisms of bilirubin toxicity and
pre-clinical therapies**

Settore scientifico-disciplinare: Gastroenterologia (MED/12)

Ph.D. Student:
Eleonora Vianello

Doctoral Coordinator: Prof.ssa Germana Meroni

Università degli Studi di Trieste

 **Supervisor:** Prof. Claudio Tiribelli
Università degli Studi di Trieste

Tutor: Dr. Silvia Gazzin

Fondazione Italiana Fegato ONLUS

Supervisor: Prof. Claudio Tiribelli
Università degli Studi di Trieste
Fondazione Italiana Fegato ONLUS

Tutor: Dr. Silvia Gazzin
Fondazione Italiana Fegato ONLUS

External Advisor: Prof. Giampiero Leanza
Università degli Studi di Trieste

Referees: Prof. Gianluca Tell
Università degli Studi di Udine
Dr. Sean Riordan
Children's Mercy Hospitals and Clinics, Kansas City

Opponent: Dr. Sean Riordan

*A mio marito,
perché è bello “guardare insieme nella stessa direzione”.*

ABSTRACT

Introduction. Neonatal jaundice is a common and benign condition usually resolved during the first week of life. Neonates with very high level of unconjugated bilirubin (UCB), with an increase of the free bilirubin (Bf), may develop encephalopathy, with different grade of severity. Typical symptoms include motor disorder, auditory dysfunction, memory and learning deficits, reflecting selective damage respectively for cerebellum and basal ganglia, inferior colliculus, and hippocampus. Several studies reported that bilirubin may activate signal cascades that culminate to cell survival or death, as well as modulation of mRNA expression of genes involved in. Histone acetylation, an epigenetic mechanism responsible for the gene expression regulation via opening/closing of the chromatin, was never investigated in bilirubin-induced central nervous system (CNS) damage until now. The involvement of histone acetylation in common and rare neuropathologies was widely described, and also the potential neuroprotective action of drugs that regulate this epigenetic process.

Aims. By the use of the animal model for hyperbilirubinemia (Gunn rat), we purpose to investigate the modulation of the acetyl-histone H3 (lys14) (H3K14ac) in five brain regions (Cortex: Cx; Cerebellum: Cll; Superior Colliculi: SC; Inferior Colliculi: IC; Hippocampus: Hip) of hyperbilirubinemic animals (jj) vs. non hyperbilirubinemic littermates at four post natal ages (P2, P9, P17 and old). Moreover, we would like to individuate the genes regulated by H3K14ac in jj cerebella vs. controls at P9 and eventually interpret the biological effects of this epigenetic modulation performing histological stainings.

Results. Western blot analysis of H3K14ac level in all the brain regions and ages considered revealed a modulation of this protein that is region- and age-dependent. A significant increase of H3K14ac was observed in Cll, IC, and Hip in P9 jj animals, while a significant decrease was present in Cll and IC at P17 and Cx in older jj rats. ChIP-seq was performed in order to link the effect of hyperbilirubinemia on the H3K14ac with the genes controlled by this epigenetic mechanism in cerebella of P9 animals. Our data on H3K14ac in Cll and the fact that the cerebellar hypoplasia is the hallmark of hyperbilirubinemic Gunn rat supported this choice. Our results revealed that a very high number of genes regulated by H3K14ac was silenced in jj rats, while other few genes seemed to be activated in hyperbilirubinemic subjects. The gene ontology analysis showed that cellular development and differentiation, proliferation and migration, as well as apoptosis were the most modulated

biological processes in jj rats. These ChIP-Seq data were confirmed by our histological findings, that revealed higher cell density with reduction of the fibrillary component and a possible impairment of cell differentiation.

Conclusions. This work reported for the first time the involvement of histone acetylation alterations in the brain of hyperbilirubinemic animals with a strong regulation of the gene expression. The complete panel of genes we obtained seemed to well-correlate with the bilirubin-induced damage that evidenced the development impairment. These data contribute to better understand the bio-molecular mechanisms that cause bilirubin toxicity but also might open to new therapeutical strategies in kernicterus, testing the neuroprotective properties of drugs that regulate the histone acetylation.

RIASSUNTO

Introduzione. L'ittero neonatale è una condizione comune e benigna che si risolve entro la prima settimana di vita. Alcuni neonati possono sviluppare iperbilirubinemia con livelli molto elevati di bilirubina non coniugata (UCB), e un incremento di bilirubina libera (Bf) non legata ad albumina ed in grado di penetrare nel sistema nervoso centrale. Questi neonati possono sviluppare encefalopatia, caratterizzata da diversi gradi di severità. I sintomi principali di questa patologia comprendono disabilità motorie, disfunzioni uditive e deficit nella memoria e nell'apprendimento. Questi sintomi sono legati al danno selettivo che bilirubina è in grado di operare rispettivamente su cervelletto e gangli della base, collicoli inferiori ed ippocampo. Molti lavori hanno dimostrato che bilirubina è in grado di attivare diverse cascate di segnale che culminano in processi di sopravvivenza cellulare o morte, così come di modulare l'espressione dell'mRNA dei geni coinvolti in queste vie di segnale. L'acetilazione istonica, meccanismo direttamente coinvolto nella regolazione dell'espressione genica attraverso l'apertura o chiusura della cromatina, non è mai stato preso in considerazione nel danno al sistema nervoso centrale (CNS) indotto da bilirubina fino al momento attuale. Il coinvolgimento dell'acetilazione istonica in diverse patologie cerebrali, sia comuni che rare, è stato ampiamente descritto, insieme alla possibilità di trattare alcune sintomatologie di tali patologie attraverso l'azione neuroprotettiva di farmaci che regolano questo processo epigenetico.

Obiettivi. Gli esperimenti sono stati condotti *in vivo*, usando l'animale modello che meglio rappresenta la condizione di iperbilirubinemia: il ratto Gunn. In questo lavoro il nostro scopo è quello di valutare la modulazione della acetilazione dell'istone H3 (lys 14) (H3K14ac) in cinque regioni cerebrali (Corteccia cerebrale: Cx; Cervelletto: Cll; Collicoli Superiori: SC; Collicoli Inferiori: IC; Ippocampo: Hip) degli animali iperbilirubinemici (jj) paragonati agli animali non iperbilirubinemici, considerando quattro età dopo la nascita (P2, P9, P17, adulti). Inoltre, vorremmo individuare i geni regolati da H3K14ac nel cervelletto degli animali iperbilirubinemici a 9 giorni dalla nascita, concludendo con una possibile interpretazione degli effetti biologici dati da bilirubina effettuando delle colorazioni istologiche.

Risultati. L'analisi tramite Western blot dell'espressione della proteina H3K14ac in tutte le regioni cerebrali a tutte le età considerate ha mostrato una modulazione della stessa dipendente dalla regione e dall'età. Un aumento significativo della proteina è stato osservato in Cll, IC ed Hip nei jj a P9. D'altra parte una riduzione significativa è stata rilevata in Cll ed IC

a P17, mentre in Cx negli animali jj adulti. Per relazionare gli effetti dell'iperbilirubinemia sulla modulazione del H3K14ac con i geni controllati da questo meccanismo epigenetico è stata utilizzata la ChIP-seq su campioni di cervelletto di animali P9. Questa scelta è stata supportata dai dati su H3K14ac ottenuti nei campioni di cervelletto a questa stessa età, ma anche dal fatto che l'ipoplasia del cervelletto rappresenta la caratteristica principale dei ratti Gunn iperbilirubinemici. I nostri risultati hanno mostrato che un elevato numero di geni regolati da H3K14ac erano silenziati nei jj, mentre altri pochi geni sembrano essere specificatamente attivati nell'animale iperbilirubinemico. L'analisi di *gene ontology* ha mostrato essenzialmente alterazioni dei processi di sviluppo e differenziamento cellulare, proliferazione e migrazione, ma anche apoptosi. I dati di ChIP-Seq sono stati confermati anche dai risultati istologici che hanno rivelato un'elevata densità cellulare con riduzione della componente fibrillare, ed una possibile compromissione del differenziamento e della migrazione.

Conclusioni. Questo lavoro ha riportato per la prima volta il coinvolgimento dell'acetilazione istonica nel cervello di animali iperbilirubinemici con una forte regolazione dell'espressione genica. Il quadro completo dei geni che abbiamo ottenuto sembrava correlare bene con il danno da bilirubina che ha evidenziato una compromissione dello sviluppo cerebrale. I nostri dati rappresentano un valido contributo nella migliore comprensione dei meccanismi biomolecolari che causano la tossicità da bilirubina, ma possono anche aprire nuove strade a strategie terapeutiche che vedono la possibilità di testare le proprietà neuroprotettive di farmaci che regolano l'acetilazione istonica.

TABLE OF CONTENTS

TABLE OF CONTENTS	V
LIST OF FIGURES	VII
LIST OF TABLES	IX
ABBREVIATIONS	X
1 INTRODUCTION.....	1
1.1 BILIRUBIN	1
1.1.1 <i>BILIRUBIN METABOLISM</i>	1
1.1.2 <i>CLINICAL ASPECTS OF BILIRUBIN NEUROTOXIC PROPERTIES</i>	4
1.1.3 <i>DISORDERS OF BILIRUBIN METABOLISM</i>	5
1.1.3.1 NEONATAL JAUNDICE	5
1.1.3.2 BILIRUBIN ENCEPHALOPATHY AND KERNICTERUS	6
1.1.3.3 CRIGLER-NAJJAR SYNDROME.....	7
1.1.3.4 GILBERT'S SYNDROME.....	8
1.1.4 <i>PREVENTION AND TREATMENT OF SEVERE HYPERBILIRUBINEMIA</i>	9
1.1.4.1 PHOTOTHERAPY	9
1.1.4.2 EXCHANGE TRANSFUSION	10
1.1.4.3 PHARMACOLOGICAL STRATEGIES	10
1.1.5 <i>ANIMAL MODELS FOR HYPERBILIRUBINEMIA</i>	11
1.1.6 <i>MOLECULAR BASIS OF BILIRUBIN NEUROTOXICITY</i>	13
1.2 EPIGENETICS.....	16
1.2.1 <i>HISTONE ACETYLTATION</i>	19
1.2.2 <i>HISTONE ACETYLTATION IN NEUROPATHOLOGIES AND NEW THERAPEUTIC PERSPECTIVES</i> ..	21
2 AIMS	25
3 MATERIALS AND METHODS	26
3.1 EXPERIMENTAL PLAN	26
3.2 ANIMAL MODEL AND BRAIN REGIONS DISSECTION	26
3.3 GENOTYPING.....	28
3.4 TOTAL SERUM BILIRUBIN DETERMINATION	29
3.5 TOTAL PROTEIN EXTRACTION AND WESTERN BLOT.....	30
3.6 CHROMATIN IMMUNOPRECIPITATION ASSAY.....	31
3.6.1 <i>WESTERN BLOT FOR ChIP CONTROL</i>	32
3.6.2 <i>RT-qPCR FOR ChIP CONTROL</i>	33
3.7 CHIP-SEQ.....	34
3.7.1 <i>DNA Library Preparation</i>	34
3.7.2 <i>Libraries Denaturation and Dilution</i>	36

3.8	COMPARATIVE ANALYSIS OF THE DNA SEQUENCES OF JJ AND CONTROLS	36
3.9	VALIDATION OF SELECTED GENES	37
3.9.1	RNA EXTRACTION AND RETROTRANSCRIPTION.....	37
3.9.2	RT-qPCR.....	38
3.10	HISTOLOGY.....	40
3.10.1	HEMATOXYLIN – EOSIN.....	40
3.10.2	CRESYL VIOLET STAINING (NISSL STAINING).....	41
3.11	STATISTICAL ANALYSIS.....	41
4	RESULTS	42
4.1	CHARACTERIZATION OF THE ANIMAL MODEL.....	42
4.1.1	TOTAL SERUM BILIRUBIN MEASUREMENT.....	42
4.1.2	CEREBELLAR GROWTH EVALUATION.....	44
4.2	HISTONE H3 ACETYLATION.....	45
4.3	CHIP ASSAY.....	50
4.4	COMPARATIVE ANALYSIS OF THE DNA SEQUENCES OF JJ AND CONTROLS	53
4.5	HISTOLOGICAL ANALYSIS	62
5	DISCUSSION AND CONCLUSION.....	69
6	BIBLIOGRAPHY	74
7	PUBLICATIONS	94
7.1	PEER REVIEWED PAPERS.....	94
7.2	POSTER PRESENTATIONS AND ABSTRACTS.....	94
8	ACKNOWLEDGMENTS.....	97

LIST OF FIGURES

FIGURE 1-1. HEME DEGRADATION AND BILIRUBIN PRODUCTION.	2
FIGURE 1-2. BILIRUBIN TRANSPORTATION ACROSS THE HEPATOCYTE.	4
FIGURE 1-3. JAUNDICE AND KERNICTERUS IN NEWBORNS.	7
FIGURE 1-4. GUNN RATS AND BRAIN COMPARISON BETWEEN JJ AND JJ/JJ.	13
FIGURE 1-5. MECHANISMS INVOLVED IN CHROMATIN MODIFICATION.	17
FIGURE 1-6. STRUCTURE OF THE NUCLEOSOME CORE AT 1.9 Å RESOLUTION.	18
FIGURE 1-7. TRANSCRIPTIONAL ACTIVATION BY HISTONE ACETYLATION.	20
FIGURE 1-8. EFFECT OF HDAC INHIBITORS ON CHROMATIN OPENING AND TRANSCRIPTION ACTIVATION.	24
FIGURE 3-1. BRAIN FROM P9 JJ RAT, DORSAL VIEW, AND DISSECTION PROCEDURE.	27
FIGURE 3-2. DNA LIBRARY PREPARATION FLOWCHART.	35
FIGURE 3-3. ILLUMINA® MISEQ® SYSTEM (FIGURE TAKEN FROM THE BROCHURE OF THE MACHINERY).	36
FIGURE 4-1. COMPARISON OF TSB IN DIFFERENT GUNN RAT GENOTYPES AT 4 POST-NATAL AGES.	43
FIGURE 4-2. REPRESENTATIVE GENOTYPING RESULTS IN JJ, JJ, AND JJ GUNN RATS.	43
FIGURE 4-3. COMPARISON OF CEREBELLUM WEIGHT IN DIFFERENT GUNN RAT GENOTYPES AT 4 POST-NATAL AGES.	44
FIGURE 4-4. CONTROL OF THE SPECIFICITY OF THE ANTI-H3K14AC ANTIBODY IN RAT BRAIN.	45
FIGURE 4-5. H3K14AC IN THE BRAIN OF THE 2-DAYS OLD JJ GUNN RAT.	46
FIGURE 4-6. H3K14AC IN THE BRAIN OF 9-DAYS OLD GUNN RATS.	47
FIGURE 4-7. H3K14AC IN THE BRAIN OF 17-DAYS OLD GUNN RATS.	48
FIGURE 4-8. H3K14AC IN THE BRAIN OF OLDER (>P60) GUNN RATS.	49
FIGURE 4-9. EVALUATION OF CHROMATIN SHEARING CONDITIONS.	51
FIGURE 4-10. WESTERN BLOT CONTROL FOR THE SUCCESS OF CHIP.	52
FIGURE 4-11. RT-QPCR CONTROL FOR THE SUCCESS OF CHIP.	53
FIGURE 4-12. PEAK ANNOTATION OF THE JJ COMPARED TO THE CONTROL.	54
FIGURE 4-13. PEAK ANNOTATION OF THE CONTROL COMPARED TO THE JJ RAT.	55
FIGURE 4-14. GENE ONTOLOGY ANALYSIS IN JJ VS. CONTROL.	56
FIGURE 4-15. GENE ONTOLOGY ANALYSIS IN JJ VS. CONTROL.	57
FIGURE 4-16. GENE ONTOLOGY ANALYSIS IN CONTROL VS. JJ.	58
FIGURE 4-17. GENE ONTOLOGY ANALYSIS IN CONTROL VS. JJ.	59

FIGURE 4-18. GENE ONTOLOGY ANALYSIS IN CONTROL VS. JJ.....	60
FIGURE 4-19. GENE ONTOLOGY ANALYSIS IN CONTROL VS. JJ.....	61
FIGURE 4-20. VIEW OF CEREBELLUM (CLL) SLICES.....	63
FIGURE 4-21. VIEW OF FRONTAL CEREBRAL CORTEX (CX) SLICES.	64
FIGURE 4-22. VIEW OF CEREBRAL CORTEX (CX) OVER THE HIPPOCAMPUS SLICES.....	65
FIGURE 4-23. VIEW OF HIPPOCAMPUS (HIP) SLICES.	66
FIGURE 4-24. VIEW OF INFERIOR COLLICULI (IC) SLICES.	67
FIGURE 4-25. VIEW OF SUPERIOR COLLICULI (SC) SLICES.....	68

LIST OF TABLES

TABLE 3-1. PCR PARAMETERS FOR THE AMPLIFICATION OF THE UGT1A1 GENE.....	28
TABLE 3-2. RT-QPCR PARAMETERS FOR THE AMPLIFICATION OF THE GENOMIC SEQUENCE OF INTEREST.....	33
TABLE 3-3. PRIMER SEQUENCES DESIGNED FOR THE ANALYSIS.....	33
TABLE 3-4. PCR ENRICHMENT OF ADAPTOR-LIGATED DNA PARAMETERS.....	35
TABLE 3-5. PRIMER SEQUENCES DESIGNED FOR THE ANALYSIS.....	38
TABLE 3-6. RT-QPCR PARAMETERS FOR THE AMPLIFICATION OF THE GENOMIC SEQUENCE OF INTEREST.....	39

ABBREVIATIONS

BVR: biliverdin reductase
TSB: total serum bilirubin
CB: conjugated bilirubin
UCB: unconjugated bilirubin
Bf: free bilirubin
UGT: uridine diphosphoglucuronate glucuronosyltransferase
CNS: central nervous system
BIND: bilirubin-induced neurological dysfunction
ABE: acute bilirubin encephalopathy
CN: Crigler-Najjar
BG: bilirubin glucuronide
GPc: globus pallidus pars externa
GPi: globus pallidus pars interna
STN: subthalamic nucleus
EGL: external granular layer
ML: molecular layer
IGL: internal granular layer
PTM: post-translational modification
HAT: histone acetyl-transferase
HDAC: histone deacetylase
H3K14ac: acetyl histone H3 (lys14)
LINE: long interspersed nuclear element
TSS: Transcriptional Start Site
TTS: Transcriptional Termination Site
UTR: Un-Translated Region

*“Non quia difficilia sunt non audemus,
sed quia non audemus difficilia sunt.”*

L. A. Seneca

1 INTRODUCTION

1.1 BILIRUBIN

Bilirubin (from Latin “*bile*” = bile and “*ruber*” = red) is a yellow pigment characterized by an open chain of four pyrrole-like rings (tetrapyrrole), derived from the porphyrin family of molecules, and it results from the enzymatic conversion of heme and hemoglobin. Despite the hypothesized antioxidant role of bilirubin observed in adults with mild levels of bilirubin without any kind of liver disease (Gilbert’s syndrome), high levels of bilirubin in newborn could compromise central nervous system leading to permanent disabilities or, at worst, death.

1.1.1 BILIRUBIN METABOLISM

Bilirubin produced in humans mostly derives from the degradation of erythrocyte hemoglobin in the spleen (80%), from the turnover of myoglobin, cytochromes and other hemoproteins (15-20%), and from the breakdown of immature red blood cells in the bone marrow^{1,2}. A healthy adult human produces 250-400 mg of bilirubin per day².

In the first step, heme group is broken in carbon monoxide (CO), ferrous iron (Fe²⁺) and biliverdin by the heme oxygenase-1 (HO-1) enzyme, consuming nicotinamide-adenine dinucleotide phosphate (NADPH) as reducing agent and three molecules of oxygen (O₂). Subsequently, biliverdin is converted to bilirubin by the cytosolic biliverdin reductase enzyme (BVR), in the presence of NADPH^{3,4}.

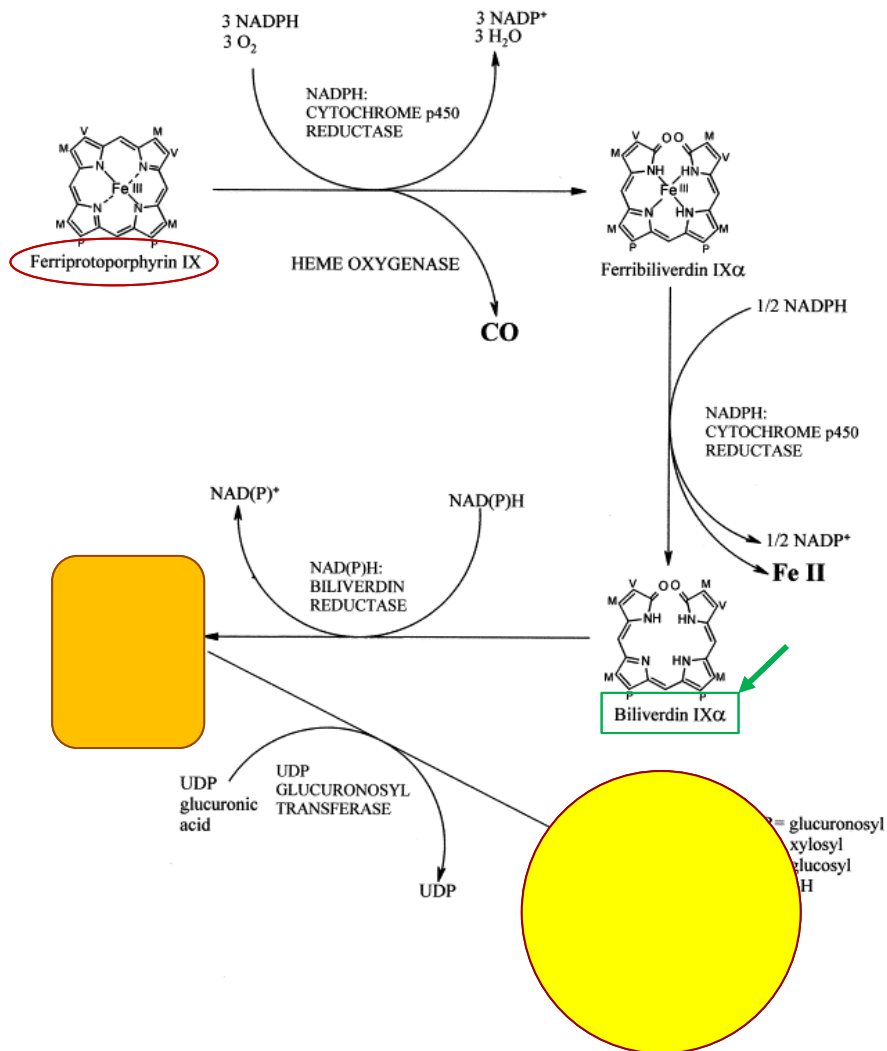


Figure 1-1. Heme degradation and bilirubin production.

Hemoglobin is converted to biliverdin by heme oxygenase. Subsequent conversion of biliverdin in unconjugated bilirubin by biliverdin reductase. Unconjugated bilirubin is transformed in conjugated bilirubin by UDP-glucuronosyl transferase enzyme (modified from Ryter et al., 2000⁵).

The bilirubin detectable in blood by clinically available measurement techniques is the total serum bilirubin (TSB), both conjugated, or direct bilirubin (CB), and unconjugated or indirect (UCB).

Due to its hydrophobic nature, almost all UCB is tightly but reversibly bound to albumin in adults ⁶ and α -fetoprotein in newborns, to be targeted to the liver ⁷. Only less than 0.1% of the UCB is not bound to albumin and it is named free bilirubin (Bf) ⁸. This small portion of lipophilic bilirubin is able to passively diffuse through membranes and accumulate inside all tissues ⁹.

In the liver, UCB can be converted into more soluble products prior to being secreted in bile ¹⁰ through the glucuronidation process. Once in the proximity of the liver, UCB is able to enter the hepatocyte via passive diffusion ⁷ and/or transporters ^{11,12}. At the sinusoidal membrane, UCB dissociates from albumin, it is internalized and transferred to the endoplasmic reticulum (ER) where it is conjugated with one/two molecules of glucuronic acid by the uridine diphosphoglucuronate glucuronosyltransferase enzyme (UGT1A1) ¹³.

CB, in the form of mono and diglucuronides ^{14,15}, is secreted into the bile canaliculus by the ATP-dependent transporter multidrug resistance-associated protein MRP2 ¹⁶. A fraction of intracellular CB not excreted into bile is transferred back to the blood by the sinusoidal transporters MRP3 (ABCC3: ATP-binding cassette transporter 3) and reabsorbed in downstream hepatocytes via OATP1B1 and OATP1B3 transporters (organic anion-transporting polypeptide). This is a liver-blood shuttling loop for bilirubin glucuronide crucial to prevent saturation of biliary excretion ^{17,18}.

CB excreted in bile passes the small intestine and reaches the colon, in which the glucuronic acid is removed by intestinal bacteria, and the resulting bilirubin is converted to urobilinogen, oxidized to stercobilin and excreted by feces. Some of the urobilinogen is reabsorbed by the enterohepatic circulation and transferred to the kidney, in which it is transformed in urobilin and excreted by urine ^{19,20}.

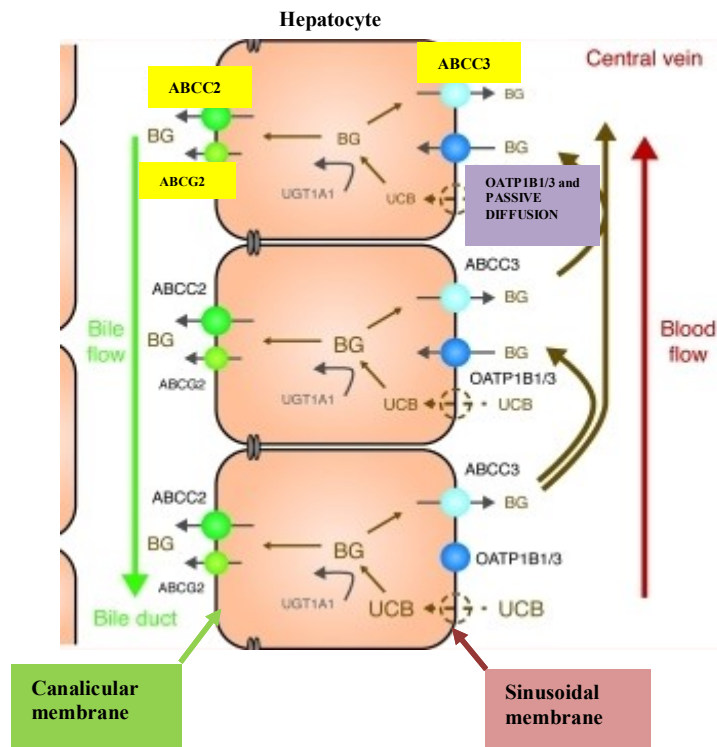


Figure 1-2. Bilirubin transportation across the hepatocyte.

Hepatocytes are organized between the portal tract and the bile duct. In this scheme of the hepatocyte, the localization of transporters across the plasma membrane is evidenced. Bilirubin enters the hepatocyte through passive diffusion or OATP transporters at the level of the sinusoidal membrane. Once UCB is converted in BG (bilirubin glucuronides), it is secreted into the bile duct through ABC transporters (modified from van de Steeg E. et al. 2012¹⁸).

1.1.2 CLINICAL ASPECTS OF BILIRUBIN NEUROTOXIC PROPERTIES

Bilirubin has a double-edged role in the body: antioxidant and protective on the one hand, whereas neurotoxic on the other hand, mostly depending on its concentration.

The toxic effect is typically manifested in newborn babies and it is supposed to be due to the interaction between the level and the duration of central nervous system (CNS) exposure to Bf²¹ and the molecular characteristics of the developing CNS^{22,23}. Only Bf is able to cross the

endothelial cells that form the Blood-Brain Interfaces (BBI) impairing the normal cellular function^{24,25}.

Neonatal jaundice has been noticed through the centuries, but the scientific description seems to have started in the last half of the 18th century.

In 1904, Schmorl presented the results of autopsies of 120 jaundiced babies and reported only six cases of a staining phenomenon of some brain areas, coining the term “kernicterus”, which refers to the intense yellow coloring of the basal ganglia and medulla oblongata²⁶. Due to this finding, the selective and observable deposition of bilirubin in specific brain regions has been considered the main cause of the bilirubin damage for several years.

Later, this concept was doubted²⁷. The experimental finding that the same bilirubin concentration was measured in different brain regions of the well-characterized animal model for hyperbilirubinemia (Gunn rat) supported the idea that the selective brain damage observed could be due to the different regional vulnerability to bilirubin toxicity^{28–30}, rather than to the preferential bilirubin deposition in the brain.

1.1.3 DISORDERS OF BILIRUBIN METABOLISM

Abnormalities in bilirubin metabolism (uptake from the circulation, intracellular binding, and storage, conjugation, biliary excretion) may result in hyperbilirubinemia, that can be divided into two types: unconjugated (indirect) or conjugated (direct).

In this work, I will describe only the unconjugated hyperbilirubinemia because it represents the main cause of bilirubin encephalopathies and the focus of this thesis.

1.1.3.1 NEONATAL JAUNDICE

Neonatal jaundice is a common and generally benign condition, affecting more than half of newborns, due to an abnormal elevation of circulating bilirubin in the transitional period after birth. The yellowish color of the skin and conjunctiva is a direct consequence of the increased levels of serum bilirubin, that reaches the peak at about 72 hours after birth (5-10 mg/dL) and

subsequently declines to normal adult levels in 7-10 days (≤ 1 mg/dL)³¹. Physiologic jaundice is determined by a combination of several events. Firstly, the increased bilirubin production is due to a shortened red blood cell lifespan and subsequent increased catabolism of hemoglobin into UCB. Then, the bilirubin disposal mechanisms located in the liver are immature in neonates: low hepatocellular transporter levels, as well as low activity of UGT enzyme, results in retention of UCB in babies³¹⁻³³. Moreover, the conversion of UCB into urobilinogen processed by intestinal bacteria is not yet active. This benign condition is usually resolved during the first week of life without any kind of treatment³⁴⁻³⁶.

Hemolytic conditions, inherited defects in conjugation, prematurity, as well as epidemiologic or environmental risk factors could additionally contribute to neonatal physiological jaundice. If hyperbilirubinemia is not properly diagnosed, supervised and possibly treated, it may progress in more severe complications producing a complex pattern of neurologic dysfunctions.

1.1.3.2 BILIRUBIN ENCEPHALOPATHY AND KERNICTERUS

The extent and pattern of neurological damage and sequelae is influenced by the amount and the duration of bilirubin neurotoxicity. In particular, two conditions of bilirubin encephalopathy, with several levels of severity, have been well characterized from the clinical point of view: acute and chronic³⁶.

Less severe hyperbilirubinemia can produce subtle encephalopathy, or bilirubin-induced neurological dysfunction (BIND). Typical disabilities without classical findings of kernicterus are movement disorders, isolated hearing loss and auditory dysfunction (AN auditory neuropathy; AD: auditory dys-synchrony) that could be associated with cognitive dysfunction³⁶.

Acute bilirubin encephalopathy (ABE) includes abnormalities of tone (hypotonia and/or hypertonia), decreased feeding, lethargy, high-pitched cry. Fever and seizures may occur, at worst death³⁶.

Chronic bilirubin encephalopathy, also called kernicterus, is characterized by a tetrad of 1) abnormal motor control, movements and muscle tone 2) auditory processing disturbance with or without hearing loss, 3) oculomotor impairments (upward vertical gaze), 4) dysplasia of the enamel of deciduous (baby) teeth. Selective damage of the globus pallidus pars externa (GPe) and

interna (GPi), substantia nigra reticulata, subthalamic nucleus (STN), brainstem auditory, vestibular, and oculomotor nuclei, hippocampus, cerebellum, was reported. Movement disorders are caused by the selective lesions in the basal ganglia. Abnormal tone and coordination may also correspond to lesions of the cerebellum and specific brainstem nuclei involved with truncal tone and vestibular function. Lesions of the auditory brainstem nuclei lead to auditory processing disorders, hearing loss/deafness ³⁶.

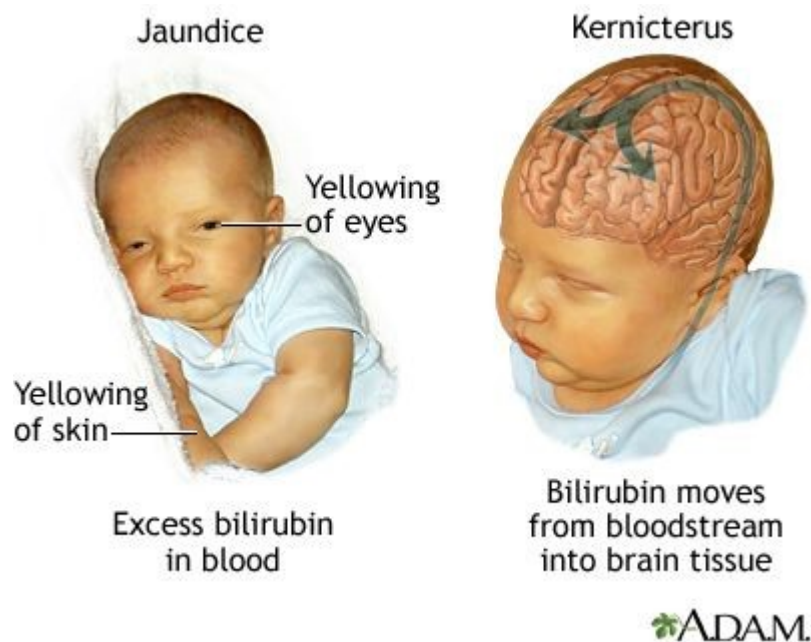


Figure 1-3. Jaundice and Kernicterus in newborns.

Neonatal jaundice is a physiological condition characterized by excess bilirubin in blood that is easily detectable because of the yellow color of the skin and the eyes. Bilirubin can reach the brain passing the blood-brain barrier and lead to a more severe condition, named kernicterus. (ADAM encyclopedia).

1.1.3.3 CRIGLER-NAJJAR SYNDROME

Crigler-Najjar syndrome types I (CN1) and II (CN2) are rare, inherited autosomal recessive diseases that are characterized by lifelong non-hemolytic unconjugated hyperbilirubinemia ³⁷. The risk of developing severe neurologic complications, such as movement and hearing impairments, and mental retardation, is high in patients with CN syndrome. Treatments are aimed at reduction

of serum bilirubin levels. Phototherapy is the routine treatment, but it becomes less effective after puberty because of skin thickening, pigmentation, and decreased surface area in relation to body mass. Plasmapheresis during a crisis is another possibility, but orthotopic liver transplantation is surely the only curative therapy³⁸. Gene therapy methods could be a promising solution: the correction of hyperbilirubinemia by the injection of a vector expressing the corrected human UGT1a1 was reported in Gunn rats³⁹ and also in hyperbilirubinemic mice model^{40,41}.

High serum levels of UCB are due to the partial or complete absence of the enzyme uridine diphosphate-glucuronosyltransferase 1 (UGT1A1), located in the liver and responsible of the bilirubin glucuronidation. The UGT1A1 is encoded by the UGT1a1 gene, which contains five consecutive exons located at the 3' end of the UGT1A locus on chromosome 2q37. Point mutations of the gene UGT1a1 are the basis of differences in CN syndrome. While CN1 results from genetic changes that cause premature truncation or critical amino acid residue substitution, CN2 is caused by substitution of single amino acid residues that markedly reduce, but do not abolish, the catalytic enzyme activity^{42,43}. Therefore, the level of serum bilirubin is different in CN1 and CN2: higher in the first syndrome (20-25 mg/dL, until 50 mg/dL during fasting or intercurrent illness), lower in the second (7-20 mg/dL, until 40 mg/dL during fasting or intercurrent illness), resulting in less severe complications. In CN2, phenobarbital administration is able to reduce over 25% serum bilirubin level^{42,44}.

1.1.3.4 GILBERT'S SYNDROME

Other names for Gilbert's syndrome are "constitutional hepatic dysfunction" or "familial nonhemolytic jaundice"⁴⁵. This condition is characterized by mild, chronic, and unconjugated hyperbilirubinemia in absence of hemolysis or any other liver diseases. The hepatic-UGT activity reduction leads to increase of serum bilirubin level up to 3 mg/dL or higher during fasting or intercurrent illness⁴⁶.

This syndrome is due to the TA insertion within dinucleotide repeat in the promoter region of UGT1a1 gene. The normal TATAA element sequence is A(TA)₆TAA, whereas in Gilbert syndrome the sequence is A(TA)₇TAA. The variant TATAA element reduces the expression of the structurally normal enzyme⁴⁷.

Gilbert's syndrome is considered innocuous, so no treatment is required, but its diagnosis is important to avoid confusion with other hepatobiliary disorders leading to hepatic injury.

1.1.4 PREVENTION AND TREATMENT OF SEVERE HYPERBILIRUBINEMIA

The clinical practice guidelines reported by the AAP (American Academy of Pediatrics) Subcommittee on Hyperbilirubinemia (2004) for the management of jaundice were addressed to reduce the incidence of severe hyperbilirubinemia and bilirubin encephalopathy in newborns^{48,49}. The main purposes of these guidelines are:

- development of newborn nursery protocol for identification, evaluation, and management of hyperbilirubinemia in the hospital;
- measurement of the total serum bilirubin (TSB) in the first 24 hours;
- provide information about newborn jaundice to parents;
- supply indications for the use of phototherapy, exchange transfusion and newer pharmacologic therapies^{48,49}.

1.1.4.1 PHOTOTHERAPY

Phototherapy represents the conventional treatment for hyperbilirubinemia and its aim is to reduce UCB concentration to non-toxic levels, preventing its deposition into the brain tissue. It was firstly introduced by Cremer and colleagues in 1958⁵⁰. The principle of action is based on the capacity of the blue-green light with a wavelength around 400-520 nm to photo-oxidize the hydrophobic UCB to more polar isomers that can be easily excreted in the urine and stool⁵¹.

The efficacy of phototherapy is determined by some relevant aspects: the wavelength range, the intensity of the light and the body surface exposed to the light⁵².

Rare side effects of phototherapy were observed: development of allergic diseases, impairment of thermoregulation, retinal impairments, dehydration are few examples⁵³. Considering that bilirubin neurotoxicity is principally due to the bilirubin portion not bound to

albumin (Bf) and poor information was collected about the potential toxicity of bilirubin breakdown products, a recent study conducted by Jasprova and colleagues demonstrated that bilirubin photoisomers not only don't interfere in bilirubin-albumin interaction but also in cell viability⁵⁴.

1.1.4.2 EXCHANGE TRANSFUSION

Exchange transfusion is recommended in infants with very severe unconjugated hyperbilirubinemia (serum bilirubin level of 20 mg/dL or higher) and the risk to develop acute bilirubin encephalopathy, with insufficient response to phototherapy. With this very invasive treatment, hyperbilirubinemic blood is removed and replaced with fresh non-jaundiced blood, also providing fresh albumin with binding sites for bilirubin⁵⁵. Adverse events such as cardiac arrest, coagulopathies, thrombosis are frequent and the mortality rate is high (03-2.0%)⁵⁶.

1.1.4.3 PHARMACOLOGICAL STRATEGIES

Alternative treatment strategies have concentrated on pharmacological approaches⁵⁷ with the aim of decreasing the production of UCB, increasing the hepatic clearance of UCB, interrupting the enterohepatic circulation of UCB.

UCB production can be decreased using two inhibitors of HO activity: metalloporphyrins⁵⁸, a synthetic heme analog in which other metals replace the central iron atom of heme, or D-penicillamine, a chelating agent⁵⁹. Both these drugs need further clinical investigation regarding safety and efficacy, before routine clinical use.

Increasing UCB conjugation could be a possible strategy to reduce plasma UCB levels. Phenobarbital is an anti-epileptic drug that is able to enhance UCB clearance and conjugation by activating the phenobarbital enhancer module in the promoter sequence of UGT1a1⁶⁰. It has been used to treat neonatal jaundice due to several reasons since 1960, and it is also useful to distinguish between type I and type II Crigler-Najjar syndrome because in the first case it is not effective.

Intravenous immune globulin (IVIG): reduces jaundice in many cases of neonatal isoimmunization. Recommended doses are 500 mg/Kg bodyweight of human virus inactivated

IVIG, infused over a 2-hour period. The risk for not responding to IVIG administration if bilirubin rate rises ≥ 1 mg/dL/h ^{61,62}.

Pharmacologic agents that provide neuroprotection by directly targeting the adverse effects of unconjugated bilirubin in the CNS are attractive options. Minocycline is a semi-synthetic second-generation tetracycline that seems to have protective effects. While it contrasts apoptosis, inflammation, and excitotoxicity *in vitro*, instead it prevents bilirubin-induced cerebellar hypoplasia and auditory dysfunction in Gunn rats ^{63,64}. Unfortunately, the use of this drug presents relevant side effect on developing bone and dentition.

1.1.5 ANIMAL MODELS FOR HYPERBILIRUBINEMIA

In 1938, Gunn Charles Kenneth published an important paper in *The journal of Heredity* ⁶⁵, describing a genetic mutation in the Wistar rat strain (*Rattus norvegicus*) that results in an autosomal recessive hereditary non-hemolytic unconjugated hyperbilirubinemia. The mutant rats have been named Gunn rats (commercial name: Hds Blue:Gunn-UDPGT) after their discoverer.

The abnormal increased amount of bilirubin pigment is due to the absence of bilirubin glucuronidation activity in the liver caused by the Ugt1a single-base deletion frameshift mutation that results in inactive bilirubin-conjugating enzyme UDP-glucuronyltransferase ⁶⁶, causing jaundice, represented by the “j” in the name of the strain. The enzyme defect is one of the mutations present in the human Crigler-Najjar type I syndrome ⁶⁷.

These animals are normal at birth and become jaundiced within 24 hours. Serum bilirubin levels continue to rise in hyperbilirubinemic (jj) newborn until about 15 mg/dL during the first two weeks of life and decline to adult levels (around 6 mg/dL) after approximately 30 days ^{68,69}. In contrast, homozygous (JJ) or heterozygous (Jj) non-hyperbilirubinemic animals do not show abnormalities, having identical bilirubin levels of about 0.20 mg/dL.

Colonies of Gunn rats are maintained throughout the world, with varied breeding practices fostering the development of distinct subpopulations of Gunn rats ⁷⁰. Besides the total bilirubin concentration, hyperbilirubinemic animals present some recurrent phenotypic characteristics, even if relevant differences could occur in some subpopulations more than in others. Symptoms such as lag growth ⁷¹, neurological difficulties like occasional ataxia, wobbly gait or partial paralysis of

the hind limbs, different mortality rate were observed decades ago^{70,72,73}. By the time, the Gunn rats have been changed showing a decrease in the severity of the phenotype, even if the most important typical features, the high level of UCB and the cerebellar hypoplasia, have been well preserved. For this reason, Gunn rat remains one of the most representative animal models for the study of hyperbilirubinemia.

As previously mentioned, a part high level of serum UCB, another important hallmark is the brain selective impairment, especially the marked cerebellar hypoplasia^{28,74-76}. Since the rat cerebellum is known to undergo to a complex and intensive developmental activity, especially after birth⁷⁷, cerebellar hypoplasia could be the result of a combination of the postnatal cerebellar neurogenesis and the action of bilirubin. The first abnormalities in the cerebellum were found over the age of 3 days after birth⁷⁸, but the critical period for bilirubin-induced cerebellar hypoplasia was identified 6-10 days after birth^{28,73,75}.

Both total cerebellar volume and growth of cerebellar vermis and lobules, especially the anterior, are significantly reduced in jj animals if compared to non-hyperbilirubinemic controls.

Histological investigations showed a marked alteration of cerebellar layer architecture: external granular layer (EGL), molecular layer (ML) and internal granular layer (IGL) are thinner, presenting a lower cell density, depending on the age considered. Purkinje cells are the most degenerated in terms of density and structure: the most striking histological feature are cytoplasmic alterations, such as vacuolation of Golgi vesicles or cisternae and dilated endoplasmic reticulum^{74-76,79}. Also, the Purkinje cell layer appears extremely disorganized, being buried in the internal cell layer. Synaptogenesis and myelination are also reported to be compromised^{76,80}. A study performed in our lab both *in vivo* and *in vitro* showed that the typical cerebellar hypoplasia of the Gunn rat might be in part due to the cell cycle perturbation and the enhancement of apoptosis triggered by the high level of UCB⁷⁹.

Despite the selective deposition of bilirubin in the brain has been considered for several years the main cause of regional damage observed in the brain, findings from different studies on Gunn rat revealed that there was no significant differences in the bilirubin concentrations between brain regions²⁸⁻³⁰. Thus, the reasons for the brain regions selective intrinsic vulnerability need to be further explored.

Later on, the hyperbilirubinemic model has been recreated in the mouse. Some research groups focused on the examination of the physiological importance of the UGT1A1 in the

metabolism of bilirubin and produced genetically engineered mice in which the UGT1A1 enzyme is inactive. One knockout mouse for UGT1 (UGT1^{-/-}) was developed by Nguyen and colleagues, inserting a NEO cassette that produced the complete interruption of the exon 4 of the UGT1 gene cluster⁸¹. Another mouse model was generated some years later by the introduction of a 1-base deletion in UGT1 exon 4 that produced an in-frame premature stop codon, generating a truncated and inactive form of the protein⁴⁰. Despite the same high TSB level and cerebellar impairment, the phenotype of the mice model is more severe than that observed in Gunn rat: stronger brain damage due to UCB results in death within two weeks after birth.



Figure 1-4. Gunn rats and brain comparison between jj and JJ/Jj.

(A) Gunn rat 2 days after birth. To be noticed, the difference in skin color that allow the recognition of the hyperbilirubinemic animals (jj) on the left and the non-hyperbilirubinemic ones, both wild type (JJ) and heterozygous (Jj), on the right. (B) The brain of Gunn rat are macroscopically characterized by differences in color and in the cerebellum size: on the left brain of hyperbilirubinemic rat (jj) with evident cerebellar hypoplasia, on the right brain of non-hyperbilirubinemic animal.

1.1.6 MOLECULAR BASIS OF BILIRUBIN NEUROTOXICITY

Bilirubin toxicity for the central nervous system has been widely studied for decades all over the world *in vitro*, *ex vivo*, and *in vivo*. Although progress has been reached in clarifying the principal causes of bilirubin-induced encephalopathy, the complete sequence of molecular events that produce brain damage is not fully understood.

Bilirubin has been reported to be selectively neurotoxic both for specific brain region and cell types^{23,82–84}, due to different bilirubin exposure and cell sensitivity to injury⁸⁵.

Neurons are the most sensitive cells to UCB attack. Macroscopical changes, such as reduction of dendrites and axons arborization as well as reduction of dendritic spines and synapses have been observed ^{80,86–88}.

Besides neurons, other cell types have been reported to be responsive to UCB action. Microglia ^{89,90} and astrocytes ⁹¹ secrete inflammatory mediators and glutamate to contrast the bilirubin-induced neurotoxicity. The inflammatory, excitotoxic and oxidative stress response to UCB insult have been confirmed in recent works using organotypic cultures ^{23,92}.

Typical lipidic nature of plasma membrane, especially myelin-rich membrane ^{80,93,94}, allows bilirubin to enter the cells diffusing spontaneously through the phospholipidic bilayer perturbing its permeability and physiology ^{95,96}. Increased UCB concentration was also reported to compromise oligodendrocyte maturation and myelination ⁹⁷.

The activation of complex signal cascades culminates to survival or death processes. Examples of the processes modulated by UCB are the following: cell cycle perturbation ⁷⁹, oxidative stress activation ^{83,98,99} and antioxidant response ¹⁰⁰, excitotoxicity ^{101–103}, apoptosis pathway activation ^{84,104}, inflammation ^{84,91}.

Bilirubin can also modulate potential protection/adaptation mechanisms against its toxicity for the brain. The real efficiency on adaptation and protection mechanisms against bilirubin toxicity is still difficult to understand and evaluate. Examples are: transporters at the level of BBI that seem to be responsible for bilirubin efflux from the brain ^{105,106}, detoxification mechanisms involving the glutathione S-transferase (GSTs) enzymes ^{68,107}, and bilirubin oxidation by “bilirubin oxidase” that belongs to the cytochromes P450 family ^{27,30,108}.

All the processes mentioned above are characterized by the modulation of a wide range of genes and proteins.

Two interesting studies, conducted on SH-SY5Y neuroblastoma cell line, showed that UCB induces the expression of proteins implicated in cell proliferation, intracellular trafficking, protein degradation and oxidative stress response ¹⁰⁹, as well as the significant upregulation of around 230 genes after 24 hours of treatment with 140 nM Bf, based on a False Discovery Rate (FDR) of about 10% ¹¹⁰.

Several studies that aimed to deepen specific pathways triggered by UCB reported the modulation of the mRNA expression of genes involved in.

The cell cycle perturbation was accompanied by the modulation of cyclins and cyclin-dependent kinase 2⁷⁹.

The oxidative stress of the endoplasmic reticulum was counteracted by the activation of the antioxidant Nrf2 pathway, with a subsequent up-regulation of cytoprotective genes that mediate cell survival (*xCT*, *GLY1*, *γGCL-m*, *γGCL-c*, *HO-1*, *NQO1*, *FTH*, *ME1*, *ATF3*)¹⁰⁰. Another marker of oxidative stress (*SRXNI*) was also up-regulated. Alteration of oxidative stress was also demonstrated in other studies^{5,99,103,111,112}.

Apoptosis was mediated by the activation of pro-apoptotic *CHOP*⁸⁴. The activation of the apoptotic process was confirmed also in other works^{102,104}.

Inflammation markers, such as *Il1β*, *Il6*, *Cox2*, *Il8*, *TNFα*, resulted to be increased^{23,84}. The role of bilirubin in triggering the inflammation pathways was reported also in other proteomic studies^{89,97,113}.

Bilirubin oxidation by cytochrome P450 family of enzymes was probably driven by the activation of the transcription of *Cyp1a1* and *Cyp1a2*^{30,108}.

mRNA of the *Mrp1* bilirubin transporter, located at the level of the blood-brain-interfaces, was reported to be enhanced¹⁰⁶.

The detoxification mechanism determined by the activation of the glutathione enzyme was also induced by the up-regulation of mRNA encoding Na⁺-independent cysteine:glutamate exchanger System Xc⁻ (*SLC7A11* and *SLC3A2* genes)¹⁰⁷. Another work not already published conducted in our lab showed the modulation of other relevant genes linked to the glutathione system (*Gsta2*, *Gsta3*, *Gstm3*, *Gstm4*, *Gstmπ*).

The impairment of the oligodendrocytes myelination process was combined with the modulation of the mRNA levels of two markers of oligodendrocytes differentiation (*Olig1* and *Olig2*)⁹⁷.

These intricate interacting pathways, that are also characterized by significant modulation of gene expression, suggest that mechanisms that have a crucial role in the regulation of gene expression, such as epigenetic mechanisms, should have a strong impact in unconjugated bilirubin toxicity.

1.2 EPIGENETICS

The term “epigenetics”, coined by the developmental biologist Conrad H. Waddington during the mid-twentieth century, was derived from the Greek word “*epigenesis*” that literally means “in addition to changes in genetic sequence”¹¹⁴. During the 1990s growing interests on epigenetics lead to an evolution of this term, that started to include any process that program genes to be differentially expressed in different context, altering gene function without changing the DNA sequence, and leads to modifications that can be transmitted to daughter cells^{115,116}.

Epigenetic processes are involved in the regulation of gene expression in many physiological processes, and epigenetic aberrations often contribute essentially to the onset and progression of human diseases, such as cancer, neurological disorders, inflammatory diseases and viral infections, via the loss or gain of function of epigenetic regulatory proteins¹¹⁷.

Many types of epigenetic processes have been identified, such as chemical modifications at the level of nucleotides (DNA methylation and RNA interference (RNAi)), modifications at the level of histones (posttranslational modifications (PTMs) of histone proteins and histone variants), and nucleosome remodeling, (ATP-dependent processes that regulate the accessibility of nucleosomal DNA).

Most transcriptional regulatory events cause changes to chromatin structure and composition, which result from the recruitment of chromatin-modifying enzymes by transcription factors and by transcriptional machinery itself^{118,119}.

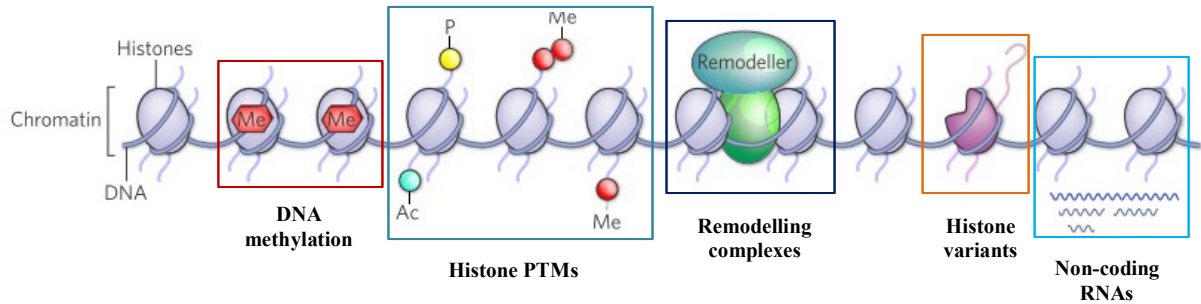


Figure 1-5. Mechanisms involved in chromatin modification.

DNA methylation, histone modification, remodeling by chromatin-remodelling complexes, insertion of histone variants, non-coding RNAs (ncRNAs). All are essential contributors to the development and cell-fate determination of tissues (modified from Dulac 2010¹²⁰).

Chromatin is the state in which DNA is packaged within the cell. The fundamental unit of chromatin is the nucleosome, a protein-DNA complex discovered in 1974. Each individual nucleosome consists of an octamer of the four globular core histones (H3, H4, H2A, H2B) around which 147 base pairs of DNA are wrapped. Each nucleosome core particle is separated from the next by a region of DNA linker about 80 nucleotide pairs long. The histone core has an NH₂-terminal amino acid “tail”, which protrudes out of the tight DNA-histone core^{121,122}.

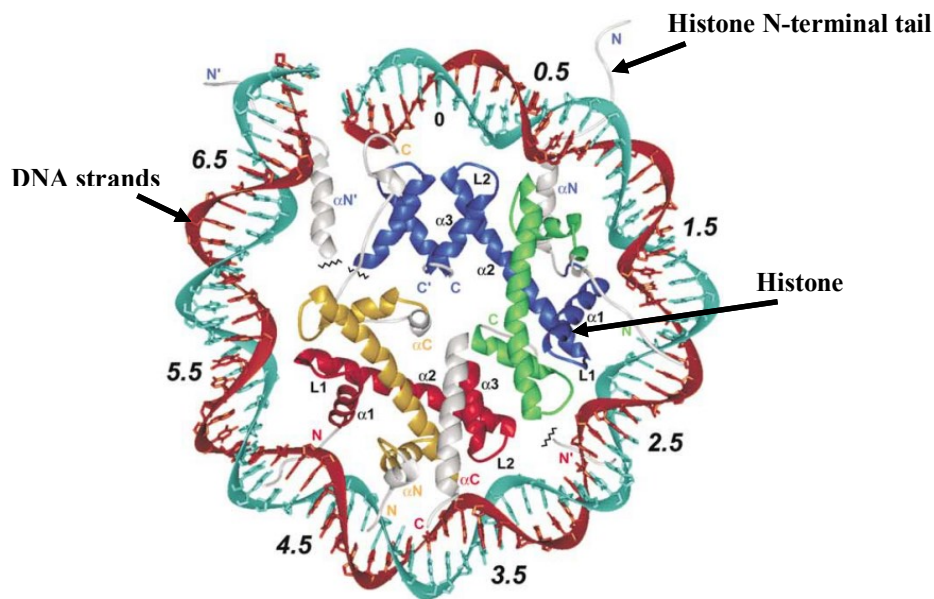


Figure 1-6. Structure of the nucleosome core at 1.9 Å resolution.

DNA strands are cyan and brown. The histone-fold domains of the histone proteins are blue for H3, green for H4, yellow for H2A and red for H2B. The histone-fold extensions and N-terminal tail regions are white (modified from Davey et al, 2002 ¹²²).

The NH₂-terminal tails are subjected to several covalent modifications, defined as post-translational modifications (PTMs), such as acetylation, methylation, phosphorylation, ubiquitination, and sumoylation. Due to their chemical properties, these epigenetic modifications can alter the condensation of the chromatin and the accessibility of the DNA to the transcriptional machinery ^{123,124}. The more condensed and “inaccessible” form of chromatin (heterochromatin) is converted in a less packed and more “accessible” chromatin (euchromatin), disrupting the contact between nucleosomes and DNA ^{118,119}. Thus, basic biological functions, i.e. transcription, replication and repair of DNA, are allowed thanks to the turning on or keeping off specific genes. The timing of the appearance of a modification depends on the signaling conditions within the cell.

1.2.1 HISTONE ACETYLATION

Histone acetylation has recently received great attention, especially in the nervous system^{116,120,125–131}, because of the knowledge of the enzymatic activity machinery and signal transduction mechanisms that regulate this post-translational modification, both in physiological and pathological conditions.

The acetylation and deacetylation of histones, occurring on lysine (K) residues located on the histone tails are dynamic processes, balanced in healthy conditions¹³². Two classes of functionally antagonistic enzymes, the histone acetyltransferases (HATs) and the histone deacetylases (HDACs), are responsible for the addition or removal of the acetate groups from acetyl coenzyme A (acetyl-CoA)¹³³. The acetyl group addition neutralizes the positive charge of the ϵ -amino group of the lysine, leading to a decreased affinity between the histone tail and the negatively charged DNA¹³⁴. The consequence of this is a remodeling of chromatin from a tightly packed configuration to a loosely packed configuration, which subsequently leads to transcriptional activation. Conversely, the removal of the acetyl groups may cause chromatin structure to condense and result in transcriptional silencing^{123,124,135–139}.

The pivotal role of histone acetylation in the activation of gene transcription is also determined by the fact that HAT complexes possess coactivator activity: they promote TATA-binding protein (TBP) or other general transcription factor association with the basal promoter. In fact, the acetylation is enriched at specific sites in the promoter and 5' end of the coding regions of genes that are ready to be transcribed¹²⁴.

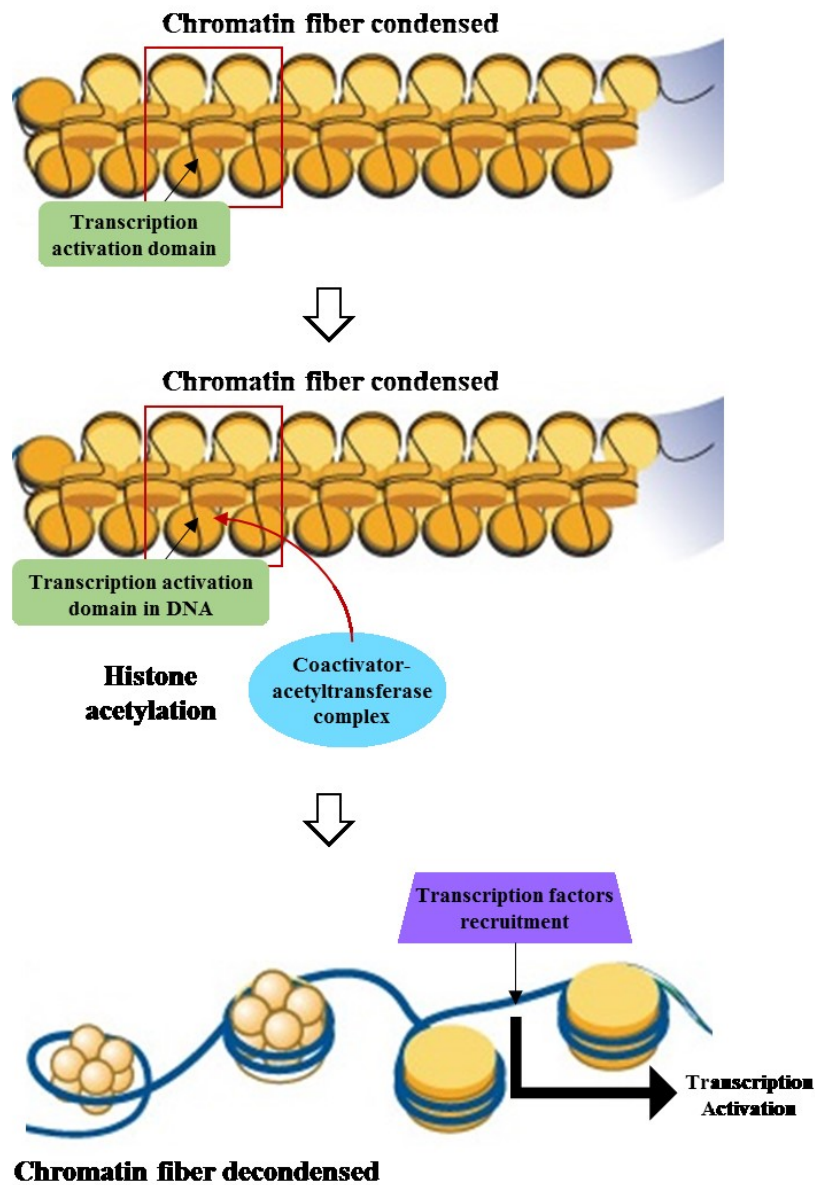


Figure 1-7. Transcriptional activation by histone acetylation.

The coactivator-acetyltransferase (HAT) complex (blue) is targeted by the DNA-binding transcription factors (green) to open the condensed and inactive chromatin. The HAT complex decondenses chromatin by acetylation of the histone tails, that starts to be transcriptionally active. The HAT complex also facilitates recruitment of the basal transcriptional machinery (violet) to the accessible promoter chromatin.

1.2.2 HISTONE ACETYLATION IN NEUROPATHOLOGIES AND NEW THERAPEUTIC PERSPECTIVES

The epigenetic regulation of gene expression plays an important modulatory role in many biological processes throughout the brain, such as development and differentiation, synaptic plasticity, learning, and memory, as well as the maintenance and survival of neurons^{116,128}.

The brain is one of the most heterogeneous tissues overall, thus the complexity of epigenetic modifications is further potentiated. Different brain regions respond differently to the same environmental challenge, as well as the same brain area, made up of the intricate interaction of different cell types, could be characterized by a heterogeneous epigenetic profile¹³⁰.

Over the past decade, epigenetic regulation has been widely explored and considered an integral part of a multitude of physiological brain function both in health and disease.

Aberrant epigenetic programs of gene expression in neurodevelopmental, psychiatric, neurodegenerative disorders have been described in several studies. In particular, histone acetylation was the most studied chromatin modification because of its relevant role in neuroplasticity^{120,126,129,140,141} and memory formation¹⁴². The deregulation of the HAT/HDAC balance, resulting in alterations of gene transcription and common cell damage mechanisms, including excitotoxicity, calcium overload, oxidative stress, acute inflammation, and apoptosis, has been implicated in several neurological disorders¹⁴³.

Examples of common neurological diseases in which this mechanism is unbalanced are Alzheimer's Disease (AD) and dementia^{142,144–146}, Autism Spectrum Disorder (ASD)^{147,148}, Multiple Sclerosis (MS)¹⁴⁹, Amyotrophic Lateral Sclerosis (ALS)¹⁵⁰, Parkinson's Disease (PD)^{151–153}, stroke and brain trauma^{143,154}.

Also, rare diseases were reported, such as Huntington's Disease (HD)^{155–157}, Friedreich's ataxia (FRDA)^{158,159}, Rett syndrome (RTT)^{160–162}, Niemann-Pick disease (NPD)¹⁶³, and psychiatric disorders^{164–168}, like schizophrenia.

Once CNS disorders were demonstrated to share common mechanisms of cell damage that are triggered also by epigenetic alterations, the question that researchers worldwide purpose to answer is if it is possible to correct these epigenetic alterations.

Certainly, therapeutics targeted at epigenetic mechanisms (via epigenetic drugs), that despite the reversibility of epigenetic modification, would represent a recent ambitious challenge in the approach to treat CNS conditions ^{115,169}.

Several epigenetic drugs are approved as drugs for other indications, for example, cancer, or are both in pre-clinical and clinical trials.

Examples of epigenetically targeted drugs that may have used in CNS indications and are able to reverse histone acetylation aberrations include the following: HDAC inhibitors ^{143,170–176} and HAT inhibitors ^{169,177–179}.

The knowledge about the efficacy of the HDACis against several diseases was extensively consolidated, in contrast, despite their potential, the inhibitors for HATs need further investigations because too many questions remain unsolved between their biological activity in *in vitro* studies and their use as therapeutic agents ¹⁷⁹.

For this reason, I will mention in this chapter only some examples of the most relevant studies that showed the neuroprotective role of the HDAC inhibitors against programmed cell death or excitotoxicity in some brain pathologies.

Current HDAC inhibitors can be divided into three families: the hydroxymates (trichostatin A and vorinostat), the short-chain fatty acids (sodium butyrate and valproate), and the benzamides (MS-275). Before knowing their activity on histone acetylation, some of these compounds, such as valproate, were widely used mainly as mood stabilizers in neuropsychiatric disorders.

The promising clinical application of the HDAC inhibitors was firstly targeted to the treatment of different types of cancer ^{180–182}, with hundreds of clinical trials ongoing, and more recently to neuropathologies.

In mouse models for the most common neurodegenerative disorder, Alzheimer's disease, HDAC inhibitors tested were capable of reversing memory deficits ^{183,184}. Clinical trials on the efficacy and safety of nicotinamide (ClinicalTrials.gov: NCT00580931) and valproate (ClinicalTrials.gov: NCT00071721 and NCT01729598) in Alzheimer's disease patients have started a few years ago.

HDACis were also tested in Parkinson's *in vivo* models. Valproic acid, sodium butyrate and trichostatin A (TSA) were demonstrated to have survival-promoting and protective effects on dopaminergic neurons ^{185,186}. Moreover, sodium butyrate was reported to attenuate the motor deficits in 6-hydroxydopamine (6-OHDA)-induced experimental PD animal models ¹⁸⁷.

The effectiveness of HDAC inhibitors was also demonstrated in amyotrophic lateral sclerosis. Preclinical studies reported that TSA was able to delay the disease progression and increase the ALS mice survival^{188,189}, and some clinical trials were launched to test valproic acid and sodium valproate in human patients (ClinicalTrials.gov: NCT00107770 and NCT00136110).

Several studies reported the anti-inflammatory, restorative and neuroprotective effects of HDACis also in stroke^{190–193} and brain trauma^{194–197}.

The neuroprotective properties of HDAC inhibitors were observed also in animal models for the rare Huntington's disease. An amelioration of the neurodegenerative phenotype and the transcriptional abnormalities after the treatment by HDAC inhibitors was reported^{198–200}. The candidate HDACi sodium phenylbutyrate was tested in human patients and a phase II clinical trial was launched in 2005 (ClinicalTrials.gov: NCT00212316; Hogarth 2007).

Recent interesting works focused on neurodevelopmental disorders revealed the amelioration of some typical signs after the therapy with HDACis. Animal models for autistic spectrum disorder showed an amelioration of their social behavior and cognition deficits after the treatment with sodium butyrate²⁰¹, or valproate²⁰². Clinical trials were also launched to test the valproate on children and adolescent autistic patients (ClinicalTrials.gov: NCT00211757). The use of HDAC inhibitors could have interesting new implications also in Friedreich Ataxia mouse model^{158,159} and Rett syndrome²⁰³.

This intriguing general picture of the involvement of epigenetic machinery in neurodevelopmental, neuropsychiatric and neurodegenerative disorders, with the original and attracting possibility to restore these diseases, need to be better clarified and completed.

Especially the therapeutic potential of the drugs that act on histone acetylation mechanism might pertain also to the hyperbilirubinemic condition.

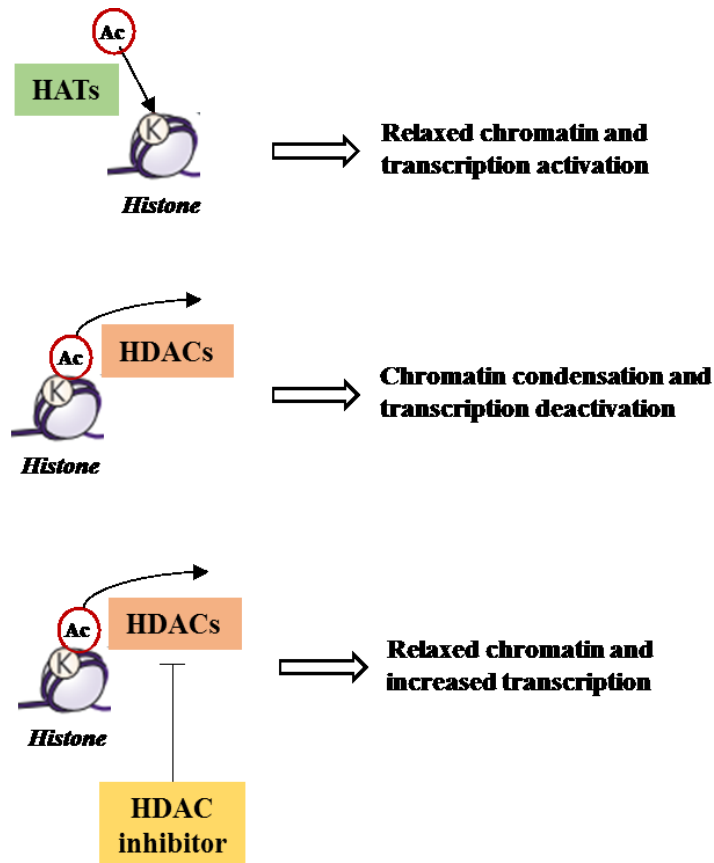


Figure 1-8. Effect of HDAC inhibitors on chromatin opening and transcription activation.

The action of the enzymes histone acetyltransferases (HATs) and histone deacetylases (HDACs) determines the acetylation/deacetylation of the histone lysine residues and the subsequent opening/closing of the chromatin structure and activation/deactivation of transcriptional gene expression. HDAC inhibitors block the deacetylation leading to a more relaxed chromatin conformation and transcriptional upregulation.

2 AIMS

The selectivity of bilirubin toxicity in specific brain regions, despite the same bilirubin level detected in each of them, and its capability in altering gene expression have been widely investigated and confirmed.

The involvement of epigenetic mechanisms able to regulate the expression of genes that control damage/resistance pathways in bilirubin neurotoxicity has not been explored till now.

In the present study we intend to:

- Evaluate the presence of altered levels of the acetyl-histone H3 (lys 14) in 5 brain regions (cortex, cerebellum, hippocampus, superior colliculi, inferior colliculi) of hyperbilirubinemic animals *vs* control at 4 post-natal ages.
- Individuate the genes regulated by acetyl-histone H3 (lys 14) in hyperbilirubinemic animals *vs.* control.
- Interpret the biological effects of this epigenetic modulation.

3 MATERIALS AND METHODS

3.1 EXPERIMENTAL PLAN

The involvement of histone acetylation in the brain of hyperbilirubinemic animals was explored in this study starting by the evaluation of the acetyl histone H3 (lys 14) (H3K14ac) levels by Western blot. Thereafter, a map of the genes regulated by the H3K14ac was obtained by chromatin immunoprecipitation assay followed by sequencing of the DNA fragments (ChIP-Seq). By the comparison of the list of ChIP-Seq genes present in hyperbilirubinemic subjects *vs.* controls, both the genes which transcription was activated as well as silenced in hyperbilirubinemia were extrapolated.

Finally, the histological analysis was performed as a relevant support for the biomolecular interpretation of the genetic results.

3.2 ANIMAL MODEL AND BRAIN REGIONS DISSECTION

Gunn rats, at two (P2), nine (P9), seventeen (P17) days after birth, and adults (more than 60 days after birth) were obtained from the Specific Pathogen Free (SPF) animal facility of CBM S.c.a.r.l. (AREA Science Park, Basovizza). Hyperbilirubinemic homozygous (jj) Gunn rats, and normo-bilirubinemic homozygous (JJ) or heterozygous (Jj) littermates as control were used.

This study was authorized by the local ethical committee for animal care and by the competent Italian Ministry. Animal care and procedures were performed according to the guidelines approved by the Italian Law (decree 87-848) and European Community directive

(86-606-ECC). Maximal effort to minimize the number of the animals and their suffering was done (RRR rule).

Animals were sacrificed by decapitation, under deep anesthesia for the cases that required it, according to the ethical rules. The anesthesia was administered by intramuscular injection of a solution composed by Rompun 2% (dose 1.5 mg/100Kg) and Zoletil 100 (dose 20 mg/Kg).

Brains were removed and placed in ice-cold PBS (137 mM NaCl, 2.7 mM KCl, 10 mM Na₂HPO₄, 1.8 mM KH₂PO₄, pH 7.4). Under the stereomicroscope, cortex (Cx), cerebellum (Cll), inferior colliculi (IC), superior colliculi (SC) and hippocampi (Hip) were dissected, cleared from meninges and choroid plexuses. Cerebella were carefully weighted to evaluate the cerebellar size, as a measure of the hypoplasia, characterizing the hyperbilirubinemic Gunn rats. All the brain regions were stored at -80°C until use.

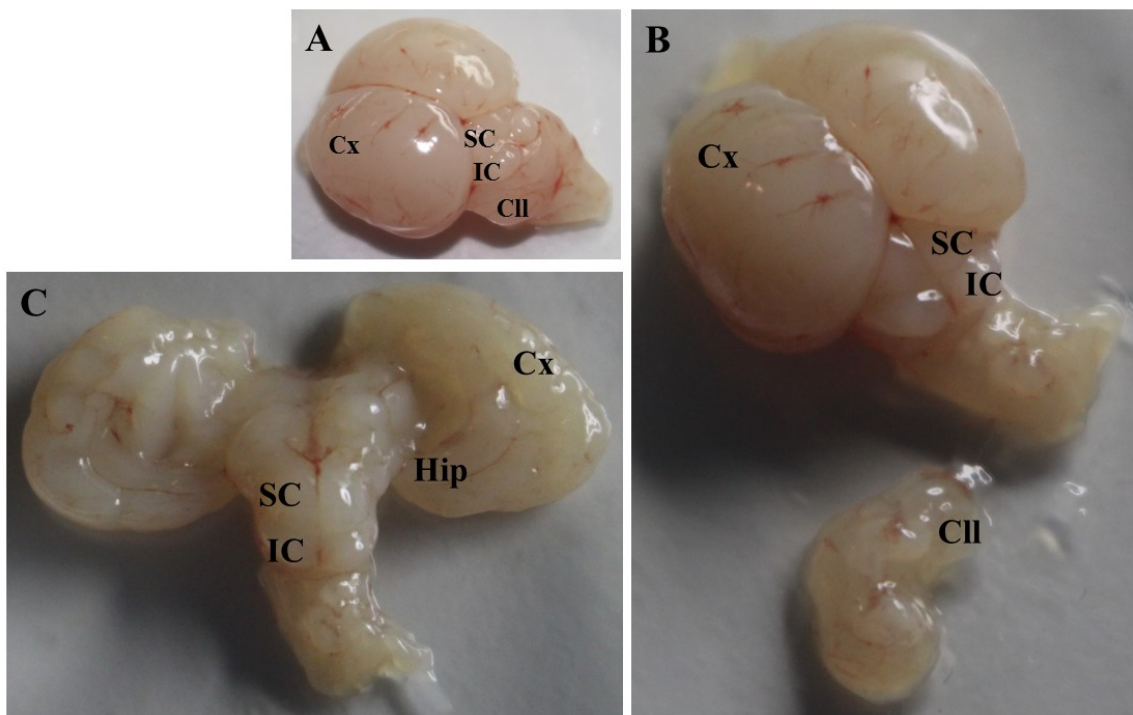


Figure 3-1. Brain from P9 jj rat, dorsal view, and dissection procedure.

Brain regions of interest were carefully dissected. (A) Entire brain vision with in evidence Cortex (Cx), Superior Colliculi (SC), Inferior Colliculi (IC) and Cerebellum (Cll). (B) Cll was removed and cleared from meninges and choroid plexuses. (C) View of the Hippocampus (Hip) in both the hemispheres.

3.3 GENOTYPING

At birth, homozygous jaundice pups (jj) were easily distinguished from the non-hyperbilirubinemic littermates by simple examination of the yellow coloration of the tegument. The genotyping procedure is necessary to distinguish the non-hyperbilirubinemic wild type (JJ) and the heterozygous animals (Jj), by the enzymatic restriction of PCR fragments encompassing the point mutation in the common exon of the UGT1 gene family.

Briefly, rapid whole genome DNA extraction was performed using the HotSHOT method: around of 2 mm of rat tail was heated at 98°C for 1 hour in 75 μ L of buffer (25 mM NaOH, 0.2 mM EDTA) and then neutralized with an equal volume of 40 mM Tris-HCl pH 5.5 buffer.

The amplification of the UGT1a1 genomic sequence was performed by the PCR method diluting the sample and the UGT1a1 gene specific primers (Forward: GGGATTCTCAGAATCTAGACATTGT; Reverse: TCGTTTGGTTCTTTTCTATTACTGACC) in the SSo AdvancedTM Universal SYBR[®] Green Supermix (BioRad, Hercules, CA, USA) for a total volume of 30 μ L. The PCR conditions were settled up as reported below.

Cycle Step	Temp	Time	Cycles
Initial Denaturation	94°C	3 min	1
Denaturation	94°C	1 min	Repeated 35 times
Anneal	55°C	1 min	
Extension	72°C	1 min	
Final Extension	72°C	5 min	Repeated 80 times
Infinite hold	4°C	∞	

Table 3-1. PCR parameters for the amplification of the UGT1a1 gene.

The control of the PCR product and the DNA quantification were performed by gel electrophoresis.

10 μ L of the amplicon were digested at 60°C for 3 hours in 30 μ L mix prepared with 3 μ L of NEBuffer 3.1 10X (B7203S, New England BioLabs[®] Inc, MA, USA), 0.3 μ L of the restriction enzyme *Bst*NI, 100% activity in NEBuffer 3.1 (R0168S, New England BioLabs[®] Inc, MA, USA).

The amplicon underwent electrophoresis using 3% agarose gel. The results were observed under UV light with a transilluminator (Euroclone, Milan, Italy) and pictures were taken with a KODAK DC290 Zoom Digital Camera (Kodak Rochester, NY, USA).

3.4 TOTAL SERUM BILIRUBIN DETERMINATION

Blood was obtained from the animals by decapitation under anesthesia when required by the ethical rules as reported above, and centrifuged at 2000 g for 10 min, RT, twice. Serum was collected under the dim light condition to minimize bilirubin photo-oxidation and immediately frozen at 20°C until use.

The quantification of total bilirubin in serum was performed following the Jendrassik-Gröf method based on the diazo-reaction²⁰⁴.

Briefly, bilirubin in serum was coupled with diazotized sulfanilic acid (Sulfanilic Acid solution: 28.9 mM $C_6H_7NO_3S$, 15 mL HCl 1N; Sodium Nitrite solution: 72.45 mM $NaNO_2$; sulfanilic acid and sodium nitrite solutions are mixed in 40:1 ratio to prepare diazo reagent), and caffeine reagent (0.41 M CH_3COONa , 0.39 M C_6H_5COONa , 0.01 M EDTA, 0.19 M $C_8H_{10}N_4O_2$) to form a pink color compound. Ascorbic acid (0.23 M $C_6H_8O_6$) was used to block the reaction. The final addition of alkaline tartrate solution (0.40 M NaOH, 1.13 M $KNaC_4H_4O_6 \cdot 4H_2O$) converted the pink acid bilirubin to green colored compound (peak absorbance: 607 nm). The intensity of the color produced is directly proportional to total bilirubin present in serum. For the final calculation of bilirubin concentration, the absorbance values of each sample were interpolated to a standard curve performed by a dilution of a stock solution of bilirubin (bilirubin maximum concentration: 0.34 mM; bilirubin minimum concentration: 8 μ M).

3.5 TOTAL PROTEIN EXTRACTION AND WESTERN BLOT

The brain regions of interest (Cx, Cll, Hip, IC, SC) were dissected and mechanically homogenized by glass-glass Dounce. Proteins were extracted using the brain homogenization buffer (sucrose 0.25 M, KH₂PO₄ 40.2 mM, K₂HPO₄ 9.8 mM, EDTA 1 mM, DTT 0.1 mM, pH 7.4) and quantified by the Bicinchoninic Acid Protein Assay (BCA)²⁰⁵, following the instruction provided by the supplier (B-9643 and C2284, Sigma, Missouri, USA).

15-25 µg of proteins were denatured with 10% of β-mercaptoethanol (Sigma Chemical, St. Louis, MO, USA) and by 5 min boiling. Then, samples were loaded and separated by 12% sodium dodecyl sulphate-polyacrylamide gel (SDS-PAGE) by electrophoresis (electrophoresis buffer: 25 mM Tris-Base, 192 mM glycine, 0.1% SDS) in a Hoefer SE 250 System (Amersham BioSciences, UK). Molecular weight standards (10-170 kDa, #26616, Thermo Fisher Scientific, Waltham, MA, USA) were used as marker proteins.

After SDS-PAGE, proteins were electro-transferred with a wet blotting system at 100V for 60 min (Bio-Rad Laboratories, Hercules, CA, USA) onto immune-blot PVDF membranes (0.2 µm; Whatman Schleicher and Schuell, Dassel, Germany), in transfer buffer (25 mM Tris-Base, 192 M glycine, 0.1% SDS, 20% methanol). The efficiency of the transfer was assessed by lack of Coomassie blue coloration of the gel after blotting, and Ponceau staining of the PVDF membrane (Coomassie blue solution and Ponceau solution for protein detection: Sigma, St. Louis, MO, USA).

Membranes were blocked for 1.5 hours at room temperature in 3% defatted milk dissolved in T-TBS (0.2% Tween 20; 20 mM Tris-HCl pH 7.5; 500 mM NaCl) and incubated O/N at 4°C with primary antibodies. The rabbit polyclonal anti-acetyl histone H3 (lys14) antibody (final concentration 0.7 µg/mL, 07-353, Merck Millipore, Temecula, CA, USA) and rabbit polyclonal anti-actin A2066 (normalization, final concentration of 0.07 µg/mL, Sigma Chemical, St. Louis, MO, USA), were diluted in 3% defatted milk T-TBS.

The following day, membranes were washed three times with 3% defatted milk T-TBS and incubated for 2 hours with the secondary antibody anti-rabbit IgG peroxidase (Dako,

Agilent Technologies, Santa Clara, CA, USA) at the final concentration of 0.0625 µg/mL in 3% defatted milk T-TBS.

Protein bands, respectively at 17 kDa (H3K14ac) and 42 kDa (actin), were detected by peroxidase reaction according to the manufacturer's protocol using a chemiluminescence procedure (ECL-Plus Western blotting Detection Reagents, GE-Healthcare Bio-Science, Italy) and visualized on X-ray films (BioMax Light, Kodak Rochester, NY, USA).

3.6 CHROMATIN IMMUNOPRECIPITATION ASSAY

Chromatin immunoprecipitation (ChIP) is a powerful method to identify regions of the genome associated with some specific proteins, such as histone subunits or post-translational modifications.

The assay was performed following the complete protocol provided by the Magna ChIPTM G Tissue Kit (#17-20000, Merck Millipore, Temecula, CA, USA). All the reagents were provided by the kit. Some conditions for ChIP were settled-up for better results: cross-link time, sonication, antibody amount.

Based on the Western blot results (for details see “Results” section), 40-50 mg of Cll of P9 animals, both hyperbilirubinemic (jj) and non-hyperbilirubinemic (JJ/Jj) ones were homogenized and cross-linked with 1% formaldehyde for 5 min, RT. The excess formaldehyde was quenched by addition of glycine and samples were resuspended in tissue lysis buffer.

Chromatin was sheared to an average size of 100-400 base pairs by sonication (Sonopuls HD 3100, Bandelin, Germany), keeping the sample in ice to avoid overheating. The sonication parameters were: power 50%, 18 cycles of 15 seconds per cycle and 105 seconds of pause between each cycle.

Chromatin fragment size was evaluated by loading the sample on a 2% agarose gel with a 100 bp marker, after incubation with RNase A for 30 min at 37°C, with proteinase K for 2 hours at 62°C, then 10 min at 95°C.

Protein-DNA complexes were immune-precipitated with 5 µL of the rabbit polyclonal anti-acetyl histone H3 (lys14) antibody (07-353, Merck Millipore, Temecula, CA, USA). Half

part of the sample was used as a negative control by the incubation with 5 μ L of the anti-rabbit IgG peroxidase antibody (Dako, Agilent Technologies, Santa Clara, CA, USA), while 1% of the same sample was used as input DNA.

G magnetic beads were added in order to capture only the chromatin/antibody complex leaving un-bound molecules in solution.

After washing the beads using the magnetic rack (LSKMAGS08 Pure Proteome™ Magnetic Stand, Merck Millipore, Temecula, CA, USA), protein-DNA crosslink was reversed incubating the sample with proteinase K at 62°C for 2 hours, followed by incubation at 95°C for 10 minutes.

Beads were separated, the supernatant containing proteins was removed, DNA purified and stored at -20°C until use.

Western blot and Real-Time quantitative PCR (RT-qPCR) were performed to verify the ChIP procedure success.

3.6.1 WESTERN BLOT FOR ChIP CONTROL

Western blot (described in detail above) was performed to verify the success of the ChIP assay. It was performed on three 20 μ L samples collected during the ChIP procedure: one incubated with rabbit polyclonal anti-H3K14ac antibody, one incubated with the anti-rabbit IgG peroxidase antibody (negative control), both collected before the cross-link reversal, and the beads obtained after the incubation of samples and antibodies and the subsequent reverse cross-link procedure.

The membrane was incubated with the antibody of interest (anti-H3K14ac) and then with the anti-rabbit IgG peroxidase. The goal was to detect the band at 17 kDa in the immunoprecipitated sample, but not in the negative control and beads.

3.6.2 RT-qPCR FOR CHIP CONTROL

RT-qPCR is the second possible control to verify the success of the ChIP assay.

The conditions for RT-qPCR were suggested by the kit Magna ChIP™ G Tissue Kit (#17-20000, Merck Millipore, Temecula, CA, USA) used for ChIP and rearranged, as reported below.

As the H3K14ac binding sites on the DNA were never reported before in literature in this specific tissue and animal model, different primers were tested, also following some indications provided by the kit used for ChIP.

The samples were diluted in a working solution of Sso Advanced™ Universal SYBR® Green Supermix (BioRad, Hercules, CA, USA) and primer mix for a total volume of 25 µL.

Parameters for the PCR reaction are reported in the table below.

Cycle Step	Temp	Time	Cycles
Initial Denaturation	94°C	10 min	1
Denaturation	94°C	20 sec	Repeated 50 times
Anneal and Extension	60°C	1 min	
Melting	55°C	1 min	1
Melting	55°C	10 sec	Repeated 80 times
Infinite hold	4°C	∞	

Table 3-2. RT-qPCR parameters for the amplification of the genomic sequence of interest.

Primers were designed using the software Beacon Designer 4.0 (Premier Biosoft International, Palo Alto, CA, USA) on rat sequence available in GenBank.

Gene	Primer sequence: Forward	Primer sequence: Reverse	Ampl. Length
<i>Gapdh</i>	CTCTCTGCTCCTCCCTGTTC	CACCGACCTTCACCATCTTG	87
<i>Actin</i>	GGCATTGCTGACAGGATG	TGGAAGGTGGACAGTGAG	137
<i>MyoD</i>	GTCTCTCAGCCTCTTTCGGT	AGCGGCTGTAGAAATCAGGTC	108
<i>cMyc</i>	CCCAAAAAAAGGCACGGAA	TATTGAAATGCGGTCATGC	89

Table 3-3. Primer sequences designed for the analysis.

Gapdh: glyceraldehyde 3-phosphate dehydrogenase. *Actin*: beta actin. *MyoD*: myogenic differentiation. *cMyc*: v-myc avian myelocytomatosis viral oncogene homolog.

1% input, immunoprecipitated samples, and negative control were added and RT-qPCR performed in an i-Cycler IQ (Bio-Rad Laboratories, Hercules, Ca, USA).

The final analysis was performed using the fold enrichment method (relative quantification by the modified $\Delta\Delta C_t$ method)^{206,207}.

3.7 ChIP-SEQ

All the samples obtained by ChIP assay were quantified using Quant-iT™ PicoGreen® dsDNA Reagent and Kits (Thermo Fisher Scientific, Waltham, MA, USA), an ultrasensitive fluorescent nucleic acid stain able to detect and quantitate small amounts of dsDNA (double strand DNA), according to manufacturer's instruction.

3.7.1 DNA LIBRARY PREPARATION

Two different kits were tested in order to obtain good quality and quantity DNA libraries from ChIP DNA. The kits were: the NEBNext® Ultra™ II DNA Library Prep Kit for Illumina® (E7645, New England BioLabs® Inc, MA, USA), and the NEXTflex™ ChIP-Seq Kit (Illumina Compatible) (5143-01, Bioo Scientific Corp, TX, USA). Due to the better quality and the higher final concentration of the DNA libraries obtained, the first one was used in this thesis's work.

Briefly, 10 ng of fragmented DNA underwent to end repair, 5' phosphorylation, dA-tailing, adaptor ligation and Uracil excision.

The cleanup of Adaptor-ligated DNA was performed without size selection using Agencourt AMPure XP magnetic beads (Beckman Coulter Life Sciences, CA, USA).

PCR enrichment of adaptor-ligated DNA followed the protocol parameters reported in the table below:

Cycle Step	Temp	Time	Cycles
Initial Denaturation	98°C	30 sec	1
Denaturation	98°C	10 sec	Repeated 10 times
Anneal and Extension	65°C	75 min	
Final Extension	65°C	5 min	1
Infinite hold	4°C	∞	

Table 3-4. PCR enrichment of Adaptor-Ligated DNA parameters.

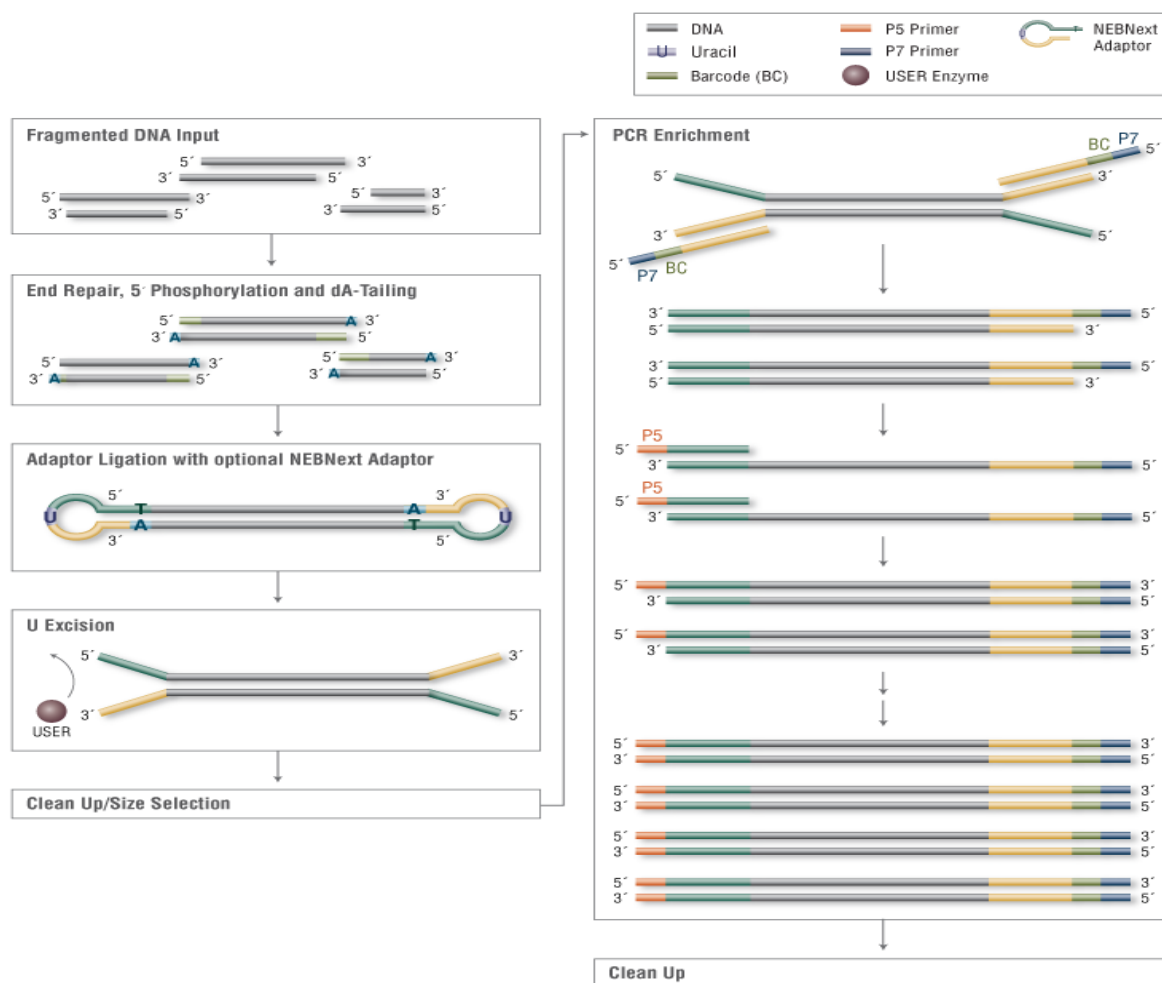


Figure 3-2. DNA library preparation flowchart.

End repair, 5' phosphorylation, dA-Tailing, Adaptor Ligation, Uracil Excision, and PCR enrichment are well represented in the scheme taken from the datasheet of the NEBNext® Ultra™ II DNA Library Prep Kit for Illumina® (E7645, New England BioLabs® Inc, MA, USA).

After the PCR cleanup, the libraries were quantified using the PicoGreen fluorescent dye, as reported above, and stored at -20°C until use.

3.7.2 LIBRARIES DENATURATION AND DILUTION

The libraries were denatured and diluted to a final concentration of 15 pM with 10% PhiX (Illumina) control. Paired-end sequencing was performed using the MiSeq reagent kit v3 2x150 in the Illumina[®] MiSeq[®] system (Illumina, San Diego, CA, USA).



Figure 3-3. Illumina[®] MiSeq[®] system (figure taken from the brochure of the machinery).

3.8 COMPARATIVE ANALYSIS OF THE DNA SEQUENCES OF jj AND CONTROLS

Reads from libraries of jj and control animals were mapped to the *Rattus norvegicus* (rn4) genome using bowtie2²⁰⁸.

Duplicate reads were filtered. The quality of the sequences was evaluated using fastQC, a quality control tool for high throughput sequence data (available online at <http://www.bioinformatics.babraham.ac.uk/projects/fastqc/>).

Peaks were called using MACS2 ²⁰⁹, which used the pool of libraries obtained from control animals, and then annotated using HOMER, a software for motif discovery and next-generation sequencing analysis ²¹⁰.

The statistical analysis used the cut-off reported below and q-values were calculated from p-values using Benjamini-Hochberg procedure:

- q-value cut-off for narrow/strong regions: 5.00e-02
- q-value cut-off for broad/weak regions: 1.00e-01.

The web-based tool GENECODIS (<http://genecodis.cnb.csic.es/>), capable of integrating diverse biological information, was used to interpret the gene lists obtained with the ChIP-Seq and to divide them in the biological processes in which they are involved in.

3.9 VALIDATION OF SELECTED GENES

After the ChIP-seq, the quantitative analysis of a limited number of interesting genes was performed by RT-qPCR.

Genes were selected following these parameters:

- Localization of the peak detected closer to the promoter or transcriptional starting site (TSS), the exon or the intron;
- Control of regulatory mechanisms of cellular differentiation, neuronal fibers maturation, and apoptosis.

3.9.1 RNA EXTRACTION AND RETROTRANSCRIPTION

The mRNA expression of genes of interest was analyzed by quantitative RT-PCR.

Total RNA of CII of P9 jj and JJ/Jj animals was extracted using Eurogold RNA Pure reagent (Euroclone, Milan, Italy).

Retrotranscription of total RNA (1 µg) was performed with High Capacity cDNA Reverse Transcription Kit (Applied Biosystems, Monza, Italy) according to the manufacturer's instructions. The reaction was run in a thermal cycler (Gene Amp PCR System 2400, Perkin-Elmer, Boston, MA, USA) at 25°C for 5 min, 37°C for 120 min, and 85°C for 5 min. the final cDNA was stored at 20°C until use.

3.9.2 RT-qPCR

For RT-qPCR, primers were designed using the Beacon designer 8.1 software (Premier Biosoft International, Palo Alto, CA, USA) on rat sequences available in GenBank (see table 3.5).

Gene	Primer sequence: Forward	Primer sequence: Reverse	Ampl. Length
<i>Anxa5</i>	TAATGACCAAAGCTGTCTCG	TTGATTGACAGCACTTCCAA	200
<i>Shox2</i>	TGAAGCTTGTAGAGTTGCAC	TCACGTTGCAATGACTATCC	80
<i>Neurod1</i>	AACGAATCCACTGTGCTTAC	TTCTTCCAAAGGCAGTAACG	133
<i>Wnt4</i>	AGTGGAGATCTGGAGAAGTG	ACGTCTACAAAGGACTGTGA	128
<i>Wnt5a</i>	CAGATGTAGCCTGTAAGTGC	CGCTGTCATACTTCTCCTTG	117
<i>Casp9</i>	TGCTAAGAAAATGGTCACGG	ATCCATCTGTGCCATAGACA	143
<i>Sema5a</i>	CAGATTGTGAGGAAATGGCA	AATGTGTGTGTAATGGAGGC	102
<i>Cdk1</i>	CTTGGACTTGCTCTCGAAA	CCAAGTCGTCAAAGTATGGG	92
<i>Bcl2l11</i>	TGTGGACTGAACTTACCTGT	CTCTAGAGCTTCAGTGAGCT	141
<i>Ctnn1</i>	CGAGAAGGAGGTTAAGGAGT	GCTTCACGCCTTCTTCATTA	110
<i>Gadd45b</i>	GCCAAACTGATGAATGTGGA	TGGATCAGGGTGAAGTGAAT	107
<i>Gadd45g</i>	GAAAGCATTGCACGAACTTC	TATGTCGCCCTCATCTTCTT	148
<i>Sod2</i>	AAGGATGGATGGAGTGGTAG	ATGTCACTCCTCTCCGAATT	131
<i>Rdh10</i>	ACCTATACCTGTGATGTGGG	GAAGGTGATGTCCAGAAACC	124
<i>Arf6</i>	ACCTCTTTCAATTGCCACTC	AAGGGGAACAAAGAAAACCC	91
<i>Cdkn2b</i>	TGAAGTGGGTTTATGCACTG	TCACCGTTTAGCAGAGATCT	132
<i>Lama5</i>	ATGTGCTCATCAAGTTTGCT	CTCCAAACAATCCCTCTTGG	125
<i>Nrg1</i>	AGCCACAAACAACAGAAACT	AAAGTTTCTCCTTCTCCGC	109

Table 3-5. Primer sequences designed for the analysis.

Anxa5: annexin A5. *Shox2*: short stature homeobox 2. *Neurod1*: neuronal differentiation 1. *Wnt4*: wingless-type MMTV integration site family, member 4. *Wnt5a*: wingless-type MMTV integration site family, member 5a. *Casp9*: caspase 9. *Sema5a*: semaphorin 5a. *Cdk1*: cyclin-dependent kinase 1. *Bcl2l11*: Bcl-2-like 11. *Ctnn1*: catenin alpha 1. *Gadd45b*: growth arrest and DNA-damage-inducible, beta. *Gadd45g*: growth arrest and DNA-damage-inducible, gamma. *Sod2*: superoxide dismutase 2. *Rdh10*: retinol dehydrogenase 10. *Arf6*: ADP-ribosylation factor 6. *Cdkn2b*: cyclin-dependent kinase inhibitor 2b. *Lama5*: laminin subunit alpha 5. *Nrg1*: neuregulin 1.

The reaction was performed in a final volume of 15 μ L in an iCycler iQ thermocycler (Bio-Rad Laboratories, Hercules, CA, USA). Briefly, 25 ng of cDNA and the corresponding gene-specific sense and anti-sense primers (250 nM each) were diluted in the SSo Advance SYBER green supermix (Bio-Rad Laboratories, Hercules, CA, USA). Amplification protocol is reported in the table below:

Cycle Step	Temp	Time	Cycles
Initial Denaturation	95°C	3 min	1
Denaturation	95°C	20 sec	Repeated 40 times
Anneal and Extension	60°C	20 sec	
Final Extension	72°C	30 sec	
Infinite hold	4°C	∞	

Table 3-6. RT-qPCR parameters for the amplification of the genomic sequence of interest.

Melting curve analysis was performed to assess product specificity. The relative quantification was made using the iCycler iQ Software, version 3.1 (Bio-Rad Laboratories, Hercules, CA, USA) by the Pfaffl modification of the $\Delta\Delta$ CT equation (CT: cycle number at which the fluorescence passes the threshold level of detection), taking into account the efficiencies of the individual genes^{206,207}.

The results were normalized to the chosen housekeeping genes and the initial amount of the template of each sample was determined as relative expression vs. one of the samples chosen as reference.

3.10 HISTOLOGY

Immediately after animals sacrifice by decapitation, the entire brain was fixed in formalin solution 4% buffered (4% of formaldehyde 37%, 33 nM NaH₂PO₄, 46 mM Na₂HPO₄), then embedded in paraffin.

Sagittal sections of the brain at 3-5 µm of thickness were obtained by the use of the microtome (Microm-hm 340e- BioOptica, Milan, Italy), affixed on the glass slides and dried at 60°C for 1 hour.

Representative sections presenting the complete panel of all the regions of interest were subjected to histochemical procedures in order to assess cell damage.

3.10.1 HEMATOXYLIN – EOSIN

Hematoxylin and eosin stain (H&E) is the most common staining technique in histopathology. The combination of the two dyes is useful for the evaluation of cell and tissue morphology. Hematoxylin is a dark blue/violet color that is basic/positive and binds to basophilic substances, such as DNA in the nucleus and RNA in the ribosomes and endoplasmic reticulum. Eosin is a red/pink color that is acidic /negative, so it binds to acidophilic substances, such as positively charged aminoacid side chains in the cytoplasm.

Sections of rat brain were stained with the H&E protocol, performed by a Leica ST5020 Multistainer (Leica Microsystem, Milan, Italy) in order to assess the presence of apoptosis, necrosis, microgliosis, edema, and cell loss. Staining was performed as follow: Xylol 2x5'; Ethanol 2x4'; H₂O 1x3'; Hematoxylin 12'; H₂O 2x6'; Eosin 1x1,30'; Ethanol 2x3'; Xylol 1x3' plus 1x2'. Histology was read by two independent pathologists, blinded to experimental design and treatment groups at the Department of Pathological Anatomy of the local Teaching Cattinara Hospital. Pictures were collected by a D-Sight plus image digital microscope & scanner (Menarini Diagnostics, Firenze, Italy).

3.10.2 CRESYL VIOLET STAINING (NISSL STAINING)

Cresyl Violet Staining is a useful method to identify the neuronal structure, staining the Nissl substance in the cytoplasm of neurons. The basic aniline dye is used to stain RNA blue: the Nissl substance (endoplasmic reticulum) appears dark blue due to the staining of ribosomal RNA.

After deparaffinization procedure (Xylol 3x5'; 100% Ethanol 2x2'; 95% Ethanol 2x2'; 80% Ethanol 1x2'; 70% Ethanol 1x2'; H₂O 2x5'), brain sections affixed on the slice were incubated for 1h in pre-filtrated 0.1% Cresyl Violet Solution (0.1% Cresyl Violet powder and 10 drops of glacial acetic acid in mQ H₂O).

Slices were washed in H₂O twice, quickly destained in 75% Ethanol, and differentiated in 95% Ethanol (95% Ethanol, 5% Chloroform, 3 drops of glacial acetic acid).

After dehydration procedure (100% Ethanol 2x5'; Xylol 2x5'), slices were mounted (Eukitt 03989, SIGMA Aldrich) and observed under optical microscope.

3.11 STATISTICAL ANALYSIS

Fold and percent changes were calculated based on corresponding controls. All data are expressed as mean \pm SD.

Data were analyzed using GraphPad InStat for Windows (GraphPad Software, Inc, La Jolla, CA, USA). Statistical significance was evaluated by the unpaired two-tailed Student's *t*-test, performed based on unequal variance as appropriate. This parametric test was chosen to evaluate the difference between the jj and the control in the analysis of the acetyl-histone H3 (lys14), considered for each age.

ANOVA test, Tukey-Kramer multiple comparison tests, was used to compare different post-natal ages in the analysis of TSB level and cerebellar weight.

In both tests, a p-value lower than 0.05 was considered statistically significant.

4 RESULTS

The original goal of my study was to investigate the involvement of histone H3 acetylation in bilirubin-induced encephalopathy, using the Gunn rats, identifying all the genes that are regulated by this epigenetic mechanism and possibly implicated in this pathology, and evaluating its possible effect on the phenotype.

4.1 CHARACTERIZATION OF THE ANIMAL MODEL

The colony was characterized by monitoring the landmark features of the Gunn strain: the TSB levels and cerebellar hypoplasia.

4.1.1 TOTAL SERUM BILIRUBIN MEASUREMENT

As Figure 4.1 shows, in hyperbilirubinemic (jj) animals TSB levels rise rapidly after birth. At P2, the TSB was about 11 mg/dL and reached the peak level at P17 (15.1 ± 2.68 mg/dL). Thereafter, in older animals, TSB decreased to the values of around 7.4 ± 2.06 mg/dL, which are typical and stable during the adulthood.

Moreover, after genotyping (Figure 4.2) allowing to distinguish heterozygous (Jj) from homozygous wild-type (JJ) animals, no detectable differences in TSB level were noticed, with a constant value of around 0.5 mg/dL all lifelong in both Gunn genotypes.

At every post-natal age, the values were statistically different ($p \leq 0.001$) if compared to the not icteric Gunn rats.

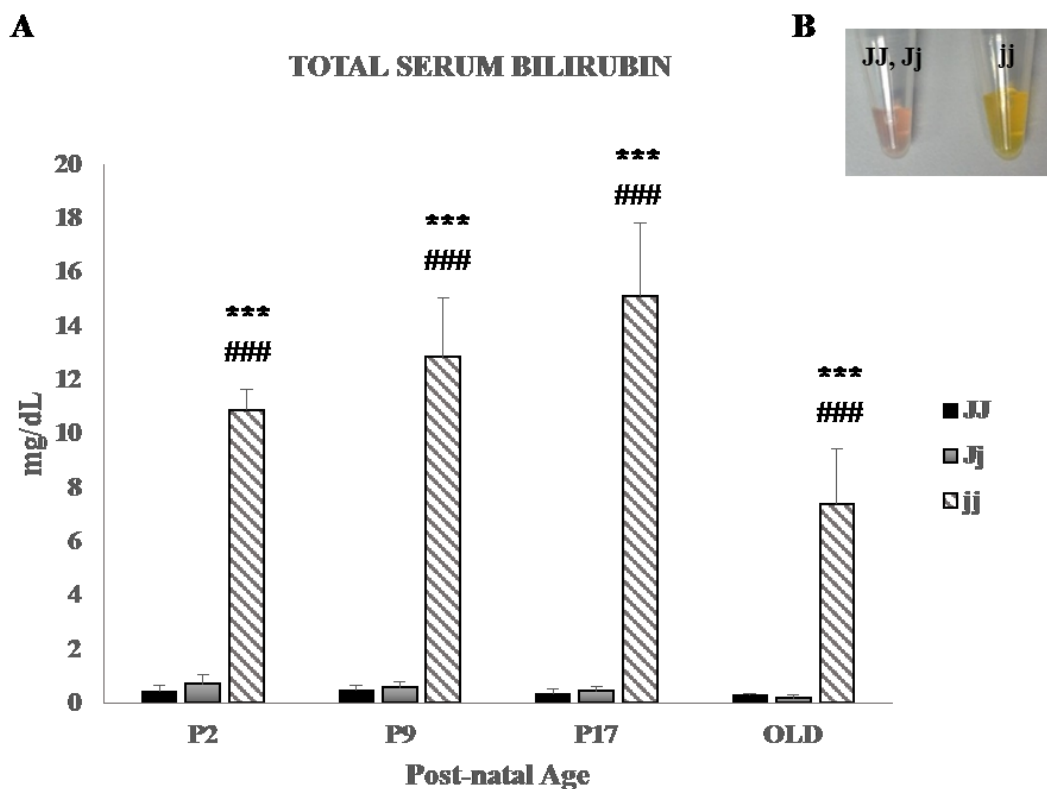


Figure 4-1. Comparison of TSB in different Gunn rat genotypes at 4 post-natal ages.

A) TSB concentration was expressed in mg/dL. P: post-natal age in days. OLD = more than 60 days old. Anova test, taking into consideration a possible variability due to the animal maturation, was applied to this analysis. The results were expressed as mean \pm SD of 10-30 animals for each age and genotype. *** and ### < 0.001 vs. JJ and Jj of the same age, respectively. B) JJ/Jj vs. jj serum appearance was represented in the image on the right upper side.

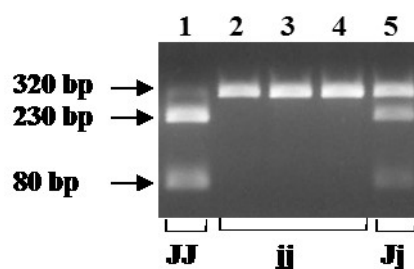


Figure 4-2. Representative genotyping results in JJ, Jj, and jj Gunn rats.

Two bands of about 230 bp and 80 bp are present in the homozygous wild-type animals (line 1), due to the presence of the *BstNI* restriction site. Three bands are visible in the heterozygous animals (line 5), while only one band of about 320 bp is visible in the homozygous hyperbilirubinemic Gunn rat (lines 2-4).

4.1.2 CEREBELLAR GROWTH EVALUATION

The effect of high levels of bilirubin is clearly manifested in the hypoplasia of the cerebellum in *jj* animals.

Cerebellar weights in *jj* and non-hyperbilirubinemic littermates (both *JJ* and *Jj*) were identical at P2 but started to show a detectable difference (around 10%) since 9 days after birth. Cerebellar growth resulted significantly impaired in *jj* animals at P17 and almost completely arrested in adult age. The cerebellar weight was about 30% lower in *jj* if compared to controls at P17 ($p \leq 0.001$), and 45% lower in *jj* older animals ($p \leq 0.001$).

Importantly, no differences in cerebellar weight were observed between *JJ* and *Jj* animals.

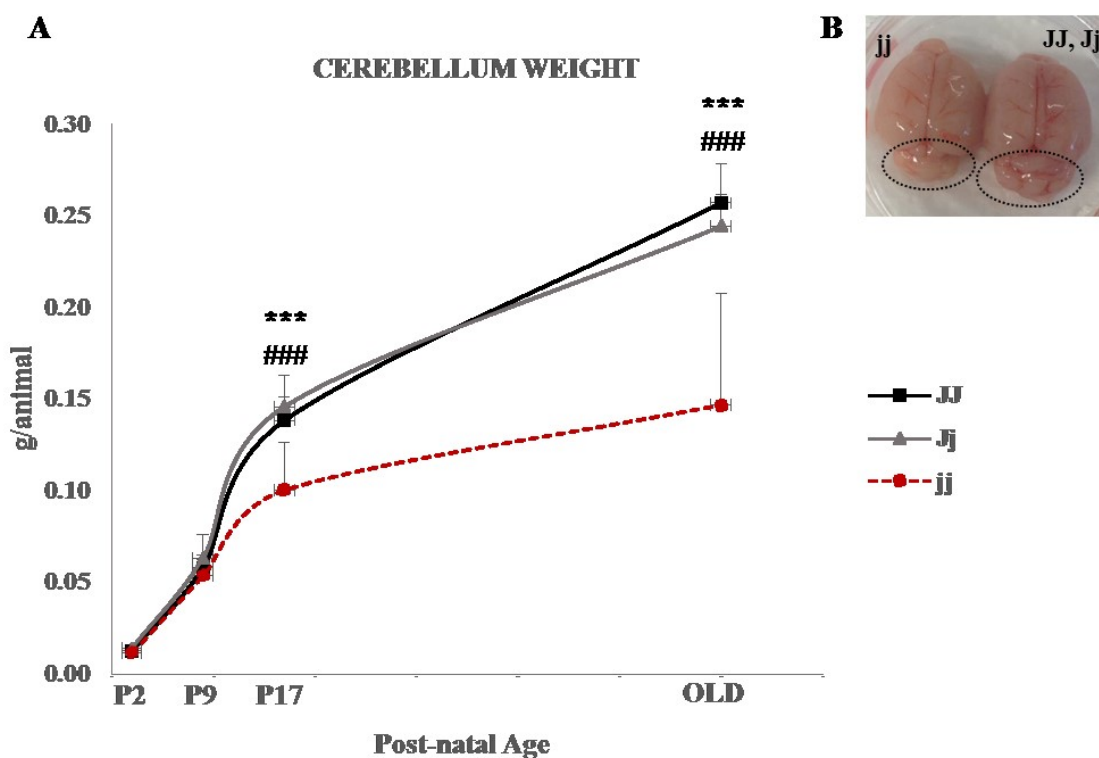


Figure 4-3. Comparison of cerebellum weight in different Gunn rat genotypes at 4 post-natal ages.

Cerebellar weight was expressed in g/animal. P: post-natal age in days. OLD= more than 60 days old. Anova test, taking into consideration a possible variability due to the animal maturation, was applied to this analysis. The results were expressed as mean \pm SD of 10-30 animals for each age and genotype. *** and ### < 0.001 vs *JJ* and *Jj* of the same age, respectively.

These results, together with the TSB data, confirm that our strain of Gunn rat possesses the typical characteristics of the animal model for neonatal hyperbilirubinemia, Crigler-Najjar type I syndrome and kernicterus. Moreover, because JJ and Jj are identical in both parameters, both genotypes were used as controls for the following analyses. This allowed also an optimization of the use of the littermates, in agreement with the ethical rules.

4.2 HISTONE H3 ACETYLATION

The screening of the levels of the acetyl-histone H3 (lys 14) (H3K14ac) was performed in different brain regions (Cx, Cll, Hip, SC, IC) of the Gunn rat at four post-natal ages (P2, P9, P17, adulthood) by Western blot.

The specificity of the antibody was first checked running one sample on 12% polyacrylamide gel. The H3K14ac was recognized as a single, defined band detectable at 17 kDa, the expected molecular weight. No other bands were detected. For such reason, the antibody was considered suitable not only for the analysis of the levels of H3K14ac but also for the immunoprecipitation of the Gunn rat brain samples.

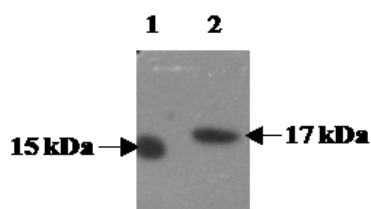


Figure 4-4. Control of the specificity of the anti-H3K14ac antibody in rat brain.

Line 1: molecular weight label; line 2: Gunn rat brain sample. No other bands were detected.

At P2, no significant differences in the level of H3K14ac jj animals compared to controls (red line) were observed for all brain regions.

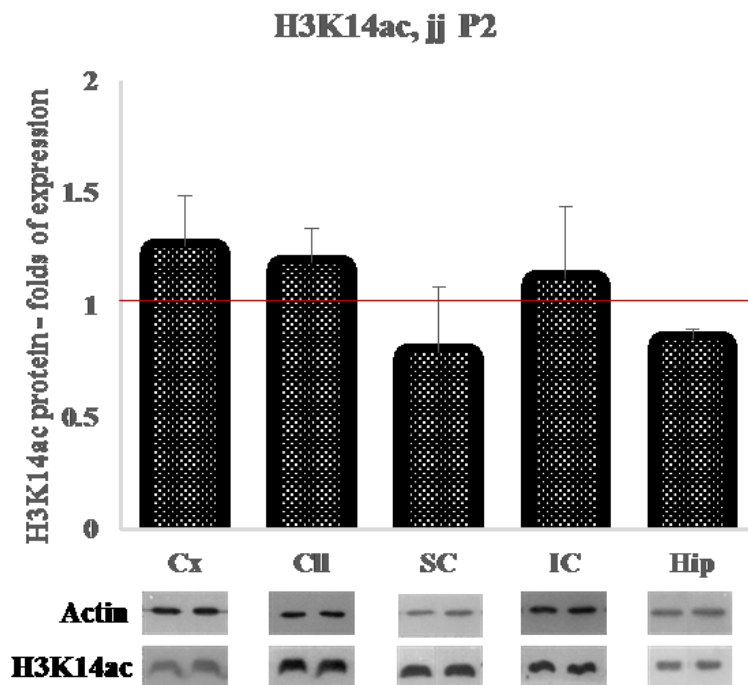


Figure 4-5. H3K14ac in the brain of the 2-days old jj Gunn rat.

The H3K14ac level was expressed as fold vs. the level in controls (red line). Actin was used to normalize the results. Cx: cerebral cortex, Cll. Cerebellum, SC: superior colliculi, IC: inferior colliculi, Hip: hippocampus. The results were expressed as mean \pm SD of 3-6 animals for each age and genotype. T-test was applied to this analysis.

At P9, the level of the H3K14ac was significantly increased in Cll (1.65 ± 0.54 fold, $p < 0.05$), Hip (1.75 ± 0.49 fold, $p < 0.05$), and in IC (2.64 ± 0.77 folds, $p < 0.01$) in jj animals compared to control pups (red line). No significant differences were reported for Cx and SC.

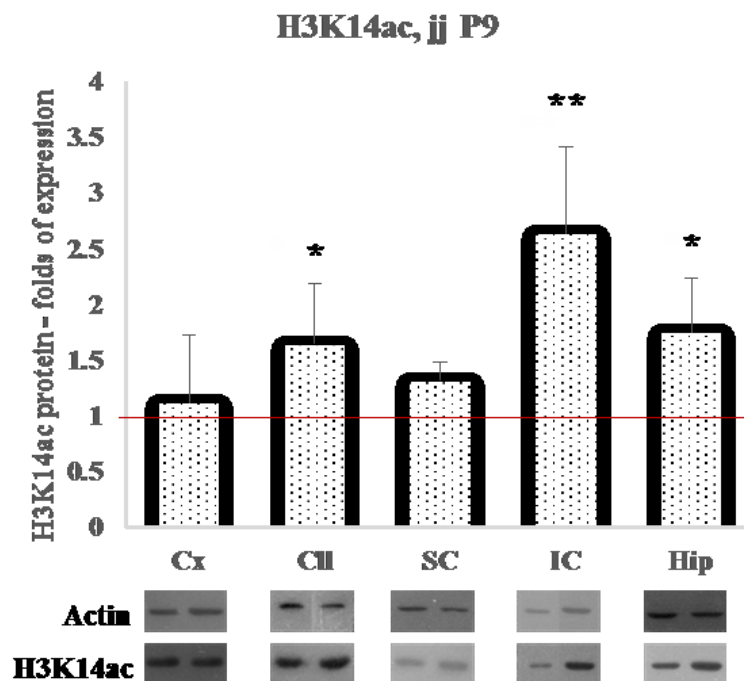


Figure 4-6. H3K14ac in the brain of 9-days old Gunn rats.

The H3K14ac level was expressed as fold vs. the level in controls (red line). Actin was used to normalize the results. Cx: cerebral cortex, Cll: Cerebellum, SC: superior colliculi, IC: inferior colliculi, Hip: hippocampus. The results were expressed as mean \pm SD of 3-6 animals for each age and genotype. T-test was applied to this analysis. * < 0.05 ; ** < 0.01 .

By contrast, at P17 the H3K14ac displayed no significant differences in Cx, Hip, and SC of jj animals if compared to the control pups. While, the level of the Histone H3 acetylation significantly decreases in Cll (0.58 ± 0.27 fold, $p < 0.05$) and IC (0.67 ± 0.18 fold, $p < 0.05$).

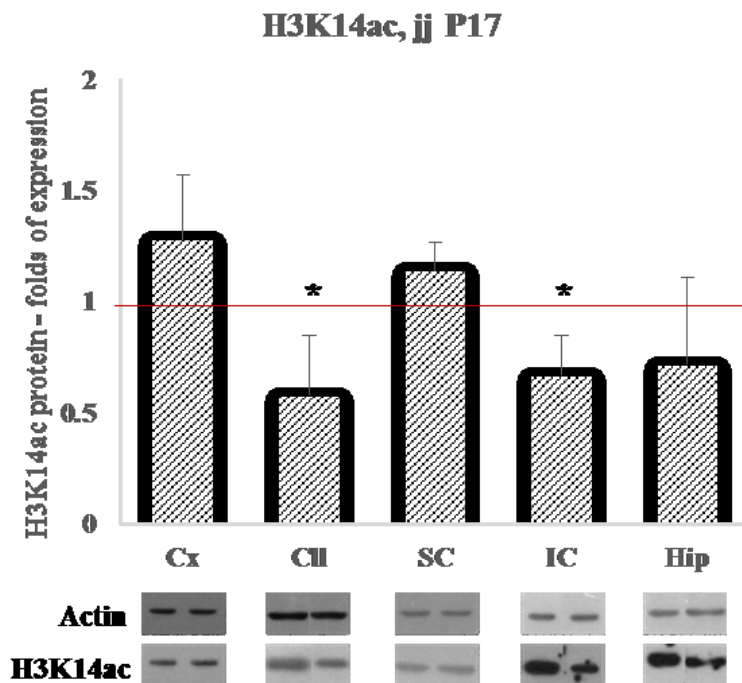


Figure 4-7. H3K14ac in the brain of 17-days old Gunn rats.

The H3K14ac level was expressed as fold vs the level in controls (red line). Actin was used to normalize the results. Cx: cerebral cortex, Cll: Cerebellum, SC: superior colliculi, IC: inferior colliculi, Hip: hippocampus. The results were expressed as mean \pm SD of 3-6 animals for each age and genotype. T-test was applied to this analysis. * < 0.05 .

In jj older animals, only Cx showed a very significant reduction of H3K14ac (0.29 ± 0.10 fold, $p < 0.01$) if compared to the age-matched controls. All the other brain regions showed no significant differences.

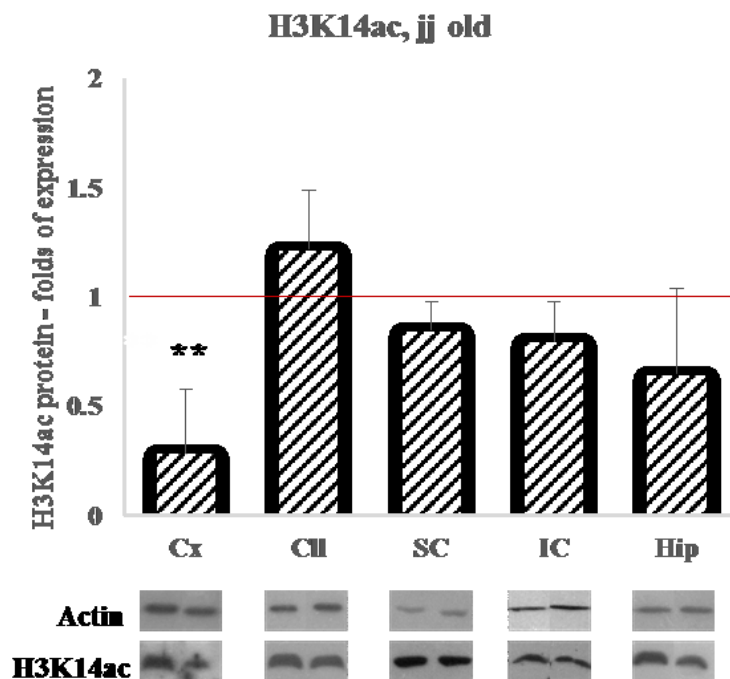


Figure 4-8. H3K14ac in the brain of older (>P60) Gunn rats.

The H3K14ac level was expressed as fold vs the level in controls (red line). Actin was used to normalize the results. Cx: cerebral cortex, Cll: Cerebellum, SC: superior colliculi, IC: inferior colliculi, Hip: hippocampus. The results were expressed as mean \pm SD of 3-6 animals for each age and genotype. T-test was applied to this analysis. ** < 0.01 .

Altogether the data we obtained revealed for the first time a modulation of the acetylation in the brain of the hyperbilirubinemic Gunn rat. Moreover, this modulation depends on the brain region and post-natal age considered.

4.3 ChIP ASSAY

To link directly the effect of hyperbilirubinemia on the H3K14ac with the genes controlled by this epigenetic mechanism, the 07-353 antibody anti-H3K14ac was used also for the chromatin immunoprecipitation.

Cerebella from P9 animals, both jj and controls, were chosen for this analysis because:

- a) cerebellum presented a significant modulation of the H3K14ac level (H3K14ac increased at P9, while decreased at P17);
- b) this CNS region is the hallmark of the hyperbilirubinemic Gunn rat, as documented by the wide existing literature;
- c) because it guaranteed a sufficient amount of tissue for the planned analysis.

The ChIP technique was settled up for the rat brain samples starting from the protocol provided by the Magna ChIP™ G Tissue Kit (#17-20000, Merck Millipore, Temecula, CA, USA).

The sonication parameters to shear the chromatin were carefully refined trying different conditions. As shown in the figure 4-9 A, three different amount (10 mg: lines 3-5, 20 mg: lines 6-8, 40-50 mg: lines 9-11) of Cll were sonicated at three different settings, maintaining the same power at 50%: (a) 6 cycles of 15 seconds per cycles and 105 seconds of pause between each cycle (lines 3, 6, 9), (b) 12 cycles of 15 seconds per cycles and 105 seconds of pause between each cycle (lines 4, 7, 10), (c) 18 cycles of 15 seconds per cycles and 105 seconds of pause between each cycle (lines 5, 8, 11). Finally the ideal tissue amount (40-50 mg) and sonication parameters (power 50%, 18 cycles of 15 seconds per cycles and 105 seconds of pause between each cycle) allowed to obtain chromatin fragments to an average size of 100-400 base pairs.

Notably, in addition to Cll, a second abundant brain region was used in this step: the cerebral cortex.

As shown in Figure 4-9 B, the Cx resulted over-fragmented using the same sonication protocol settled up for the Cll. The expected chromatin fragments for Cx (Figure 4-9 C) were obtained by decreasing the number of sonication cycles (power 50%, 10 cycles of 15 seconds per cycles and 105 seconds of pause between each cycle), revealing that the composition of tissue may influence the sonication efficiency.

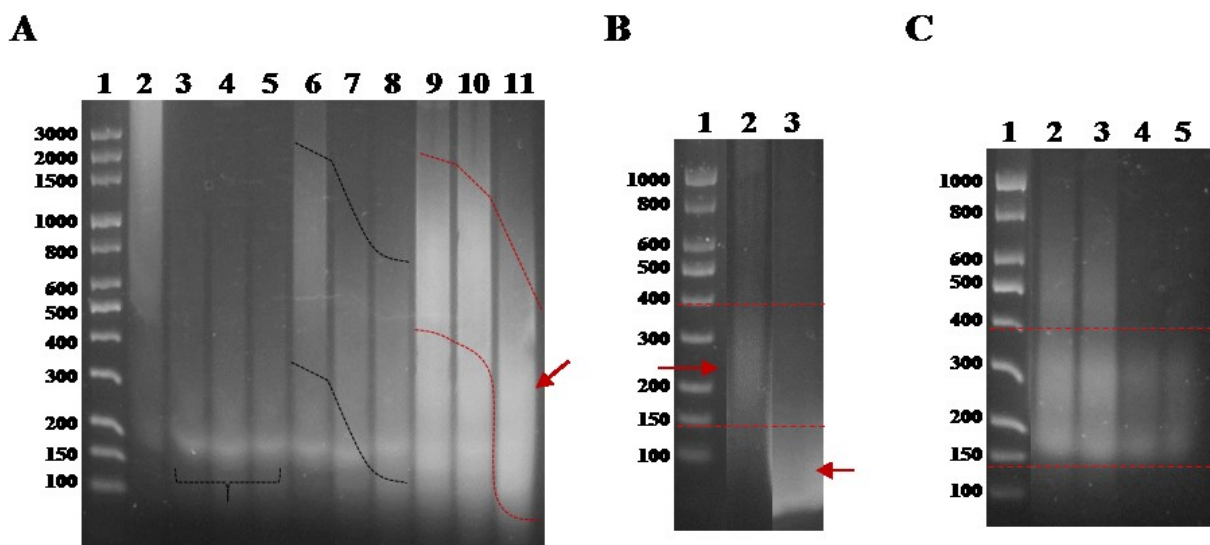


Figure 4-9. Evaluation of chromatin shearing conditions.

(A, B, C) Line 1: 100 bp marker. (A) Line 2: control, not-sonicated sample. Lines 3-5: 10 mg Cll. Lines 6-8: 20 mg Cll. Lines 9-11: 40-50 mg Cll. Sonication parameters: a (lines 3, 6, 9); b (lines 4, 7, 10); c (lines 5, 8, 11). Best sonication condition reported in line 11. (B) Line 2: Cll. Line 3: Cx. Same sonication parameters sheared Cll and Cx chromatin differently. (C) Lines 2 and 3: Cll. Lines 4 and 5: Cx. Same Cll and Cx fragments size were obtained with different sonication parameters.

The successful of the ChIP procedure was evaluated by Western blot and RT-qPCR.

The Figure 4-10 A showed the expected band at 17 kDa in the H3K14ac-sample, but not in the negative control, as expected. The 17kDa band was unexpectedly detected also in the beads-sample suggesting that the H3K14ac protein was still present, probably retaining part of the DNA. This trouble was subsequently discovered to be due to the addition of an incorrect amount of the proteinase K, thus unable to digest proteins. Bigger bands were detected also at 30 kDa and 55-70 kDa and they could be recognized as the antibody used for the ChIP and/or other non-specific proteins.

After correcting the amount of the proteinase K used for the digestion of the proteins, a very good result was obtained as reported in the Figure 4-10 B. In the figure a band at 17 kDa was detected only in the H3K14ac-sample, but not in the negative control and in the beads, suggesting that all the proteins present in the samples were correctly and completely digested by the proteinase K.

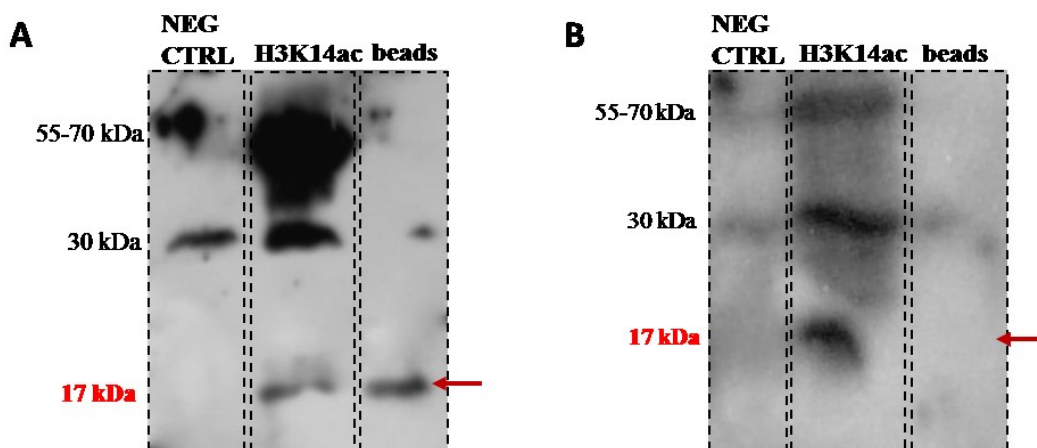


Figure 4-10. Western Blot control for the success of ChIP.

Negative control (NEG CTRL), H3K14ac and beads samples were reported. In evidence the molecular weight of 17 kDa, 30 kDa and 55-70 kDa where bands were detected.

RT-qPCR was performed on the purified DNA sample obtained from ChIP.

As a first attempt, we made a RT-qPCR using a cMyc promoter primer and a MyoD primer, as suggested by the ChIP kit. Unfortunately, we weren't able to obtain the expected enrichment (around of 100 folds between the immune-precipitated sample and the whole not-immuno-precipitated genomic DNA).

Based on our experience in the field of hyperbilirubinemia, we tested two new primers: actin and GAPDH. As showed in Figure 4-11 A and B, the results obtained were as expected for an appropriate ChIP procedure (for actin the signal in the H3K14ac-sample was about 99 folds higher than in the negative control, for GAPDH was about 150 folds higher). By this results, we do not only demonstrated the success of the ChIP on Gunn rat brain samples, but we also individuated two primers that could be used as controls for ChIP assay in bilirubin encephalopathy.

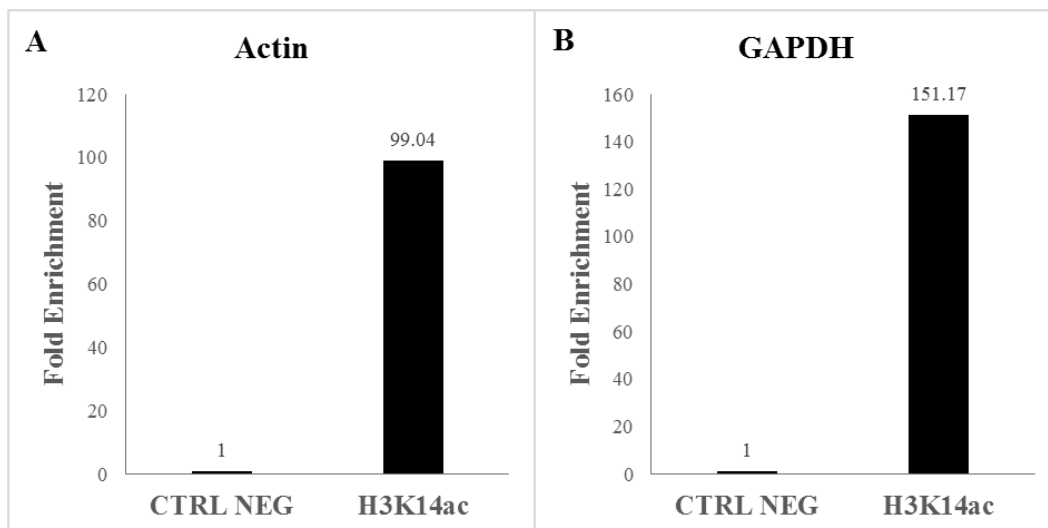


Figure 4-11. RT-qPCR control for the success of ChIP.

(B and C) Results obtained using actin and GAPDH primers: in both cases, the primers could be considered as good controls for ChIP.

Once verified the success of the ChIP, the DNA of the cerebella samples from P9 animals was purified for the following sequencing steps.

4.4 COMPARATIVE ANALYSIS OF THE DNA SEQUENCES OF *jj* AND CONTROLS

Two DNA libraries were prepared from a pool of three CII from *jj* and three CII from control ChIP DNA. In order to obtain 10 ng of libraries, the pools were prepared mixing the samples taking in consideration their respective concentration. The concentrations of the libraries obtained were: 54.2 nM for *jj* and 75.4 nM for controls.

An equal concentration (10 nM) of both (*jj* and ctrl) libraries were submitted to sequencing. After the sequencing, we obtained: 12744 reads for the *jj* pool and 15908 reads for the control pool. A good overall quality for both the runs was obtained.

The comparative analysis of the pool of libraries of 3 jj animals vs. the control resulted in the annotation of 170 significant peaks. This analysis purposed to reveal the sequences of the DNA in which hyperbilirubinemia induced chromatin opening via H3K14 acetylation.

More than the 87% of the peaks was intergenic, mostly located on satellite region or LINE (long interspersed nuclear element) region of the DNA. A very few percentage was detected in the other regions of the DNA. Only 6.5% of the peaks was found to be located in the intron region of the DNA, 4.7% of the peaks in the promoter – TSS (Transcription Start Site) region of the DNA, and the 0.6% of the peaks in the exon region of the DNA. 1.2% of the peaks was located in non-coding regions of the DNA

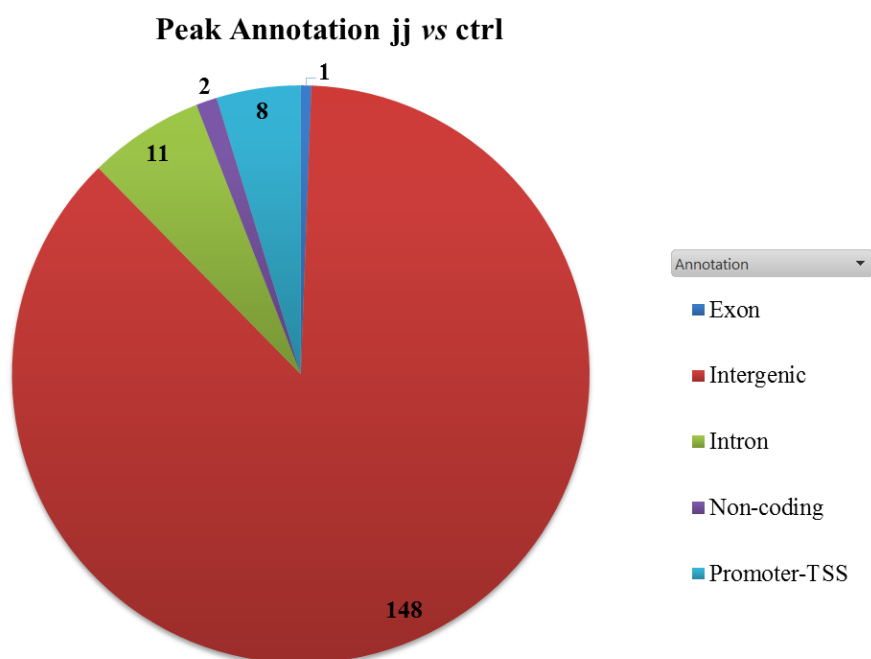


Figure 4-12. Peak annotation of the jj compared to the control.

List of the significant peaks divided according to the location into specific regions of the DNA: Exon, Intergenic, Intron, Non-coding, Promoter-TSS.

To identify the portion of the chromatin de-activated (condensed) in hyperbilirubinemic rats, the peaks obtained from hyperbilirubinemic samples were subtracted to the peaks of control animals. 3311 significant peaks present only in normobilirubinemic conditions were counted.

Despite the high percentage (37.2 %) of peaks located in the intergenic DNA, the 25.6% of the peaks was located on the promoter-TSS region of the DNA. 17.4% of the sequences was located on introns and the 12.8% was located in exons. A very low percentage (0.2%) of the peaks was located in non-coding regions of the DNA.

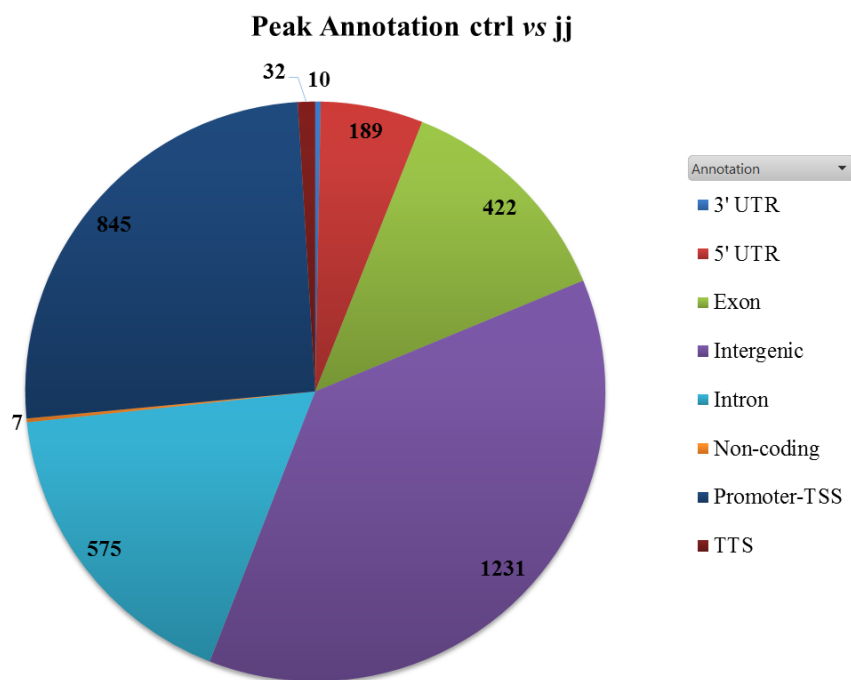


Figure 4-13. Peak annotation of the control compared to the jj rat.

List of the significant peaks divided according to the location into specific regions of the DNA: 3'UTR (Un-Translated Regions), 5'UTR, Exon, Intergenic, Intron, Non-coding, Promoter-TSS (Transcriptional Start Site), TTS (Transcriptional Termination Site).

Once the peaks were analyzed, we were able to obtain a list of single sequences both in jj and controls.

A gene ontology analysis (GeneCodis: <http://genecodis.cnb.csic.es/>) was performed both for the list of sequences in *jj vs. controls* and in *controls vs. jj*, in order to assemble the genes considering their biological function. After choosing not to consider sequences present on non-coding regions of the DNA, the overall list of sequences was divided into two groups: one included sequences located on exon, intron, promoter-TSS (Transcriptional Start Site) and TTS (Transcriptional Termination Site) regions of the DNA, the other included sequences located in intergenic regions of the DNA.

The analysis of the sequences located in exon, intron and promoter-TSS portions of the DNA in *jj vs. control* identified genes involved in regulatory pathways of the development of the nervous system, such as brain morphogenesis, development of axons and dendrites, and synapsis generation, as well as pathways that regulate the physiological cellular homeostasis.

GENE	BIOLOGICAL PROCESS
3	somatic diversification of immunoglobulins; keratan sulfate biosynthetic process; sulfur metabolic process; N-acetylglucosamine metabolic process; granulocyte differentiation
1	regulation of circadian rhythm; regulation of protein catabolic process; protein import into nucleus, translocation
1	regulation of synapse structural plasticity; radial glia guided migration of Purkinje cell; brain morphogenesis; prepulse inhibition; dendrite morphogenesis; axonogenesis
1	positive regulation of peptidyl-threonine phosphorylation; regulation of glycolysis; regulation of fatty acid metabolic process; glycogen metabolic process; regulation of protein kinase activity; regulation of catalytic activity; protein kinase cascade
1	retinoic acid biosynthetic process; nose development; neural crest cell development; embryonic viscerocranium morphogenesis; ear development; retinol metabolic process; retinal metabolic process; embryonic organ development; embryonic forelimb morphogenesis; visual perception; organ morphogenesis

Figure 4-14. Gene ontology analysis in *jj vs. control*.

Sequences located on exon, intron and promoter-TSS regions of the DNA in *jj vs. control* were grouped considering their biological functions. Number of genes and description of the biological processes were reported.

Genes that are involved in the activation of CNS developmental pathways and cellular differentiation were also identified among sequences located in intergenic regions of the DNA.

GENE	BIOLOGICAL PROCESS
6	multicellular organismal development, cell differentiation
3	cell adhesion
3	forebrain development
3	nervous system development
3	response to organic cyclic compound
3	nucleosome assembly

Figure 4-15. Gene ontology analysis in jj vs. control.

Sequences located in intergenic regions of the DNA were grouped considering their biological function. Number of genes and description of the biological processes were reported.

The analysis of the sequences located in exon, intron, promoter-TSS, TTS and UTR portions of the DNA in control vs. jj identified several groups of genes that are involved in a complex regulation of different functions.

A part 40% of genes involved in different signaling pathways (Figure 4-16) indicated more in detail in Figure 4-17, a complex developmental and differentiation pattern was controlled by 22% of genes. Cellular growth and proliferation were regulated by 13% of genes, as well as cell death process in which 9% of genes were implicated. Cellular migration was also present, with 3% of genes involved in.

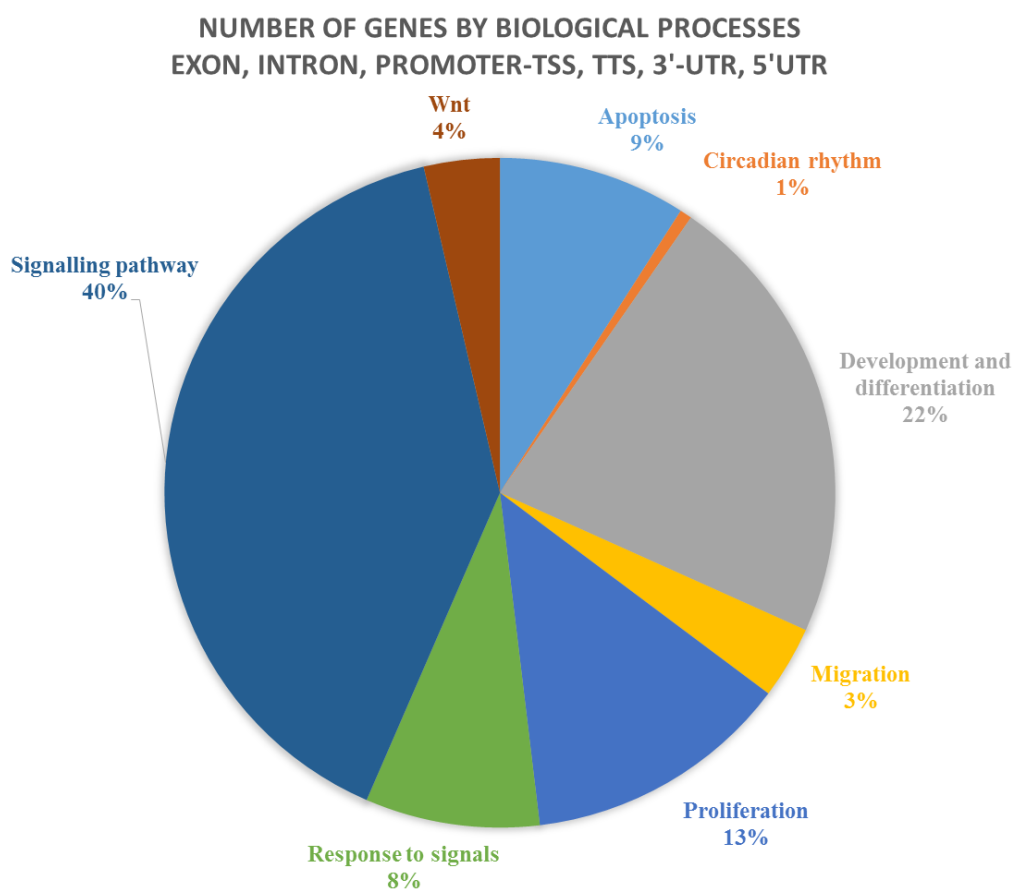


Figure 4-16. Gene ontology analysis in control vs. jj.

Percentage of genes grouped by biological function. Sequences reported are located on exon, intron, promoter-TSS, TTS and UTR regions of the DNA.

NUMBER OF GENES	BIOLOGICAL PROCESS
124	regulation of cysteine-type endopeptidase activity involved in apoptotic process; regulation of apoptotic process; regulation of neuron apoptosis
8	circadian rhythm
302	actin cytoskeleton organization; aging; anatomical structure development; angiogenesis; anterior/posterior pattern specification; axon guidance and axonogenesis; central nervous system development; cell-cell adhesion; cell development; cell differentiation; cell fate specification; cellular response to growth factor stimulus; dendritic spine morphogenesis; microtubule-based movement; neurogenesis; regulation of neuron projection development; neural tube closure; patterning of blood vessels; regulation of excitatory postsynaptic membrane potential; positive regulation of synaptic transmission, glutamatergic; synapse assembly and maturation; vasculature development
48	regulation of cell migration
176	regulation of cell cycle; cell division; cell proliferation; G1/S transition of mitotic cell cycle; mitosis; somatic stem cell maintenance
115	regulation of inflammatory response; response to axon injury; response to DNA damage stimulus; response to drug; response to hydrogen peroxide; response to mechanical stimulus; response to nutrient levels; response to organic nitrogen; response to organic substance; response to stress; response to toxin
545	cell-cell signaling; chromatin modification; GTP catabolic process; intracellular protein kinase cascade; intracellular protein transport; MAPK cascade; regulation of gene expression; regulation of protein phosphorylation and dephosphorylation; regulation of sequence-specific DNA binding transcription factor activity; regulation of transcription from RNA polymerase II promoter; regulation of transcription, DNA-dependent; nucleosome assembly; regulation of I-kappaB kinase/NF-kappaB cascade; regulation of protein ubiquitination; protein folding; protein import into nucleus; regulation of catalytic activity; regulation of signal transduction; regulation of transcription, DNA-dependent; rRNA processing; signal transduction; translation; transport; ubiquitin-dependent protein catabolic process
50	regulation of canonical and non-canonical Wnt receptor signaling pathway

Figure 4-17. Gene ontology analysis in control vs. jj.

Number of genes and description of the biological processes were reported. Sequences reported are located on exon, intron, promoter-TSS, TTS and UTR regions of the DNA.

The analysis of the sequences located in intergenic portions of the DNA in control vs. jj identified groups of genes involved in the same biological processes observed in the previous analysis.

36% of genes were involved in signaling pathways (Figure 4-18). 26% of genes controlled the cellular differentiation and central nervous system development. Cellular growth and proliferation were regulated by 9% of genes, as well as cell death process in which 13% of genes were implicated.

Figure 4-17 B showed in detail the different biological processes.

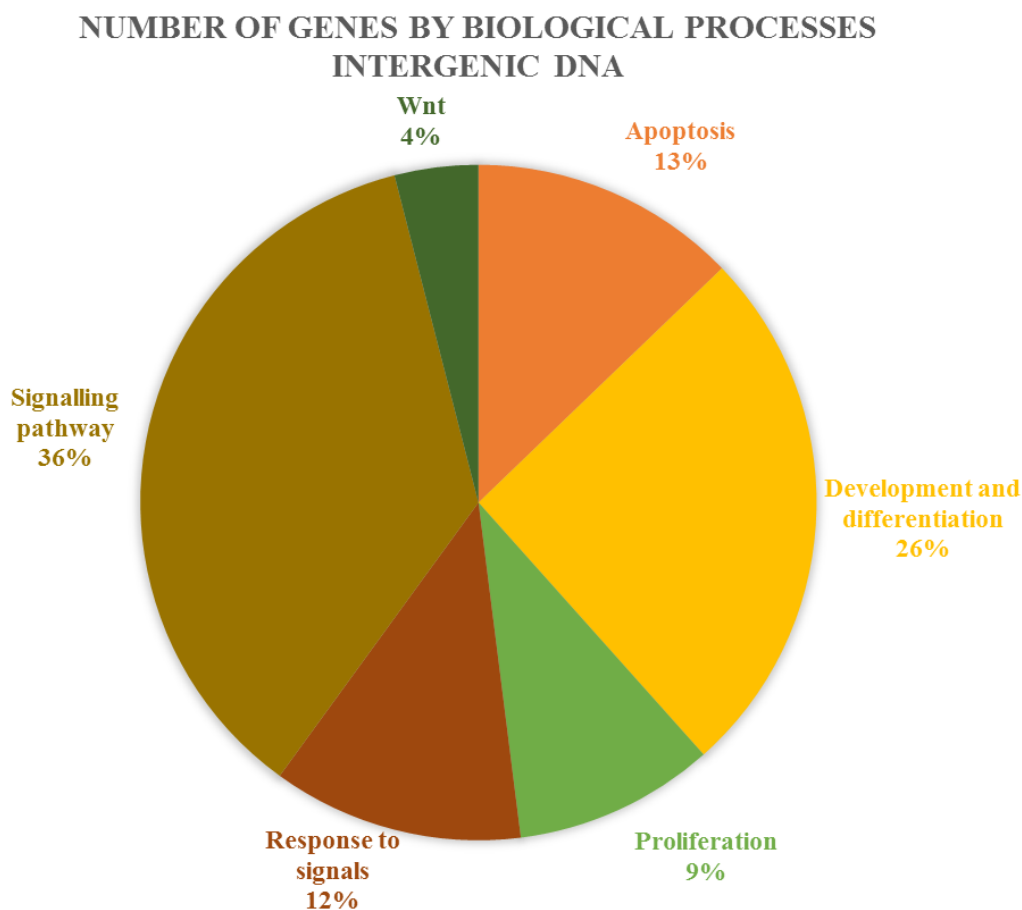


Figure 4-18. Gene ontology analysis in control vs. jj.

Percentage of genes grouped by biological function. Sequences reported are located in intergenic regions of the DNA.

NUMBER OF GENES	BIOLOGICAL PROCESS
16	regulation of apoptotic process in neuronal and non-neuronal cells
32	aging; cell development; cell (neuron, oligodendrocyte) differentiation; cell fate commitment; cell fate determination; cell maturation; central nervous system neuron development; generation of neurons; learning or memory; neuron migration; organ morphogenesis; regulation of synaptic plasticity
12	G1/S transition of mitotic cell cycle; regulation of cell proliferation; regulation of neural precursor cell proliferation; regulation of cell cycle
15	response to drug; response to ethanol; response to organic cyclic compound; response to organic nitrogen; response to stress
45	chromatin remodeling; intracellular signal transduction; regulation of sequence-specific DNA binding transcription factor activity; regulation of transcription from RNA polymerase II promoter; regulation of transcription, DNA-dependent; regulation of gene expression
5	regulation of Wnt receptor signaling pathway

Figure 4-19. Gene ontology analysis in control vs. jj.

Number of genes and description of the biological processes were reported. Sequences reported are located in intergenic regions of the DNA.

4.5 HISTOLOGICAL ANALYSIS

The histological staining, H&E and cresyl-violet were performed both in jj and control, at the same age of the ChIP-Seq analysis (P9). The entire brain was processed, allowing to obtain the complete picture of the CNS.

Both stainings revealed a wide damage in jj animals if compared to controls. A widespread arrest of the cellular differentiation and a lack of the fibrillary component, with a subsequent (apparent) cell density increase was observed.

Death due to necrotic/apoptotic processes was also observed, particularly localized in specific regions, such as inferior colliculi and some areas of the cerebral cortex, where holes are clearly visible.

In detail, in the cerebellum of jj animals, the most affected area is the Purkinje cell layer in which a general disorganization can be observed (Fig 4-20 A). In particular, the Purkinje cells seemed to be organized in more than one single layer, as it was reported in several papers that focused on the detailed description of the histological aspects in jj cerebellum⁷⁴⁻⁷⁶.

Moreover, the Purkinje cells seemed to be characterized by loss of dendritic arbor, and the cell body was not well-defined.

The external granular layer was characterized by high cell density if compared to the control, but the thickness presented no apparent differences.

The cerebellum arbor vitae, or white matter, revealed the presence of cells with meganuclei.

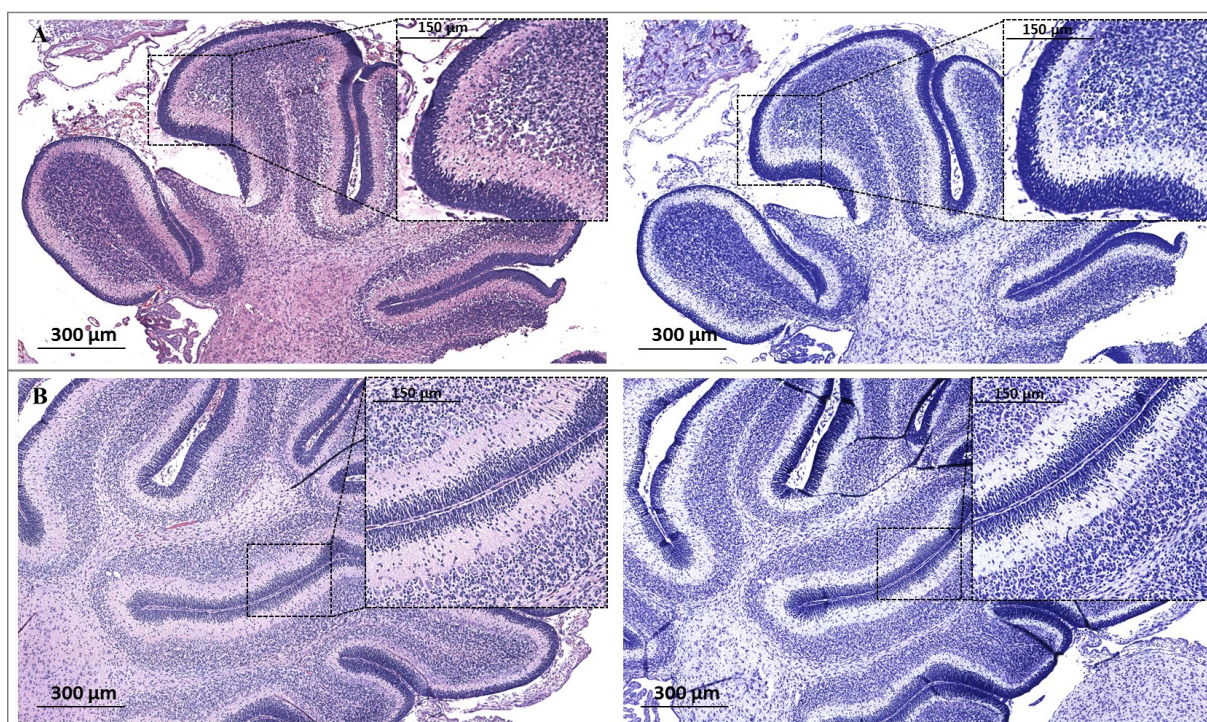


Figure 4-20. View of cerebellum (CII) slices.

(A) H&E staining (on the left) and cresyl violet staining (on the right) of P9 jj CII slice. (B) H&E staining (on the left) and cresyl violet staining (on the right) of P9 control CII slice. Both in A and B a higher magnification of a detail was reported (squares). In evidence the altered structure of the Purkinje layer in jj animals.

In the frontal cortex of jj animals a very high cell density was noticed (Fig 4-21 A). Cell bodies with a not-well developed fibrillary component appeared more compact.

A remarkable damage seemed to be due to a general atrophy and cell sufferance due to death processes and alteration of proliferation. In evidence the destruction of the normal aspect of the brain parenchyma with a consistent presence of widespread holes.

Small darker spots represented sites of microgliosis.

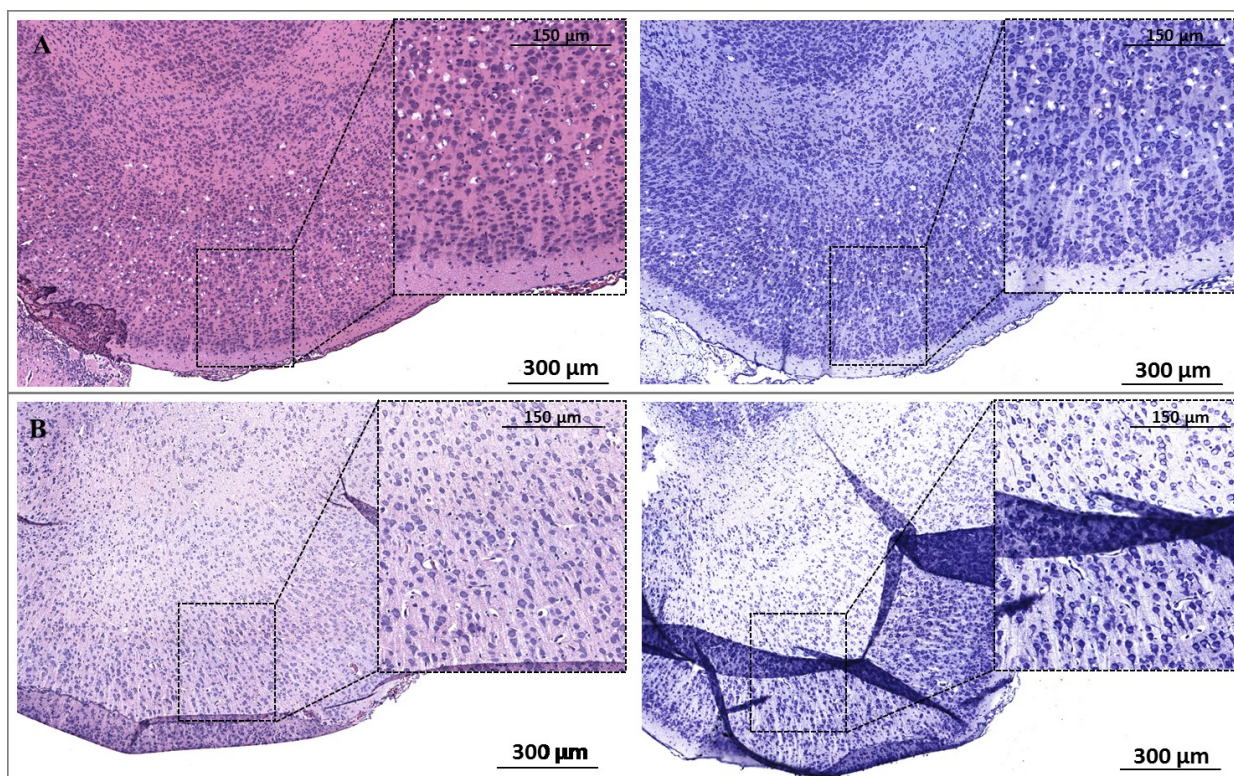


Figure 4-21. View of frontal cerebral cortex (Cx) slices.

(A) H&E staining (on the left) and cresyl violet staining (on the right) of P9 jj frontal Cx. (B) H&E staining (on the left) and cresyl violet staining (on the right) of P9 control frontal Cx slice. Both in A and B a higher magnification of a detail was reported. In evidence the high cellular density and the presence of widespread holes in jj Cx.

The same high cell density with a consistent reduction of the fibrillary component observed in the frontal cortex was also reported in the region of the cerebral cortex located over the hippocampus in jj animals if compared to the control pups (Fig 4-22 A). The high cell compaction seemed to determine the cortex thickness reduction. The distinction between nucleus and cytoplasm was very difficult, thus these cells seemed to be not well-differentiated, as well as the fibers. Death process through apoptosis and impairment of cell differentiation were noticed. Subpial ectasis and reduced thickness of the subpial white matter were observed.

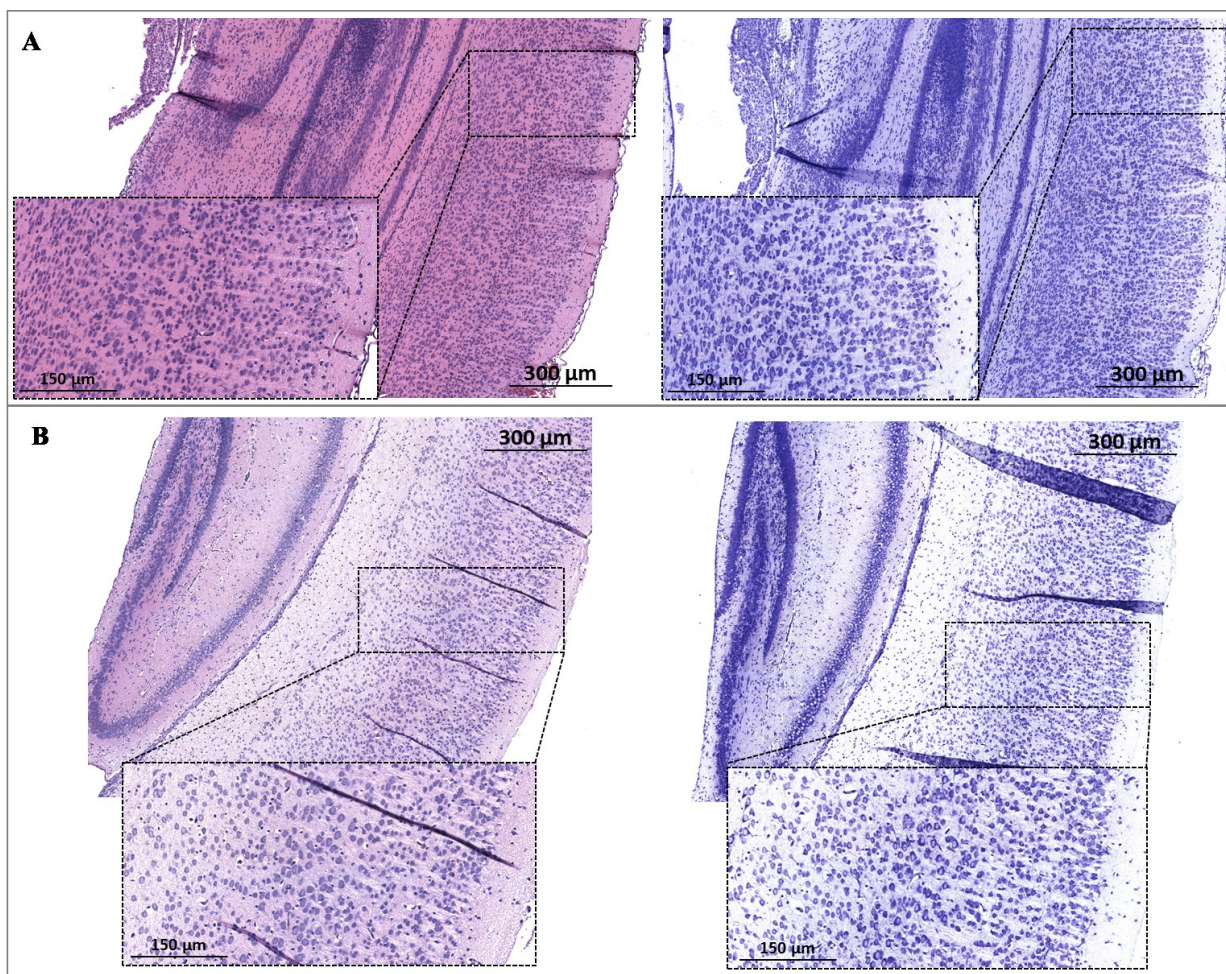


Figure 4-22. View of cerebral cortex (Cx) over the hippocampus slices.

(A) H&E staining (on the left) and cresyl violet staining (on the right) of P9 jj Cx over the hippocampus slice. (B) H&E staining (on the left) and cresyl violet staining (on the right) of P9 control Cx over the hippocampus slice. Both in A and B a higher magnification of a detail was reported. In evidence the high cellular density and thickness reduction due to the not-well differentiated fibrillary component in jj Cx.

The hippocampus of jj rats appeared thinned with very condensed cellular elements (Fig 4-23 A). Dendrites and the entire fibrillary component seemed not well-defined and generally collapsed. Cells seemed to undergo to apoptotic processes that determine a high nuclei compaction.

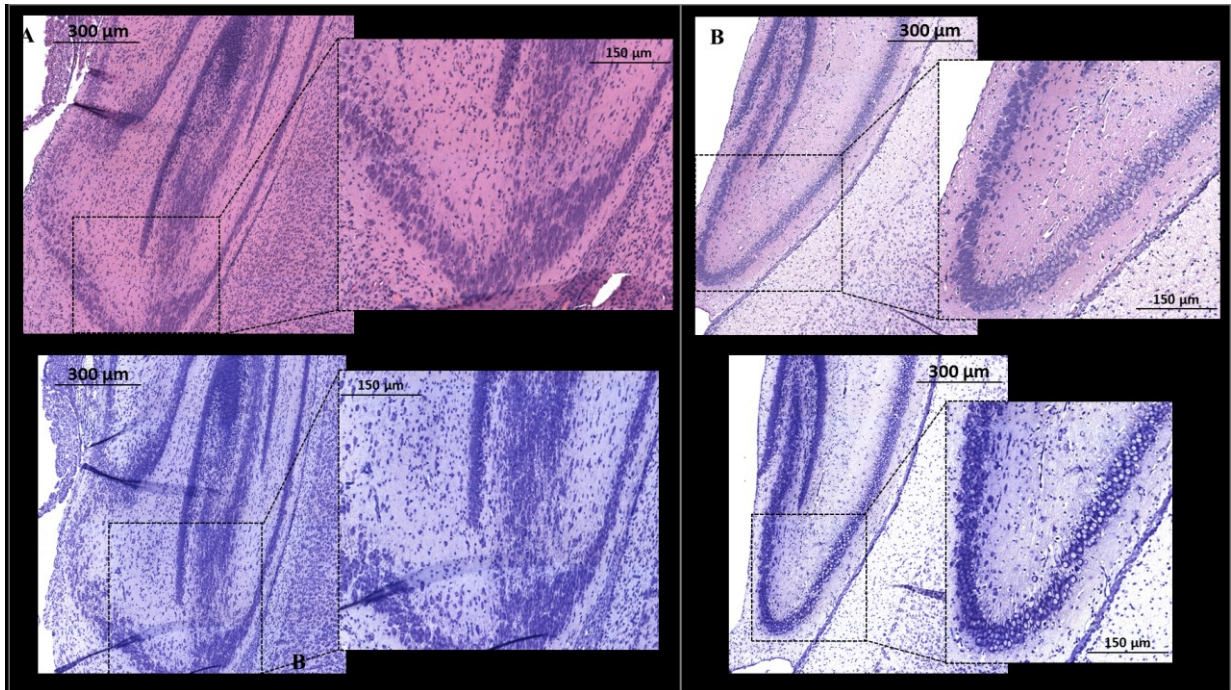


Figure 4-23. View of hippocampus (Hip) slices.

(A) H&E staining (on the left) and cresyl violet staining (on the right) of P9 jj Hip slice. (B) H&E staining (on the left) and cresyl violet staining (on the right) of P9 control Hip slice. Both in A and B a higher magnification of a detail was reported. In evidence, the hippocampal structure was extremely thinner with highly condensed cell bodies and collapsed fibrillary component.

The inferior colliculi of jj animals (Fig 4-24 A) were characterized by a general impairment of the parenchyma with widespread holes, particularly concentrated in the central area rather than the periphery. The cell morphology was not well-characterized if compared to the control one. Megacells in degeneration were detected.

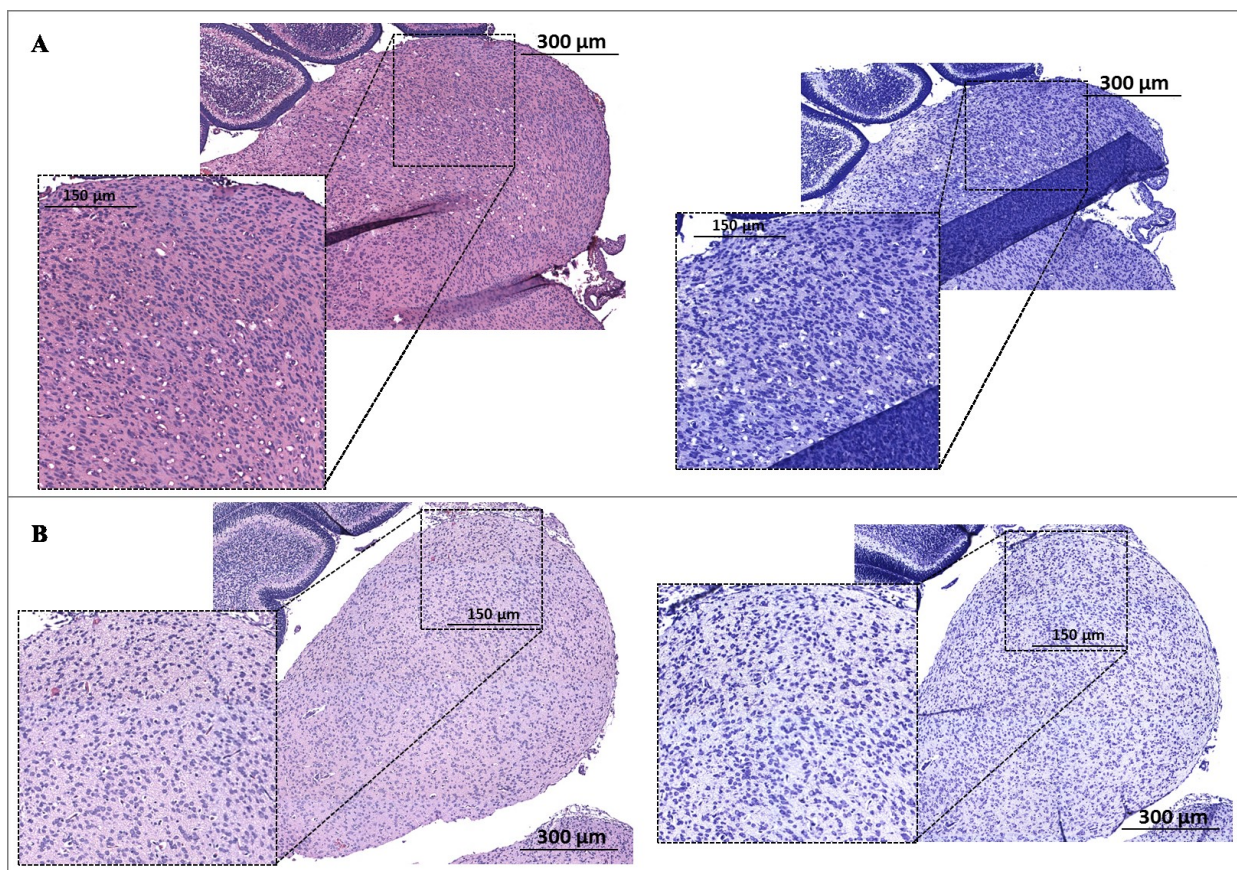


Figure 4-24. View of inferior colliculi (IC) slices.

(A) H&E staining (on the left) and cresyl violet staining (on the right) of P9 jj IC. (B) H&E staining (on the left) and cresyl violet staining (on the right) of P9 control IC slice. Both in A and B a higher magnification of a detail was reported. In evidence a general impairment of the parenchyma with widespread holes concentrated in the central area of the jj IC.

In the superior colliculi of jj pups (Fig 4-25 A) a higher cell density if compared to control was noticed. Neurons seemed to suffer: an altered and not well-designed morphology of the cell with no clear difference between nucleus, cytoplasm and the cellular membrane was observed. Swollen nuclei and macrocells were detected. Presence of microgliosis.

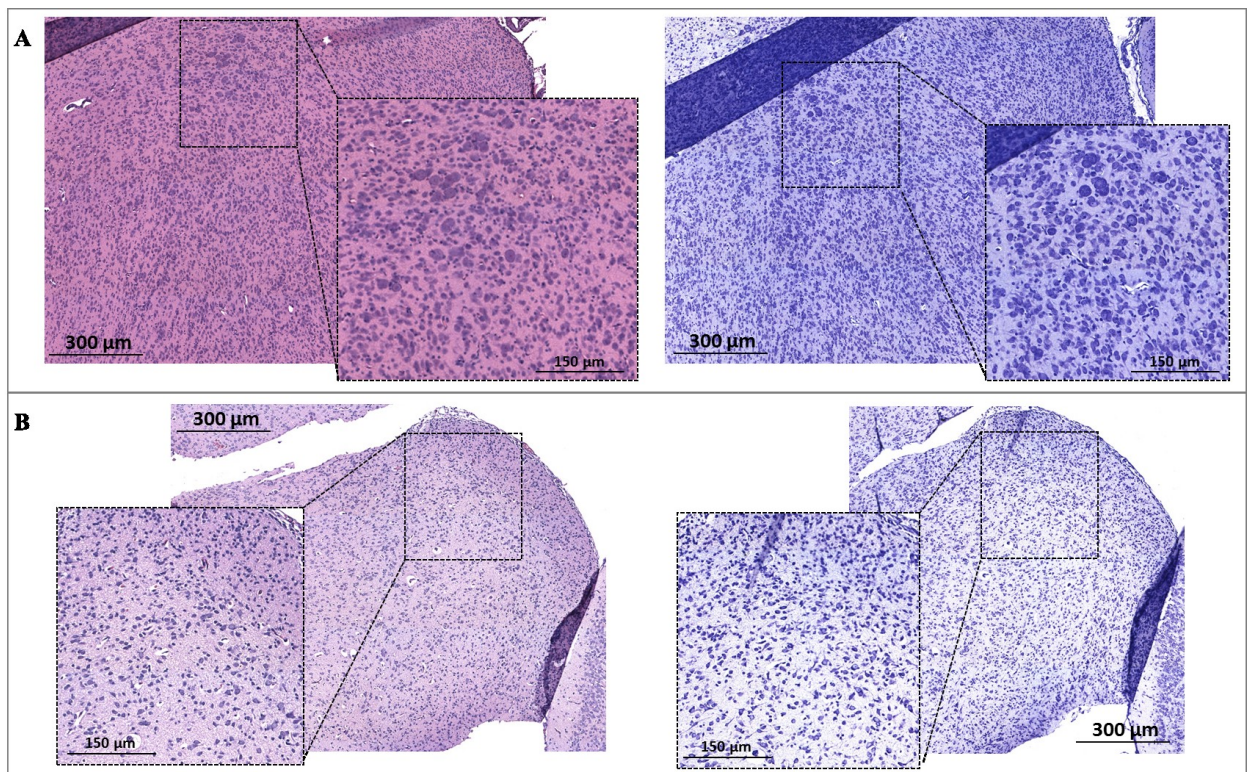


Figure 4-25. View of superior colliculi (SC) slices.

(A) H&E staining (on the left) and cresyl violet staining (on the right) of P9 jj SC slice. (B) H&E staining (on the left) and cresyl violet staining (on the right) of P9 control SC slice. Both in A and B a higher magnification of a detail was reported. In evidence not-well designed cell morphology in jj SC.

5 DISCUSSION AND CONCLUSION

Epigenetics defines those mechanisms that are directly responsible for the regulation of gene expression without changing the DNA sequence, conducting embryogenesis and influencing the development of individual's body and brain during different stages of life ²¹¹. A deregulation of these complex orchestrated events might also exert negative and diseased outcomes. In particular, histone acetylation is responsible for DNA packaging regulation with powerful influence in transcriptional activity/silencing; it is also deeply involved in brain physiological processes and pathologies ¹¹⁶.

Common cellular mechanisms impairments were described both in several brain diseases, but also in the neurological dysfunction due to high levels of bilirubin. In this disease, the activation of complex signaling pathways and the modulation of the expression of a considerable number of genes was demonstrated to be directly triggered by bilirubin ^{23,79,84,91,97,98,100,106,108-110}. Moreover, the heterogeneity of the brain, defined not only in terms of cellular composition and interaction but also considering the vulnerability of selected brain areas to environmental challenge, was observed also in bilirubin-induced encephalopathy ^{23,82,84}.

For these reasons, we decided to explore the involvement of histone acetylation in bilirubin-induced encephalopathy using the well-characterized rat model for hyperbilirubinemia.

The screening of the acetyl-histone H3 (lys 14) protein on five brain regions (Cx, Cll, Hip, SC, and IC) at three ages after birth (P2, P9, P17) and in adulthood clearly evidenced the different capability of each area to respond to the bilirubin insult, despite the same bilirubin level measured in (about 5-6nmol/g) ^{29,30}.

As first, the modulation of the H3K14ac seems to require some time of bilirubin challenge, as evidenced by the absence of detectable differences in the H3K14ac levels in all brain regions at P2. This result could be explained by a correlation with the time of exposure to bilirubin or by the fact that the early stage after birth (P2) could be less sensitive to bilirubin compared to the other ages. In rodents, the CNS experiences a dormant period immediately

after birth ²¹², possibly making the brain less sensitive to the actions of toxins ²³. In agreement, the critical period for bilirubin-induced damage was identified around 6-10 days after birth in the Gunn rat ^{28,73,75}. Thus, 48 hours of exposure to bilirubin are not enough to exert any effects on histone H3 acetylation.

In the other ages, H3K14ac expression followed an age- and region-dependent course. Cll, IC, and Hip reported a significant increase of this protein at P9, while a significant decrease was present only in Cll and IC at P17. In adulthood, these brain regions normalized the H3K14ac level (vs. ctrl), while Cx showed a significant reduction.

The upregulation of the H3K14ac in some brain regions at P9, following the increasing TSB level (about 13 mg/dL) measured at this age, might suggest the chromatin opening in DNA sequences that could be responsible for protection/resistance mechanisms activation. Otherwise, the normalization/downregulation of the H3K14ac observed at P17, despite the incessant increasing of TSB level (around 15 mg/dL), might be due to the closing of the portions of chromatin controlled by this specific epigenetic mechanism in DNA region that regulate protection/resistance pathways in place of the activation of other regulatory mechanisms for cellular damage and death. Another possible explanation could be linked to the different plasma bilirubin/albumin molar ratio (B/A) detected at these four ages and reported in the study conducted by Gazzin and colleagues in 2012 ³⁰. In this study, the B/A ratio was reported to be higher than 1 in jj at P2 and P9, increasing the risk for bilirubin neurotoxicity, while it decreases within a safe range (> 0.5) at P17 and in older animals. The trend to reduction was reflected by the amount of bilirubin in brain ³⁰. This could explain the normalization of the H3K14ac level observed during the maturation of the animal.

The marked cerebellar hypoplasia is the hallmark of the hyperbilirubinemic animal models ^{30,40,74}. Our histological results on P9 cerebellum well agree with previous works ⁷⁴⁻⁷⁶ showing a marked disorganization of the Purkinje cells still disposed in multilayer rather than in a single layer as in controls. As Altman described in his work, one phase of the normal cerebellar development is the Purkinje cells maturation, characterized by the alignment of this cell type in a monolayer and the dendrites projection towards the molecular layer ²¹³. Our findings demonstrated that bilirubin could compromise these two developmental processes, probably decelerating/delaying the cellular migration. The disorganized architecture, the degeneration of the dendritic arbor, as well as not-well-defined cell bodies, agrees with the

observation of an impairment of synaptogenesis showed in Gunn rats by Yamamura ⁷⁶, and is confirmed in the Ugt knock-in mouse ⁴⁰. Moreover, the injured myelination reported by Brito ⁸⁰ and Barateiro ⁹⁷ could be inferred also in our histological findings that evidenced a relevant fibrillary component alteration. Even if other works described a thinning of the molecular layer (ML) with lower cellular density at P9, while the external granular layer (EGL) and internal granular layer (IGL) started to reduce thickness after this age ⁷⁶, our staining seemed to show higher cellular density without reduction of this layer. An abnormal stratification of the cerebellar layers was also confirmed in the P5 Ugt knock-in mouse ⁴⁰ with a different pattern: a thinner external germinal layer and a thicker internal granular layer were observed in mutant cerebella. The main differences in the animal models and strains, as well as in the severity of the phenotype, could explain the different cerebellar architecture we found, compared to the other models. The involvement of this brain structure is finally confirmed in case reports of pre-term infants died with kernicterus ^{80,214}, corroborating the symptoms described in clinics ²¹⁵.

Although cerebellum is the most studied brain region using animal models for hyperbilirubinemia, also IC, a key part of the auditory pathway, and Hip, principal location of the memory functions, were demonstrated to be damaged by bilirubin both in *in vivo* and *ex vivo* works. Causes of the hearing loss in Gunn rat model, reflecting an auditory pathway damage, seemed to be the degeneration of excitatory synaptic terminals in the auditory brainstem ²¹⁶, but also the alteration of calcium-binding protein expression ²¹⁷. Moreover, apoptosis and necrosis ²¹⁸, as well as synaptic potential inhibition ^{219,220} and microglial activated morphology ²²¹ were reported. In clinical practice, the damage of IC was demonstrated observing alterations of the auditory evoked potentials ^{64,222–225}, while the Hip impairment was supposed by memory deficits ^{88,220}. Newborn autopsies that reported yellow staining and cellular impairment in the hippocampus and inferior colliculi ²²⁶ confirmed the clinical reports. Our histological results for Hip and IC confirmed the bilirubin-induced impairment described in the studies mentioned above. A part a general higher cell density with not-well defined cell morphology, in IC widespread holes, symptoms of tissue degeneration, were evidenced, while in Hip the general architecture of the layers appeared condensed with scarce development of the fibers.

Interestingly, Cx, usually considered resistant to bilirubin by clinicians²²⁷, is a double-edged brain region. In fact, a large number of *in vitro*^{104,108,228–230} and animal model-based works reported its sensitivity to bilirubin^{23,219,231,232}. Our histological images of P9 jj animals seemed to confirm the Cx vulnerability to bilirubin insult, displaying a general tissue sufferance, highlighting the same cell density increase and relevant reduction of the fibrillary component observed in the other regions, and also a widespread riddled aspect. Surprisingly, the H3K14ac showed no variations among the three developmental ages taken into consideration in my work, despite the higher TSB level, while reporting a significant downregulation in older animals, completely not-aligned with the other brain regions, despite the TSB was decreased at not-toxic levels. This intriguing result suggests that the neonatal and juvenile exposure to high UCB levels may have influences on epigenetic mechanisms also in aging. The absolute novelty of this work was determined by the systematic and complete evaluation of the biomolecular mechanisms of bilirubin toxicity, introducing the possible regulation of gene expression by histone acetylation, comparing different brain regions and different ages.

Despite the whole panel of histological data should be assessed in the other post natal ages, these findings suggest that bilirubin interferes with cell proliferation and blocks cell differentiation, maturation and/or migration. The ChIP-Seq results seemed to be in agreement with the histological findings and with the overall knowledge of the CNS development present in literature. Our analysis revealed that in P9 jj cerebellum very few sequences (about 200) seemed to be linked to H3K14ac, with the highest percentage of sequences (87%) located in the intergenic region of the DNA (LINE and satellite) and a lower percentage of sequences located on the promoter-TSS, intron and exon regions of the DNA. On the other hand, a very high number of sequences (over 3000) seemed to be present only in controls, thus suggesting that a very high percentage of genes controlled by H3K14ac was silenced in jj animals. Generally speaking, a part the genes that regulate physiological signaling pathways, the genes grouped by the gene ontology analysis seemed to be involved in the regulation of development and differentiation, proliferation, migration and apoptosis pathways. The fact that in jj animals these processes seemed to be inactive at this specific age revealed that the normal modeling of the cerebellum could be affected by bilirubin. Furthermore, the detection of a very high percentage of intergenic DNA compared to the coding-DNA in jj may be considered peculiar.

In fact, despite the intergenic DNA has been classified as “junk” for many years, recently its role has been reconsidered. These repetitive elements, including satellite DNA and retrotransposons, such as LINE, seemed to be part of the heterochromatin and essential for chromosome stability and gene expression regulation^{233–235}. Again, few studies reported their involvement in some diseases, hypothesizing the heterochromatin destabilization with consequent inappropriate transcription^{236,237}, as well as their linking to histone modification and DNA methylation^{238–240}. Currently, the understanding of these DNA sequences in diseases is still incomplete, especially because ChIP-seq, a very powerful tool to investigate the epigenetic regulation of genome, is limited to the investigations that are already known^{241,242}. New technologies able to analyze repeat sequences might better understanding this subject.

In conclusion, this work reported for the first time the involvement of histone acetylation in the brain of hyperbilirubinemic animals with a strong regulation of the gene expression. The complete panel of genes we obtained seemed to well-correlate with the bilirubin-induced damage that evidenced the development impairment. All together, these results represented a relevant contribution to better understand the bio-molecular mechanisms that cause bilirubin toxicity, but also might be important to consider new pre-clinical therapies in kernicterus, testing the neuroprotective properties of drugs able to regulate the histone acetylation.

In future, we plan to complete this project by:

- Completing the panel of the temporal trend of the bilirubin effect on the different brain regions by the histological staining of P2, P17, and older brains. This may contribute to improving our knowledge of this pathology.
- Analyzing a selected list of genes obtained by the ChIP-seq analysis, by RT-qPCR in all the brain regions at all the ages considered in this work in order to have more quantitative information. This could be useful to introduce new hypothesis relative to the influence of biomolecular mechanisms on the hyperbilirubinemic phenotype.
- Publishing a peer-review paper that will be of a great novelty for the study of the biomolecular mechanisms in kernicterus, introducing epigenetic and the clear bilirubin influence on CNS development.

6 BIBLIOGRAPHY

1. Ostrow, J. D., Jandl, J. H. & Schmid, R. The formation of bilirubin from hemoglobin in vivo. *J. Clin. Invest.* **41**, 1628–1637 (1962).
2. London, I. M., West, R., Shemin, D. & Rittenberg, D. On the origin of bile pigment in normal man. *J. Biol. Chem.* **184**, 351–358 (1950).
3. Tenhunen, R., Marver, H. S. & Schmid, R. The enzymatic conversion of heme to bilirubin by microsomal heme oxygenase. *Proc. Natl. Acad. Sci. U. S. A.* **61**, 748–755 (1968).
4. Vitek, L. & Ostrow, J. D. Bilirubin chemistry and metabolism; harmful and protective aspects. *Curr. Pharm. Des.* **15**, 2869–2883 (2009).
5. Ryter, S. W. & Tyrrell, R. M. The heme synthesis and degradation pathways: role in oxidant sensitivity. Heme oxygenase has both pro- and antioxidant properties. *Free Radic. Biol. Med.* **28**, 289–309 (2000).
6. Jacobsen, J. & Brodersen, R. Albumin-bilirubin binding mechanism. *J. Biol. Chem.* **258**, 6319–6326 (1983).
7. Zucker, S. D., Goessling, W. & Hoppin, A. G. Unconjugated bilirubin exhibits spontaneous diffusion through model lipid bilayers and native hepatocyte membranes. *J. Biol. Chem.* **274**, 10852–10862 (1999).
8. Ahlfors, C. E. Bilirubin-albumin binding and free bilirubin. *J. Perinatol. Off. J. Calif. Perinat. Assoc.* **21 Suppl 1**, S40-42-62 (2001).
9. Diamond, I. & Schmid, R. Experimental bilirubin encephalopathy. The mode of entry of bilirubin-14C into the central nervous system. *J. Clin. Invest.* **45**, 678–689 (1966).
10. Ostrow, J. D., Mukerjee, P. & Tiribelli, C. Structure and binding of unconjugated bilirubin: relevance for physiological and pathophysiological function. *J. Lipid Res.* **35**, 1715–1737 (1994).
11. Sticova, E. & Jirsa, M. New insights in bilirubin metabolism and their clinical implications. *World J. Gastroenterol.* **19**, 6398–6407 (2013).
12. Wolkoff, A. W. Organic anion uptake by hepatocytes. *Compr. Physiol.* **4**, 1715–1735 (2014).

13. Hauser, S. C., Ziurys, J. C. & Gollan, J. L. Subcellular distribution and regulation of hepatic bilirubin UDP-glucuronyltransferase. *J. Biol. Chem.* **259**, 4527–4533 (1984).
14. Chowdhury, J. R., Jansen, P. L., Fischberg, E. B., Daniller, A. & Arias, I. M. Hepatic conversion of bilirubin monoglucuronide to diglucuronide in uridine diphosphate-glucuronyl transferase-deficient man and rat by bilirubin glucuronoside glucuronosyltransferase. *J. Clin. Invest.* **62**, 191–196 (1978).
15. Blanckaert, N., Gollan, J. & Schmid, R. Bilirubin diglucuronide synthesis by a UDP-glucuronic acid-dependent enzyme system in rat liver microsomes. *Proc. Natl. Acad. Sci. U. S. A.* **76**, 2037–2041 (1979).
16. Gartung, C. & Matern, S. Molecular regulation of sinusoidal liver bile acid transporters during cholestasis. *Yale J. Biol. Med.* **70**, 355–363 (1997).
17. van de Steeg, E. *et al.* Organic anion transporting polypeptide 1a/1b-knockout mice provide insights into hepatic handling of bilirubin, bile acids, and drugs. *J. Clin. Invest.* **120**, 2942–2952 (2010).
18. van de Steeg, E. *et al.* Complete OATP1B1 and OATP1B3 deficiency causes human Rotor syndrome by interrupting conjugated bilirubin reuptake into the liver. *J. Clin. Invest.* **122**, 519–528 (2012).
19. Poland, R. L. & Odell, G. B. Physiologic jaundice: the enterohepatic circulation of bilirubin. *N. Engl. J. Med.* **284**, 1–6 (1971).
20. Gazzin, S., Masutti, F., Vitek, L. & Tiribelli, C. The molecular basis of jaundice: An old symptom revisited. *Liver Int. Off. J. Int. Assoc. Study Liver* (2016). doi:10.1111/liv.13351
21. Stevenson, D. K., Vreman, H. J. & Wong, R. J. Bilirubin production and the risk of bilirubin neurotoxicity. *Semin. Perinatol.* **35**, 121–126 (2011).
22. Rice, D. & Barone, S. Critical periods of vulnerability for the developing nervous system: evidence from humans and animal models. *Environ. Health Perspect.* **108 Suppl 3**, 511–533 (2000).
23. Dal Ben, M., Bottin, C., Zanconati, F., Tiribelli, C. & Gazzin, S. Evaluation of region selective bilirubin-induced brain damage as a basis for a pharmacological treatment. *Sci. Rep.* **7**, 41032 (2017).
24. Ghersi-Egea, J. F., Gazzin, S. & Strazielle, N. Blood-brain interfaces and bilirubin-induced neurological diseases. *Curr. Pharm. Des.* **15**, 2893–2907 (2009).
25. Gazzin, S., Strazielle, N., Tiribelli, C. & Ghersi-Egea, J.-F. Transport and metabolism at blood-brain interfaces and in neural cells: relevance to bilirubin-induced encephalopathy. *Front. Pharmacol.* **3**, 89 (2012).

26. Schmorl, C. Zur Kenntnis des ikterus neonatorum, insbesondere der dabei auftretenden gehirnveränderungen. *Verh Dtsch Pathol Ges* **6**, 109–115 (1904).
27. Hansen, T. W. Bilirubin oxidation in brain. *Mol. Genet. Metab.* **71**, 411–417 (2000).
28. Sawasaki, Y., Yamada, N. & Nakajima, H. Developmental features of cerebellar hypoplasia and brain bilirubin levels in a mutant (Gunn) rat with hereditary hyperbilirubinaemia. *J. Neurochem.* **27**, 577–583 (1976).
29. Hansen, T. W. Acute entry of bilirubin into rat brain regions. *Biol. Neonate* **67**, 203–207 (1995).
30. Gazzin, S. *et al.* Bilirubin accumulation and Cyp mRNA expression in selected brain regions of jaundiced Gunn rat pups. *Pediatr. Res.* **71**, 653–660 (2012).
31. Gourley, G. R. Bilirubin metabolism and kernicterus. *Adv. Pediatr.* **44**, 173–229 (1997).
32. Kawade, N. & Onishi, S. The prenatal and postnatal development of UDP-glucuronyltransferase activity towards bilirubin and the effect of premature birth on this activity in the human liver. *Biochem. J.* **196**, 257–260 (1981).
33. Ostrow, J. D., Pascolo, L., Shapiro, S. M. & Tiribelli, C. New concepts in bilirubin encephalopathy. *Eur. J. Clin. Invest.* **33**, 988–997 (2003).
34. Ostrow, J. D., Pascolo, L., Brites, D. & Tiribelli, C. Molecular basis of bilirubin-induced neurotoxicity. *Trends Mol. Med.* **10**, 65–70 (2004).
35. Tiribelli, C. & Ostrow, J. D. Intestinal flora and bilirubin. *J. Hepatol.* **42**, 170–172 (2005).
36. Shapiro, S. M. Chronic bilirubin encephalopathy: diagnosis and outcome. *Semin. Fetal. Neonatal Med.* **15**, 157–163 (2010).
37. Crigler, J. F. & Najjar, V. A. Congenital familial nonhemolytic jaundice with kernicterus; a new clinical entity. *AMA Am. J. Dis. Child.* **83**, 259–260 (1952).
38. van der Veere, C. N. *et al.* Current therapy for Crigler-Najjar syndrome type 1: report of a world registry. *Hepatol. Baltim. Md* **24**, 311–315 (1996).
39. Nguyen, T. H. *et al.* Therapeutic lentivirus-mediated neonatal in vivo gene therapy in hyperbilirubinemic Gunn rats. *Mol. Ther. J. Am. Soc. Gene Ther.* **12**, 852–859 (2005).

40. Bortolussi, G. *et al.* Rescue of bilirubin-induced neonatal lethality in a mouse model of Crigler-Najjar syndrome type I by AAV9-mediated gene transfer. *FASEB J. Off. Publ. Fed. Am. Soc. Exp. Biol.* **26**, 1052–1063 (2012).
41. Bortolussi, G. *et al.* Life-Long Correction of Hyperbilirubinemia with a Neonatal Liver-Specific AAV-Mediated Gene Transfer in a Lethal Mouse Model of Crigler-Najjar Syndrome. *Hum. Gene Ther.* **25**, 844–855 (2014).
42. Arias, I. M. Chronic unconjugated hyperbilirubinemia without overt signs of hemolysis in adolescents and adults. *J. Clin. Invest.* **41**, 2233–2245 (1962).
43. Kadakol, A. *et al.* Genetic lesions of bilirubin uridine-diphosphoglucuronate glucuronosyltransferase (UGT1A1) causing Crigler-Najjar and Gilbert syndromes: correlation of genotype to phenotype. *Hum. Mutat.* **16**, 297–306 (2000).
44. Ito, T. *et al.* Phenobarbital following phototherapy for Crigler-Najjar syndrome type II with good fetal outcome: a case report. *J. Obstet. Gynaecol. Res.* **27**, 33–35 (2001).
45. Gilbert, A. & Lereboullet, P. La cholemia simple familiale. *Semaine Med* **21**, 241–3 (1901).
46. Watchko, J. F. & Lin, Z. Exploring the genetic architecture of neonatal hyperbilirubinemia. *Semin. Fetal. Neonatal Med.* **15**, 169–175 (2010).
47. Bosma, P. J. *et al.* The genetic basis of the reduced expression of bilirubin UDP-glucuronosyltransferase 1 in Gilbert's syndrome. *N. Engl. J. Med.* **333**, 1171–1175 (1995).
48. Schwartz, H. P., Haberman, B. E. & Ruddy, R. M. Hyperbilirubinemia: current guidelines and emerging therapies. *Pediatr. Emerg. Care* **27**, 884–889 (2011).
49. Hyperbilirubinemia, S. on. Management of Hyperbilirubinemia in the Newborn Infant 35 or More Weeks of Gestation. *Pediatrics* **114**, 297–316 (2004).
50. Cremer, R. J., Perryman, P. W. & Richards, D. H. Influence of light on the hyperbilirubinaemia of infants. *Lancet Lond. Engl.* **1**, 1094–1097 (1958).
51. McDonagh, A. F. & Lightner, D. A. Phototherapy and the photobiology of bilirubin. *Semin. Liver Dis.* **8**, 272–283 (1988).
52. Stokowski, L. A. Fundamentals of phototherapy for neonatal jaundice. *Adv. Neonatal Care Off. J. Natl. Assoc. Neonatal Nurses* **11**, S10-21 (2011).

53. Xiong, T., Qu, Y., Cambier, S. & Mu, D. The side effects of phototherapy for neonatal jaundice: what do we know? What should we do? *Eur. J. Pediatr.* **170**, 1247–1255 (2011).
54. Jasprova, J. *et al.* The Biological Effects of Bilirubin Photoisomers. *PloS One* **11**, e0148126 (2016).
55. Schreuder, A. B. *et al.* Optimizing exchange transfusion for severe unconjugated hyperbilirubinemia: studies in the Gunn rat. *PloS One* **8**, e77179 (2013).
56. Behjati, S., Sagheb, S., Aryasepehr, S. & Yaghmai, B. Adverse events associated with neonatal exchange transfusion for hyperbilirubinemia. *Indian J. Pediatr.* **76**, 83–85 (2009).
57. Dennery, P. A. Pharmacological interventions for the treatment of neonatal jaundice. *Semin. Neonatol. SN* **7**, 111–119 (2002).
58. Schulz, S., Wong, R. J., Vreman, H. J. & Stevenson, D. K. Metalloporphyrins - an update. *Front. Pharmacol.* **3**, 68 (2012).
59. Brodersen, R., Lakatos, L. & Karmazsin, L. D-penicillamine, a non-bilirubin-displacing drug in neonatal jaundice. *Acta Paediatr. Scand.* **69**, 31–35 (1980).
60. Valaes, T., Kipouros, K., Petmezaki, S., Solman, M. & Doxiadis, S. A. Effectiveness and safety of prenatal phenobarbital for the prevention of neonatal jaundice. *Pediatr. Res.* **14**, 947–952 (1980).
61. Rubaltelli, F. F. Current drug treatment options in neonatal hyperbilirubinaemia and the prevention of kernicterus. *Drugs* **56**, 23–30 (1998).
62. Cuperus, F. J. C. *et al.* Effective treatment of unconjugated hyperbilirubinemia with oral bile salts in Gunn rats. *Gastroenterology* **136**, 673–682.e1 (2009).
63. Geiger, A. S., Rice, A. C. & Shapiro, S. M. Minocycline blocks acute bilirubin-induced neurological dysfunction in jaundiced Gunn rats. *Neonatology* **92**, 219–226 (2007).
64. Rice, A. C., Chiou, V. L., Zuckoff, S. B. & Shapiro, S. M. Profile of minocycline neuroprotection in bilirubin-induced auditory system dysfunction. *Brain Res.* **1368**, 290–298 (2011).
65. Gunn, C. K. Hereditary Acholuric Jaundice in the Rat. *Can. Med. Assoc. J.* **50**, 230–237 (1944).
66. Chowdhury, J. R., Kondapalli, R. & Chowdhury, N. R. Gunn rat: a model for inherited deficiency of bilirubin glucuronidation. *Adv. Vet. Sci. Comp. Med.* **37**, 149–173 (1993).

67. Ciotti, M., Chen, F., Rubaltelli, F. F. & Owens, I. S. Coding defect and a TATA box mutation at the bilirubin UDP-glucuronosyltransferase gene cause Crigler-Najjar type I disease. *Biochim. Biophys. Acta* **1407**, 40–50 (1998).
68. Johnson, J. A., Hayward, J. J., Kornguth, S. E. & Siegel, F. L. Effects of hyperbilirubinaemia on glutathione S-transferase isoenzymes in cerebellar cortex of the Gunn rat. *Biochem. J.* **291 (Pt 2)**, 453–461 (1993).
69. Yeary, R. A. & Grothaus, R. H. The Gunn rat as an animal model in comparative medicine. *Lab. Anim. Sci.* **21**, 362–366 (1971).
70. Stobie, P. E., Hansen, C. T., Hailey, J. R. & Levine, R. L. A difference in mortality between two strains of jaundiced rats. *Pediatrics* **87**, 88–93 (1991).
71. Leyten, R., Vroemen, J. P., Blanckaert, N. & Heirwegh, K. P. The congenic normal R/APfd and jaundiced R/APfd-j/j rat strains: a new animal model of hereditary non-haemolytic unconjugated hyperbilirubinaemia due to defective bilirubin conjugation. *Lab. Anim.* **20**, 335–342 (1986).
72. Johnson, L., Sarmiento, F., Blanc, W. A. & Day, R. Kernicterus in rats with an inherited deficiency of glucuronyl transferase. *AMA J. Dis. Child.* **97**, 591–608 (1959).
73. Keino, H. & Kashiwamata, S. Critical period of bilirubin-induced cerebellar hypoplasia in a new Sprague-Dawley strain of jaundiced Gunn rats. *Neurosci. Res.* **6**, 209–215 (1989).
74. Conlee, J. W. & Shapiro, S. M. Development of cerebellar hypoplasia in jaundiced Gunn rats: a quantitative light microscopic analysis. *Acta Neuropathol. (Berl.)* **93**, 450–460 (1997).
75. Takagishi, Y. & Yamamura, H. Purkinje cell abnormalities and synaptogenesis in genetically jaundiced rats (Gunn rats). *Brain Res.* **492**, 116–128 (1989).
76. Yamamura, H. & Takagishi, Y. Cerebellar hypoplasia in the hyperbilirubinemic Gunn rat: morphological aspects. *Nagoya J. Med. Sci.* **55**, 11–21 (1993).
77. Altman, J. & Das, G. D. Autoradiographic and histological studies of postnatal neurogenesis. I. A longitudinal investigation of the kinetics, migration and transformation of cells incorporating tritiated thymidine in neonate rats, with special reference to postnatal neurogenesis in some brain regions. *J. Comp. Neurol.* **126**, 337–389 (1966).

78. Schutta, H. S. & Johnson, L. Bilirubin encephalopathy in the Gunn rat: a fine structure study of the cerebellar cortex. *J. Neuropathol. Exp. Neurol.* **26**, 377–396 (1967).
79. Robert, M. C. *et al.* Alterations in the cell cycle in the cerebellum of hyperbilirubinemic Gunn rat: a possible link with apoptosis? *PloS One* **8**, e79073 (2013).
80. Brito, M. A. *et al.* Cerebellar axon/myelin loss, angiogenic sprouting, and neuronal increase of vascular endothelial growth factor in a preterm infant with kernicterus. *J. Child Neurol.* **27**, 615–624 (2012).
81. Nguyen, N. *et al.* Disruption of the *ugt1* locus in mice resembles human Crigler-Najjar type I disease. *J. Biol. Chem.* **283**, 7901–7911 (2008).
82. Silva, R. F. M., Rodrigues, C. M. P. & Brites, D. Rat cultured neuronal and glial cells respond differently to toxicity of unconjugated bilirubin. *Pediatr. Res.* **51**, 535–541 (2002).
83. Brito, M. A. *et al.* Unconjugated bilirubin differentially affects the redox status of neuronal and astroglial cells. *Neurobiol. Dis.* **29**, 30–40 (2008).
84. Qaisiya, M. *et al.* Bilirubin-induced ER stress contributes to the inflammatory response and apoptosis in neuronal cells. *Arch. Toxicol.* (2016). doi:10.1007/s00204-016-1835-3
85. Watchko, J. F. Kernicterus and the molecular mechanisms of bilirubin-induced CNS injury in newborns. *Neuromolecular Med.* **8**, 513–529 (2006).
86. Falcão, A. S. *et al.* Apoptosis and impairment of neurite network by short exposure of immature rat cortical neurons to unconjugated bilirubin increase with cell differentiation and are additionally enhanced by an inflammatory stimulus. *J. Neurosci. Res.* **85**, 1229–1239 (2007).
87. Fernandes, A. *et al.* Bilirubin as a determinant for altered neurogenesis, neuritogenesis, and synaptogenesis. *Dev. Neurobiol.* **69**, 568–582 (2009).
88. Chang, F.-Y., Lee, C.-C., Huang, C.-C. & Hsu, K.-S. Unconjugated bilirubin exposure impairs hippocampal long-term synaptic plasticity. *PloS One* **4**, e5876 (2009).
89. Silva, S. L. *et al.* Features of bilirubin-induced reactive microglia: from phagocytosis to inflammation. *Neurobiol. Dis.* **40**, 663–675 (2010).
90. Silva, S. L. *et al.* Neuritic growth impairment and cell death by unconjugated bilirubin is mediated by NO and glutamate, modulated by microglia, and prevented by glycoconjugated deoxycholic acid and interleukin-10. *Neuropharmacology* **62**, 2398–2408 (2012).

91. Brites, D. The evolving landscape of neurotoxicity by unconjugated bilirubin: role of glial cells and inflammation. *Front. Pharmacol.* **3**, 88 (2012).
92. Barateiro, A., Domingues, H. S., Fernandes, A., Relvas, J. B. & Brites, D. Rat cerebellar slice cultures exposed to bilirubin evidence reactive gliosis, excitotoxicity and impaired myelinogenesis that is prevented by AMPA and TNF- α inhibitors. *Mol. Neurobiol.* **49**, 424–439 (2014).
93. Brites, D. & Fernandes, A. Bilirubin-induced neural impairment: A special focus on myelination, age-related windows of susceptibility and associated co-morbidities. *Semin. Fetal. Neonatal Med.* (2014). doi:10.1016/j.siny.2014.12.002
94. Barateiro, A. *et al.* Reduced Myelination and Increased Glia Reactivity Resulting from Severe Neonatal Hyperbilirubinemia. *Mol. Pharmacol.* **89**, 84–93 (2016).
95. Zucker, S. D., Goessling, W., Bootle, E. J. & Sterritt, C. Localization of bilirubin in phospholipid bilayers by parallax analysis of fluorescence quenching. *J. Lipid Res.* **42**, 1377–1388 (2001).
96. Hansen, T., Tommarello, S. & Allen, J. Subcellular localization of bilirubin in rat brain after in vivo i.v. administration of [3 H]bilirubin. *Pediatr. Res.* **49**, 203–207 (2001).
97. Barateiro, A. *et al.* Unconjugated bilirubin restricts oligodendrocyte differentiation and axonal myelination. *Mol. Neurobiol.* **47**, 632–644 (2013).
98. Brito, M. A., Brites, D. & Butterfield, D. A. A link between hyperbilirubinemia, oxidative stress and injury to neocortical synaptosomes. *Brain Res.* **1026**, 33–43 (2004).
99. Brito, M. A. *et al.* Bilirubin injury to neurons: contribution of oxidative stress and rescue by glycoconjugated deoxycholic acid. *Neurotoxicology* **29**, 259–269 (2008).
100. Qaisiya, M., Coda Zabetta, C. D., Bellarosa, C. & Tiribelli, C. Bilirubin mediated oxidative stress involves antioxidant response activation via Nrf2 pathway. *Cell. Signal.* **26**, 512–520 (2014).
101. McDonald, J. W., Shapiro, S. M., Silverstein, F. S. & Johnston, M. V. Role of glutamate receptor-mediated excitotoxicity in bilirubin-induced brain injury in the Gunn rat model. *Exp. Neurol.* **150**, 21–29 (1998).
102. Grojean, S., Koziel, V., Vert, P. & Daval, J. L. Bilirubin induces apoptosis via activation of NMDA receptors in developing rat brain neurons. *Exp. Neurol.* **166**, 334–341 (2000).

103. Brito, M. A. *et al.* N-methyl-aspartate receptor and neuronal nitric oxide synthase activation mediate bilirubin-induced neurotoxicity. *Mol. Med. Camb. Mass* **16**, 372–380 (2010).
104. Rodrigues, C. M. P., Solá, S. & Brites, D. Bilirubin induces apoptosis via the mitochondrial pathway in developing rat brain neurons. *Hepatology. Baltim. Md* **35**, 1186–1195 (2002).
105. Gazzin, S. *et al.* Differential expression of the multidrug resistance-related proteins ABCB1 and ABCG1 between blood-brain interfaces. *J. Comp. Neurol.* **510**, 497–507 (2008).
106. Gazzin, S. *et al.* Modulation of Mrp1 (ABCG1) and Pgp (ABCB1) by bilirubin at the blood-CSF and blood-brain barriers in the Gunn rat. *PLoS One* **6**, e16165 (2011).
107. Giraudi, P. J., Bellarosa, C., Coda-Zabetta, C. D., Peruzzo, P. & Tiribelli, C. Functional induction of the cystine-glutamate exchanger system Xc(-) activity in SH-SY5Y cells by unconjugated bilirubin. *PLoS One* **6**, e29078 (2011).
108. Gambaro, S. E., Robert, M. C., Tiribelli, C. & Gazzin, S. Role of brain cytochrome P450 mono-oxygenases in bilirubin oxidation-specific induction and activity. *Arch. Toxicol.* (2014).
doi:10.1007/s00204-014-1394-4
109. Deganuto, M. *et al.* A proteomic approach to the bilirubin-induced toxicity in neuronal cells reveals a protective function of DJ-1 protein. *Proteomics* **10**, 1645–1657 (2010).
110. Calligaris, R. *et al.* A transcriptome analysis identifies molecular effectors of unconjugated bilirubin in human neuroblastoma SH-SY5Y cells. *BMC Genomics* **10**, 543 (2009).
111. Barateiro, A., Vaz, A. R., Silva, S. L., Fernandes, A. & Brites, D. ER stress, mitochondrial dysfunction and calpain/JNK activation are involved in oligodendrocyte precursor cell death by unconjugated bilirubin. *Neuromolecular Med.* **14**, 285–302 (2012).
112. Basu, S., De, D., Dev Khanna, H. & Kumar, A. Lipid peroxidation, DNA damage and total antioxidant status in neonatal hyperbilirubinemia. *J. Perinatol. Off. J. Calif. Perinat. Assoc.* **34**, 519–523 (2014).
113. Falcão, A. S., Fernandes, A., Brito, M. A., Silva, R. F. M. & Brites, D. *Acta Neuropathol. (Berl.)* **112**, 95–105 (2006).
114. Weinhold, B. Epigenetics: The Science of Change. *Environ. Health Perspect.* **114**, A160–A167 (2006).
115. Szyf, M. Prospects for the development of epigenetic drugs for CNS conditions. *Nat. Rev. Drug Discov.* **14**, 461–474 (2015).

116. Gräff, J., Kim, D., Dobbin, M. M. & Tsai, L.-H. Epigenetic regulation of gene expression in physiological and pathological brain processes. *Physiol. Rev.* **91**, 603–649 (2011).
117. Berdasco, M. & Esteller, M. Genetic syndromes caused by mutations in epigenetic genes. *Hum. Genet.* **132**, 359–383 (2013).
118. Kouzarides, T. Chromatin modifications and their function. *Cell* **128**, 693–705 (2007).
119. Taverna, S. D., Li, H., Ruthenburg, A. J., Allis, C. D. & Patel, D. J. How chromatin-binding modules interpret histone modifications: lessons from professional pocket pickers. *Nat. Struct. Mol. Biol.* **14**, 1025–1040 (2007).
120. Dulac, C. Brain function and chromatin plasticity. *Nature* **465**, 728–735 (2010).
121. Luger, K., Mäder, A. W., Richmond, R. K., Sargent, D. F. & Richmond, T. J. Crystal structure of the nucleosome core particle at 2.8 Å resolution. *Nature* **389**, 251–260 (1997).
122. Davey, C. A., Sargent, D. F., Luger, K., Maeder, A. W. & Richmond, T. J. Solvent mediated interactions in the structure of the nucleosome core particle at 1.9 Å resolution. *J. Mol. Biol.* **319**, 1097–1113 (2002).
123. Jenuwein, T. & Allis, C. D. Translating the histone code. *Science* **293**, 1074–1080 (2001).
124. Berger, S. L. Histone modifications in transcriptional regulation. *Curr. Opin. Genet. Dev.* **12**, 142–148 (2002).
125. Crosio, C., Heitz, E., Allis, C. D., Borrelli, E. & Sassone-Corsi, P. Chromatin remodeling and neuronal response: multiple signaling pathways induce specific histone H3 modifications and early gene expression in hippocampal neurons. *J. Cell Sci.* **116**, 4905–4914 (2003).
126. Fagiolini, M., Jensen, C. L. & Champagne, F. A. Epigenetic influences on brain development and plasticity. *Curr. Opin. Neurobiol.* **19**, 207–212 (2009).
127. Narayan, P. J. & Dragunow, M. High content analysis of histone acetylation in human cells and tissues. *J. Neurosci. Methods* **193**, 54–61 (2010).
128. Houston, I. *et al.* Epigenetics in the human brain. *Neuropsychopharmacol. Off. Publ. Am. Coll. Neuropsychopharmacol.* **38**, 183–197 (2013).
129. Lilja, T., Heldring, N. & Hermanson, O. Like a rolling histone: epigenetic regulation of neural stem cells and brain development by factors controlling histone acetylation and methylation. *Biochim. Biophys. Acta* **1830**, 2354–2360 (2013).

130. Zhao, Y.-Q., Jordan, I. K. & Lunyak, V. V. Epigenetics components of aging in the central nervous system. *Neurother. J. Am. Soc. Exp. Neurother.* **10**, 647–663 (2013).
131. Yao, B. *et al.* Epigenetic mechanisms in neurogenesis. *Nat. Rev. Neurosci.* **17**, 537–549 (2016).
132. Sterner, D. E. & Berger, S. L. Acetylation of histones and transcription-related factors. *Microbiol. Mol. Biol. Rev. MMBR* **64**, 435–459 (2000).
133. Marks, P. A., Miller, T. & Richon, V. M. Histone deacetylases. *Curr. Opin. Pharmacol.* **3**, 344–351 (2003).
134. Brownell, J. E. & Allis, C. D. Special HATs for special occasions: linking histone acetylation to chromatin assembly and gene activation. *Curr. Opin. Genet. Dev.* **6**, 176–184 (1996).
135. Imhof, A. & Wolffe, A. P. Transcription: gene control by targeted histone acetylation. *Curr. Biol. CB* **8**, R422–424 (1998).
136. Mizzen, C. A. & Allis, C. D. Linking histone acetylation to transcriptional regulation. *Cell. Mol. Life Sci. CMLS* **54**, 6–20 (1998).
137. Turner, B. M. Histone acetylation as an epigenetic determinant of long-term transcriptional competence. *Cell. Mol. Life Sci. CMLS* **54**, 21–31 (1998).
138. Struhl, K. Histone acetylation and transcriptional regulatory mechanisms. *Genes Dev.* **12**, 599–606 (1998).
139. Fukuda, H., Sano, N., Muto, S. & Horikoshi, M. Simple histone acetylation plays a complex role in the regulation of gene expression. *Brief. Funct. Genomic. Proteomic.* **5**, 190–208 (2006).
140. Bell, K. F. S. *et al.* Neuronal development is promoted by weakened intrinsic antioxidant defences due to epigenetic repression of Nrf2. *Nat. Commun.* **6**, 7066 (2015).
141. Maze, I., Noh, K.-M. & Allis, C. D. Histone regulation in the CNS: basic principles of epigenetic plasticity. *Neuropsychopharmacol. Off. Publ. Am. Coll. Neuropsychopharmacol.* **38**, 3–22 (2013).
142. Gräff, J. & Tsai, L.-H. Histone acetylation: molecular mnemonics on the chromatin. *Nat. Rev. Neurosci.* **14**, 97–111 (2013).
143. Shein, N. A. & Shohami, E. Histone deacetylase inhibitors as therapeutic agents for acute central nervous system injuries. *Mol. Med. Camb. Mass* **17**, 448–456 (2011).

144. Gu, X., Sun, J., Li, S., Wu, X. & Li, L. Oxidative stress induces DNA demethylation and histone acetylation in SH-SY5Y cells: potential epigenetic mechanisms in gene transcription in A β production. *Neurobiol. Aging* **34**, 1069–1079 (2013).
145. Lu, X. *et al.* Histone acetyltransferase p300 mediates histone acetylation of PS1 and BACE1 in a cellular model of Alzheimer's disease. *PloS One* **9**, e103067 (2014).
146. Narayan, P. J., Lill, C., Faull, R., Curtis, M. A. & Dragunow, M. Increased acetyl and total histone levels in post-mortem Alzheimer's disease brain. *Neurobiol. Dis.* **74**, 281–294 (2015).
147. Sun, W. *et al.* Histone Acetylome-wide Association Study of Autism Spectrum Disorder. *Cell* **167**, 1385–1397.e11 (2016).
148. López, A. J. & Wood, M. A. Role of nucleosome remodeling in neurodevelopmental and intellectual disability disorders. *Front. Behav. Neurosci.* **9**, 100 (2015).
149. Küçükali, C. İ., Kürtüncü, M., Çoban, A., Çebi, M. & Tüzün, E. Epigenetics of multiple sclerosis: an updated review. *Neuromolecular Med.* **17**, 83–96 (2015).
150. Janssen, C. *et al.* Differential histone deacetylase mRNA expression patterns in amyotrophic lateral sclerosis. *J. Neuropathol. Exp. Neurol.* **69**, 573–581 (2010).
151. Jin, H. *et al.* Histone Hyperacetylation Up-regulates Protein Kinase C δ in Dopaminergic Neurons to Induce Cell Death: RELEVANCE TO EPIGENETIC MECHANISMS OF NEURODEGENERATION IN PARKINSON DISEASE. *J. Biol. Chem.* **289**, 34743–34767 (2014).
152. Gebremedhin, K. G. & Rademacher, D. J. Histone H3 acetylation in the postmortem Parkinson's disease primary motor cortex. *Neurosci. Lett.* **627**, 121–125 (2016).
153. Park, G. *et al.* Regulation of Histone Acetylation by Autophagy in Parkinson Disease. *J. Biol. Chem.* **291**, 3531–3540 (2016).
154. Gao, W.-M. *et al.* Immunohistochemical analysis of histone H3 acetylation and methylation--evidence for altered epigenetic signaling following traumatic brain injury in immature rats. *Brain Res.* **1070**, 31–34 (2006).
155. Sadri-Vakili, G. *et al.* Histones associated with downregulated genes are hypo-acetylated in Huntington's disease models. *Hum. Mol. Genet.* **16**, 1293–1306 (2007).

156. Stack, E. C. *et al.* Modulation of nucleosome dynamics in Huntington's disease. *Hum. Mol. Genet.* **16**, 1164–1175 (2007).
157. Lee, J., Hwang, Y. J., Ryu, H., Kowall, N. W. & Ryu, H. Nucleolar dysfunction in Huntington's disease. *Biochim. Biophys. Acta* **1842**, 785–790 (2014).
158. Rai, M. *et al.* HDAC inhibitors correct frataxin deficiency in a Friedreich ataxia mouse model. *PLoS One* **3**, e1958 (2008).
159. Soragni, E. *et al.* Epigenetic therapy for Friedreich ataxia. *Ann. Neurol.* **76**, 489–508 (2014).
160. Shahbazian, M. *et al.* Mice with truncated MeCP2 recapitulate many Rett syndrome features and display hyperacetylation of histone H3. *Neuron* **35**, 243–254 (2002).
161. Urdinguio, R. G., Pino, I., Ropero, S., Fraga, M. F. & Esteller, M. Histone H3 and H4 modification profiles in a Rett syndrome mouse model. *Epigenetics Off. J. DNA Methylation Soc.* **2**, 11–14 (2007).
162. Adachi, M., Autry, A. E., Covington, H. E. & Monteggia, L. M. MeCP2-mediated transcription repression in the basolateral amygdala may underlie heightened anxiety in a mouse model of Rett syndrome. *J. Neurosci. Off. J. Soc. Neurosci.* **29**, 4218–4227 (2009).
163. Alam, M. S., Getz, M. & Haldar, K. Chronic administration of an HDAC inhibitor treats both neurological and systemic Niemann-Pick type C disease in a mouse model. *Sci. Transl. Med.* **8**, 326ra23 (2016).
164. Chen, Y., Sharma, R. P., Costa, R. H., Costa, E. & Grayson, D. R. On the epigenetic regulation of the human reelin promoter. *Nucleic Acids Res.* **30**, 2930–2939 (2002).
165. Tremolizzo, L. *et al.* An epigenetic mouse model for molecular and behavioral neuropathologies related to schizophrenia vulnerability. *Proc. Natl. Acad. Sci. U. S. A.* **99**, 17095–17100 (2002).
166. Tsankova, N. M. *et al.* Sustained hippocampal chromatin regulation in a mouse model of depression and antidepressant action. *Nat. Neurosci.* **9**, 519–525 (2006).
167. Tsankova, N., Renthal, W., Kumar, A. & Nestler, E. J. Epigenetic regulation in psychiatric disorders. *Nat. Rev. Neurosci.* **8**, 355–367 (2007).
168. Tang, B., Dean, B. & Thomas, E. A. Disease- and age-related changes in histone acetylation at gene promoters in psychiatric disorders. *Transl. Psychiatry* **1**, e64 (2011).
169. Mai, A. *et al.* Small-molecule inhibitors of histone acetyltransferase activity: identification and biological properties. *J. Med. Chem.* **49**, 6897–6907 (2006).

170. Ganai, S. A., Ramadoss, M. & Mahadevan, V. Histone Deacetylase (HDAC) Inhibitors - emerging roles in neuronal memory, learning, synaptic plasticity and neural regeneration. *Curr. Neuropharmacol.* **14**, 55–71 (2016).
171. Dokmanovic, M., Clarke, C. & Marks, P. A. Histone deacetylase inhibitors: overview and perspectives. *Mol. Cancer Res. MCR* **5**, 981–989 (2007).
172. Kazantsev, A. G. & Thompson, L. M. Therapeutic application of histone deacetylase inhibitors for central nervous system disorders. *Nat. Rev. Drug Discov.* **7**, 854–868 (2008).
173. Abel, T. & Zukin, R. S. Epigenetic targets of HDAC inhibition in neurodegenerative and psychiatric disorders. *Curr. Opin. Pharmacol.* **8**, 57–64 (2008).
174. Grayson, D. R., Kundakovic, M. & Sharma, R. P. Is there a future for histone deacetylase inhibitors in the pharmacotherapy of psychiatric disorders? *Mol. Pharmacol.* **77**, 126–135 (2010).
175. Fischer, A., Sananbenesi, F., Mungenast, A. & Tsai, L.-H. Targeting the correct HDAC(s) to treat cognitive disorders. *Trends Pharmacol. Sci.* **31**, 605–617 (2010).
176. Zwergel, Clemens, Stazi, G. & Mai, S. V. and A. Histone Deacetylase Inhibitors: Updated Studies in Various Epigenetic-Related Diseases. *J. Clin. Epigenetics* (2016).
177. Schneider, A. *et al.* Acetyltransferases (HATs) as targets for neurological therapeutics. *Neurother. J. Am. Soc. Exp. Neurother.* **10**, 568–588 (2013).
178. Gao, C. *et al.* Rational design and validation of a Tip60 histone acetyltransferase inhibitor. *Sci. Rep.* **4**, 5372 (2014).
179. Wapenaar, H. & Dekker, F. J. Histone acetyltransferases: challenges in targeting bi-substrate enzymes. *Clin. Epigenetics* **8**, 59 (2016).
180. West, A. C. & Johnstone, R. W. New and emerging HDAC inhibitors for cancer treatment. *J. Clin. Invest.* **124**, 30–39 (2014).
181. Ververis, K., Hiong, A., Karagiannis, T. C. & Licciardi, P. V. Histone deacetylase inhibitors (HDACIs): multitargeted anticancer agents. *Biol. Targets Ther.* **7**, 47–60 (2013).
182. Gryder, B. E., Sodji, Q. H. & Oyelere, A. K. Targeted cancer therapy: giving histone deacetylase inhibitors all they need to succeed. *Future Med. Chem.* **4**, 505–524 (2012).

183. Liu, D. *et al.* Nicotinamide forestalls pathology and cognitive decline in Alzheimer mice: evidence for improved neuronal bioenergetics and autophagy procession. *Neurobiol. Aging* **34**, 1564–1580 (2013).
184. Kilgore, M. *et al.* Inhibitors of class 1 histone deacetylases reverse contextual memory deficits in a mouse model of Alzheimer’s disease. *Neuropsychopharmacol. Off. Publ. Am. Coll. Neuropsychopharmacol.* **35**, 870–880 (2010).
185. Wu, X. *et al.* Histone deacetylase inhibitors up-regulate astrocyte GDNF and BDNF gene transcription and protect dopaminergic neurons. *Int. J. Neuropsychopharmacol. Off. Sci. J. Coll. Int. Neuropsychopharmacol. CINP* **11**, 1123–1134 (2008).
186. Kidd, S. K. & Schneider, J. S. Protective effects of valproic acid on the nigrostriatal dopamine system in a 1-methyl-4-phenyl-1,2,3,6-tetrahydropyridine mouse model of Parkinson’s disease. *Neuroscience* **194**, 189–194 (2011).
187. Sharma, S., Taliyan, R. & Singh, S. Beneficial effects of sodium butyrate in 6-OHDA induced neurotoxicity and behavioral abnormalities: Modulation of histone deacetylase activity. *Behav. Brain Res.* **291**, 306–314 (2015).
188. Yoo, Y.-E. & Ko, C.-P. Treatment with trichostatin A initiated after disease onset delays disease progression and increases survival in a mouse model of amyotrophic lateral sclerosis. *Exp. Neurol.* **231**, 147–159 (2011).
189. Lee, J. *et al.* Therapeutic targeting of epigenetic components in amyotrophic lateral sclerosis (ALS). *Curr. Med. Chem.* **21**, 3576–3582 (2014).
190. Kim, H. J. *et al.* Histone deacetylase inhibitors exhibit anti-inflammatory and neuroprotective effects in a rat permanent ischemic model of stroke: multiple mechanisms of action. *J. Pharmacol. Exp. Ther.* **321**, 892–901 (2007).
191. Kim, H. J., Leeds, P. & Chuang, D.-M. The HDAC inhibitor, sodium butyrate, stimulates neurogenesis in the ischemic brain. *J. Neurochem.* **110**, 1226–1240 (2009).
192. Langley, B., Brochier, C. & Riviuccio, M. A. Targeting histone deacetylases as a multifaceted approach to treat the diverse outcomes of stroke. *Stroke J. Cereb. Circ.* **40**, 2899–2905 (2009).

193. Fleiss, B., Nilsson, M. K. L., Blomgren, K. & Mallard, C. Neuroprotection by the histone deacetylase inhibitor trichostatin A in a model of lipopolysaccharide-sensitized neonatal hypoxic-ischaemic brain injury. *J. Neuroinflammation* **9**, 70 (2012).
194. Zhang, B. *et al.* HDAC inhibitor increases histone H3 acetylation and reduces microglia inflammatory response following traumatic brain injury in rats. *Brain Res.* **1226**, 181–191 (2008).
195. Dash, P. K., Orsi, S. A. & Moore, A. N. Histone deacetylase inhibition combined with behavioral therapy enhances learning and memory following traumatic brain injury. *Neuroscience* **163**, 1–8 (2009).
196. Shein, N. A. *et al.* Histone deacetylase inhibitor ITF2357 is neuroprotective, improves functional recovery, and induces glial apoptosis following experimental traumatic brain injury. *FASEB J. Off. Publ. Fed. Am. Soc. Exp. Biol.* **23**, 4266–4275 (2009).
197. Dash, P. K. *et al.* Valproate administered after traumatic brain injury provides neuroprotection and improves cognitive function in rats. *PloS One* **5**, e11383 (2010).
198. Thomas, E. A. *et al.* The HDAC inhibitor 4b ameliorates the disease phenotype and transcriptional abnormalities in Huntington's disease transgenic mice. *Proc. Natl. Acad. Sci. U. S. A.* **105**, 15564–15569 (2008).
199. Ferrante, R. J. *et al.* Histone deacetylase inhibition by sodium butyrate chemotherapy ameliorates the neurodegenerative phenotype in Huntington's disease mice. *J. Neurosci. Off. J. Soc. Neurosci.* **23**, 9418–9427 (2003).
200. Jia, H. *et al.* The Effects of Pharmacological Inhibition of Histone Deacetylase 3 (HDAC3) in Huntington's Disease Mice. *PloS One* **11**, e0152498 (2016).
201. Kratsman, N., Getselter, D. & Elliott, E. Sodium butyrate attenuates social behavior deficits and modifies the transcription of inhibitory/excitatory genes in the frontal cortex of an autism model. *Neuropharmacology* **102**, 136–145 (2016).
202. Foley, A. G., Cassidy, A. W. & Regan, C. M. Pentyl-4-yn-VPA, a histone deacetylase inhibitor, ameliorates deficits in social behavior and cognition in a rodent model of autism spectrum disorders. *Eur. J. Pharmacol.* **727**, 80–86 (2014).

203. Xu, X., Kozikowski, A. P. & Pozzo-Miller, L. A selective histone deacetylase-6 inhibitor improves BDNF trafficking in hippocampal neurons from Mecp2 knockout mice: implications for Rett syndrome. *Front. Cell. Neurosci.* **8**, 68 (2014).
204. Doumas, B. T. *et al.* Candidate reference method for determination of total bilirubin in serum: development and validation. *Clin. Chem.* **31**, 1779–1789 (1985).
205. Smith, P. K. *et al.* Measurement of protein using bicinchoninic acid. *Anal. Biochem.* **150**, 76–85 (1985).
206. Pickrell, J. K. *et al.* Understanding mechanisms underlying human gene expression variation with RNA sequencing. *Nature* **464**, 768–772 (2010).
207. Pfaffl, M. W. A new mathematical model for relative quantification in real-time RT-PCR. *Nucleic Acids Res.* **29**, e45 (2001).
208. Langmead, B. & Salzberg, S. L. Fast gapped-read alignment with Bowtie 2. *Nat. Methods* **9**, 357–359 (2012).
209. Zhang, Y. *et al.* Model-based analysis of ChIP-Seq (MACS). *Genome Biol.* **9**, R137 (2008).
210. Heinz, S. *et al.* Simple combinations of lineage-determining transcription factors prime cis-regulatory elements required for macrophage and B cell identities. *Mol. Cell* **38**, 576–589 (2010).
211. Kanherkar, R. R., Bhatia-Dey, N. & Csoka, A. B. Epigenetics across the human lifespan. *Front. Cell Dev. Biol.* **2**, 49 (2014).
212. Bandeira, F., Lent, R. & Herculano-Houzel, S. Changing numbers of neuronal and non-neuronal cells underlie postnatal brain growth in the rat. *Proc. Natl. Acad. Sci. U. S. A.* **106**, 14108–14113 (2009).
213. Altman, J. Postnatal development of the cerebellar cortex in the rat. II. Phases in the maturation of Purkinje cells and of the molecular layer. *J. Comp. Neurol.* **145**, 399–463 (1972).
214. Tabarki, B., Khalifa, M., Yacoub, M., Tlili, K. & Essoussi, A. S. Cerebellar symptoms heralding bilirubin encephalopathy in Crigler-Najjar syndrome. *Pediatr. Neurol.* **27**, 234–236 (2002).
215. Watchko, J. F., Painter, M. J. & Panigrahy, A. Are the neuromotor disabilities of bilirubin-induced neurologic dysfunction disorders related to the cerebellum and its connections? *Semin. Fetal. Neonatal Med.* **20**, 47–51 (2015).
216. Haustein, M. D. *et al.* Acute hyperbilirubinaemia induces presynaptic neurodegeneration at a central glutamatergic synapse. *J. Physiol.* **588**, 4683–4693 (2010).

217. Spencer, R. F., Shaia, W. T., Gleason, A. T., Sismanis, A. & Shapiro, S. M. Changes in calcium-binding protein expression in the auditory brainstem nuclei of the jaundiced Gunn rat. *Hear. Res.* **171**, 129–141 (2002).
218. Song, S., Hu, Y., Gu, X., Si, F. & Hua, Z. A novel newborn rat kernicterus model created by injecting a bilirubin solution into the cisterna magna. *PLoS One* **9**, e96171 (2014).
219. Hansen, T. W., Bratlid, D. & Walaas, S. I. Bilirubin decreases phosphorylation of synapsin I, a synaptic vesicle-associated neuronal phosphoprotein, in intact synaptosomes from rat cerebral cortex. *Pediatr. Res.* **23**, 219–223 (1988).
220. Zhang, L., Liu, W., Tanswell, A. K. & Luo, X. The effects of bilirubin on evoked potentials and long-term potentiation in rat hippocampus in vivo. *Pediatr. Res.* **53**, 939–944 (2003).
221. Liaury, K. *et al.* Morphological features of microglial cells in the hippocampal dentate gyrus of Gunn rat: a possible schizophrenia animal model. *J. Neuroinflammation* **9**, 56 (2012).
222. Akinpelu, O. V., Waissbluth, S. & Daniel, S. J. Auditory risk of hyperbilirubinemia in term newborns: a systematic review. *Int. J. Pediatr. Otorhinolaryngol.* **77**, 898–905 (2013).
223. Schreuder, A. B. *et al.* Albumin administration protects against bilirubin-induced auditory brainstem dysfunction in Gunn rat pups. *Liver Int. Off. J. Int. Assoc. Study Liver* **33**, 1557–1565 (2013).
224. Agrawal, V. K., Shukla, R., Misra, P. K., Kapoor, R. K. & Malik, G. K. Brainstem auditory evoked response in newborns with hyperbilirubinemia. *Indian Pediatr.* **35**, 513–518 (1998).
225. Sharma, P. *et al.* Brainstem evoked response audiometry (BAER) in neonates with hyperbilirubinemia. *Indian J. Pediatr.* **73**, 413–416 (2006).
226. Hachiya, Y. & Hayashi, M. Bilirubin encephalopathy: a study of neuronal subpopulations and neurodegenerative mechanisms in 12 autopsy cases. *Brain Dev.* **30**, 269–278 (2008).
227. Shapiro, S. M. Definition of the clinical spectrum of kernicterus and bilirubin-induced neurologic dysfunction (BIND). *J. Perinatol. Off. J. Calif. Perinat. Assoc.* **25**, 54–59 (2005).
228. Vaz, A. R. *et al.* Selective vulnerability of rat brain regions to unconjugated bilirubin. *Mol. Cell. Neurosci.* **48**, 82–93 (2011).
229. Fernandes, A. *et al.* Inflammatory signalling pathways involved in astroglial activation by unconjugated bilirubin. *J. Neurochem.* **96**, 1667–1679 (2006).

230. Falcão, A. S., Fernandes, A., Brito, M. A., Silva, R. F. M. & Brites, D. Bilirubin-induced inflammatory response, glutamate release, and cell death in rat cortical astrocytes are enhanced in younger cells. *Neurobiol. Dis.* **20**, 199–206 (2005).
231. Hu, W. *et al.* Ex vivo (1)H nuclear magnetic resonance spectroscopy reveals systematic alterations in cerebral metabolites as the key pathogenetic mechanism of bilirubin encephalopathy. *Mol. Brain* **7**, 87 (2014).
232. Gürses, D., Kiliç, I. & Sahiner, T. Effects of hyperbilirubinemia on cerebrocortical electrical activity in newborns. *Pediatr. Res.* **52**, 125–130 (2002).
233. Ayarpadikannan, S. & Kim, H.-S. The impact of transposable elements in genome evolution and genetic instability and their implications in various diseases. *Genomics Inform.* **12**, 98–104 (2014).
234. Charlesworth, B., Sniegowski, P. & Stephan, W. The evolutionary dynamics of repetitive DNA in eukaryotes. *Nature* **371**, 215–220 (1994).
235. Nishibuchi, G. & Déjardin, J. The molecular basis of the organization of repetitive DNA-containing constitutive heterochromatin in mammals. *Chromosome Res. Int. J. Mol. Supramol. Evol. Asp. Chromosome Biol.* (2017). doi:10.1007/s10577-016-9547-3
236. Maze, I. *et al.* Cocaine dynamically regulates heterochromatin and repetitive element unsilencing in nucleus accumbens. *Proc. Natl. Acad. Sci. U. S. A.* **108**, 3035–3040 (2011).
237. Wood, J. G. & Helfand, S. L. Chromatin structure and transposable elements in organismal aging. *Front. Genet.* **4**, 274 (2013).
238. Ryu, S. H., Kang, K., Yoo, T., Joe, C. O. & Chung, J. H. Transcriptional repression of repeat-derived transcripts correlates with histone hypoacetylation at repetitive DNA elements in aged mice brain. *Exp. Gerontol.* **46**, 811–818 (2011).
239. Neven, K. Y. *et al.* Repetitive element hypermethylation in multiple sclerosis patients. *BMC Genet.* **17**, 84 (2016).
240. Bollati, V. *et al.* DNA methylation in repetitive elements and Alzheimer disease. *Brain. Behav. Immun.* **25**, 1078–1083 (2011).
241. Day, D. S., Luquette, L. J., Park, P. J. & Kharchenko, P. V. Estimating enrichment of repetitive elements from high-throughput sequence data. *Genome Biol.* **11**, R69 (2010).

242. Treangen, T. J. & Salzberg, S. L. Repetitive DNA and next-generation sequencing: computational challenges and solutions. *Nat. Rev. Genet.* **13**, 36–46 (2011).

7 PUBLICATIONS

7.1 PEER REVIEWED PAPERS

Robert MC, Furlan G, Rosso N, Gambaro SE, Apitsionak F, **Vianello E**, Tiribelli C, Gazzin S; “Alteration in the Cell Cycle in the Cerebellum of Hyperbilirubinemic Gunn Rat: A Possible Link with Apoptosis? PLOS ONE. 2013 Nov 1;8(11):e79073. doi: 10.1371/journal.pone.0079073.

Bortolussi G, Zentilin L, Vanikova J, Bockor L, Bellarosa C, Mancarella A, **Vianello E**, Tiribelli C, Giacca M, Vitek L, Muro AF; “Life-long correction of hyperbilirubinemia with a neonatal liver-specific AAV-mediated gene transfer in a lethal mouse model of Crigler-Najjar Syndrome”. Hum Gene Ther. 2014 Sep;25(9):844-55. doi: 10.1089/hum.2013.233.

Jasprova J, Dal Ben M, **Vianello E**, Goncharova I, Urbanova M, Vyroubalova K, Gazzin S, Tiribelli C, Sticha M, Cerna M, Vitek L. “The Biological Effects of Bilirubin Photoisomers.” PLOS ONE. 2016 Feb 1;11(2):e0148126. doi: 10.1371/journal.pone.0148126.

7.2 POSTER PRESENTATIONS AND ABSTRACTS

Zarattini P, Barbetta D, Bramante A, **Vianello E**, Lorenzon A, Gazzin S, Stebel M, Zennaro C, Tiribelli C. “Upgrading Gunn rat health and welfare by colony rederivation: the effect on the animal model.” Poster presented at the XXII AISAL Symposium “Innovation in laboratory animal science. The future is now.” In conjunction with the Board of Management

of FELASA (2015, Oct. 22-24). Abstract published in Comparative Medicine journal “Abstract of Scientific Papers: AISAL Symposium Naples.” Comp Med. 2016 Feb; 66(1): 73-79.

Vianello E, Berengeno A, Gazzin S, Tiribelli C. “mRNA profiling in toxicity or protection mechanisms involved in bilirubin-induced neuronal damage”. Poster at Conference “RNA Metabolism: Changing Paradigms in Neurodegeneration”, 2014, May 26-29, Trieste.

Vianello E, Berengeno A, Gazzin S, Tiribelli C. “Screening for different genes involved in toxicity or protection mechanisms in bilirubin-induced neuronal damage”. Poster at Conference 9th FENS Forum of Neuroscience. 2014, July 5-9, Milan.

Vanikova J, Goncarova I, Urbanova M, Vyroubalova K, **Vianello E**, Dal Ben M, Gazzin S, Tiribelli C, Sticha M, Cerna M, Vitek L. “Bilirubin Photoisomers do not affect bilirubin binding to albumin”. Poster at Conference 8th International Conference on Heme Oxygenase, BioIron and Oxidative Stress. 2014, Oct. 8-11, Sydney.

Vianello E, Tiribelli C, Gazzin S. “Histone acetylation in hyperbilirubinemia: An unexplored mechanism for bilirubin-induced encephalopathy and kernicterus.” Poster at Conference Environment & Health: Epigenetic mechanisms to design repair solutions. 2015, March 26/27, Vipava SLO.

Vianello E, Tiribelli C, Gazzin S. “Epigenetics in hyperbilirubinemia: the involvement of histone acetylation in bilirubin-induced encephalopathy”. Poster at Conference Don Ostrow Trieste Yellow Retreat. 2015, Sept. 02/03, Trieste.

Vianello E, Tiribelli C, Gazzin S. “Bilirubin-induced encephalopathy and epigenetics: Age-dependent modulation of histone H3 (lys14) acetylation in hyperbilirubinemic rat brain.” Poster at Conference 10th FENS Forum of Neuroscience. 2016, July 02-06, Copenhagen.

Berengeno A, Fazzari F, Robert C, Apitsionak F, Gambaro S, Furlan G, Dal Ben M, **Vianello E**, Tiribelli C, Gazzin S. “An *in vivo* map for the regional and developmental regulated

bilirubin-induced neurotoxicity.” Poster at Conference Joint Franco-Italian-Swiss multinational meeting on blood-brain interfaces. 2016, Oct. 24-26, Lion.

8 ACKNOWLEDGMENTS



Fondazione Italiana Fegato

Prof. Claudio Tiribelli

Dr. Silvia Gazzin

Matteo Dal Ben, Veronica Marin, Natalia Rosso, Cristina Bellarosa, Devis Pascut, Pablo Giraudi, Cecilia Sukowati, Nicole Parmisan, Rusdina Bte Ladju, Yogi Pratama, Rosario Bongiovanni, Beatrice Anfuso, Mohammed Qaisiya, Chiara Greco, Carlos Coda Zabetta, Sandra Leal



SPF Animal Facility of CBM S.c.a.r.l. (AREA Science Park, Basovizza, Trieste)

Andrea Lorenzon and Alessandra Bramante



Centro di coordinamento regionale Malattie Rare FVG, Azienda Ospedaliero Universitaria Santa Maria della Misericordia, Udine

Andrea Dardis and Stefania Zampieri



Dipartimento di Anatomia Patologica, Ospedale di Cattinara, Trieste

Prof. Fabrizio Zanconati and Cristina Bottin



Cancer Genomics Lab, Fondazione Edo ed Elvo Tempia, Biella

Giovanna Chiorino, Paola Ostano, Fabio Tordini